AN INVESTIGATION INTO THE BEHAVIOUR OF SIMPLY-SUPPORTED BAMBOO-GEOTEXTILE COMPOSITE SYSTEM

SAW JING XIEN

A project report submitted in partial fulfilment of the requirements for the award of Bachelor of Engineering (Hons.) Civil Engineering

Faculty of Engineering and Science
Universiti Tunku Abdul Rahman

May 2015

DECLARATION

I hereby declare that this project report is based on my original work except for citations and quotations which have been duly acknowledged. I also declare that it has not been previously and concurrently submitted for any other degree or award at UTAR or other institutions.

Signature : _____

Name : SAW JING XIEN

ID No. : 1101011

Date : _____

APPROVAL FOR SUBMISSION

I certify that this project report entitled **"AN INVESTIGATION INTO THE BEHAVIOUR OF SIMPLY-SUPPORTED BAMBOO-GEOTEXTILE COMPOSITE SYSTEM"** was prepared by **SAW JING XIEN** has met the required standard for submission in partial fulfilment of the requirements for the award of Bachelor of Engineering (Hons.) Civil Engineering at Universiti Tunku Abdul Rahman.

Approved by,

Signature : _____

Supervisor : IR. DR. LOW KAW SAI

Date : _____

ACKNOWLEDGEMENTS

I would like to thank everyone who had contributed to the successful completion of this project. I would also like to express my gratitude to my research supervisor, Ir. Dr. Low Kaw Sai for his invaluable advice, guidance and his enormous patience throughout the development of the research.

I am also very much thankful for Mr Hwong Guo Fu, the lab officer for providing assistance whenever possible throughout the laboratory investigation. It is also my honour to obtain guidance from Ir. Dr. Lim Siong Kang for giving valuable advices for my project.

AN INVESTIGATION INTO THE BEHAVIOUR OF SIMPLY-SUPPORTED BAMBOO-GEOTEXTILE COMPOSITE SYSTEM

ABSTRACT

Soft ground construction has been on the use as soft clay is often found throughout the coastal plains of Malaysia, East and West alike, where many of these areas are under development for urbanization pressure. However, soft clay construction has always been a challenge for geotechnical engineers as soft ground will undoubtedly pose stability and settlement problems for the structures built over it. Since soft ground are almost found everywhere across the world, its importance has long been noticed by civil engineers since long ago, and according by many solutions have been devised and deployed to counter such issues. However, unfortunately, many of the existing solutions are either too sophisticated or costly to be implemented.

Thus, in view of the existing soft ground problems and the ineffectiveness and uneconomical of methods available, an environmentally friendly and yet cost-effective method is introduced. Bamboo-geotextile composite (BGC) system a.k.a. Geobamtile system has to date been deployed successfully in several projects in Malaysia and her neighbouring countries and recorded satisfactory performance so far.

For completeness, the theories for good understanding on the behaviour of such system, so that it can be justified to be a well-developed solution based on sound engineering. This indeed constitutes the core of this investigation to provide a theoretical background for such system.

Being a structure-soil interaction problem, literature reviews are carried out in this direction. For general, it is known that in a common foundation problem,

concrete foundation is supported directly by soil continuum and the behaviour of the concrete foundation in turn is influenced by soil properties and its conditions and the behaviour of soil however is in turn influenced by the action of slab acting on it.

One of the most well-known structure-soil interaction models is the Winkler model (Winkler, 1867) that was originally developed for analysis of railroad track. Nevertheless, it is a very simple but not very accurate representation of many practical foundations. Many theories have since been developed to improve on this model by several researchers such as Filonenko-Borodich, Hetenyi, Pasternak and Vlasov. The literature review for this thesis will incorporate the selected theories which will be used in developing the current theoretical approach in conjunction with experimental studies carried out. All these constitute an effort to understand the BGC system well.

It is realized that the difficulties of using these structure-soil interaction theories for the BGC system are the determination of several parameters in particularly the modulus of subgrade reaction, k_o of the soil, which is a case-sensitive parameter, the Young modulus, E of bamboo, a natural material which exhibits inconsistent E values throughout its culm and the moment of inertia, I of the BGC system as a whole especially when bamboo culms are arranged in a criss-cross direction that gives rise to a discontinuous and non-uniform cross-section throughout the system. These problems however are a subject of investigation and will discuss in more details in this study.

TABLE OF CONTENTS

LIST OF TABLES

LIST OF FIGURES

LIST OF SYMBOLS / ABBREVIATIONS

B	width of foundation, mm
I	moment of inertia of beam, mm^4
L *or* l	length of beam, mm
E	modulus of elasticity of beam
E_s	modulus of elasticity of soil
EI	flexural rigidity of beam
k'	spring's proportionality constant
k	coefficient of subgrade reaction, N/mm^2
k_o	modulus of subgrade reaction, N/mm^3
k_{s1}	coefficient of subgrade reaction for a plate of 1 ft. wide, N/mm^3
p	vertical downward force, N
q_u	allowable bearing capacity
$q(x)$	uniformly-distributed load (UDL), N/mm
v_s	Poisson's ratio of soil
μ	non-dimensional soil mass per unit length
λ	$\sqrt[4]{\frac{k_o B}{4EI}}$, characteristic parameter of Winkler's model
X	value of sample
$\bar{X}$	mean
σ	standard deviation
CV	coefficient of variation
N	number of samples
x, y, z	coordinate axes

LIST OF APPENDICES

CHAPTER 1

INTRODUCTION

1.1 Introduction

In Malaysia, construction over soft ground has always been an important yet challenging domain in the field of civil engineering. Today, due to scarcity of good firm ground, it is inevitable to have developments built on soft ground. Accordingly, in the past decades, the construction of various structures, buildings and infrastructures on the soft ground has been on a growing trend.

The dilemma is now on the infrastructural development over soft ground. The idea of implementing new methods to support heavy engineering construction over soft clay and/or even peat economically and soundly has expectedly would receive tremendous attention. Many methods have been proposed and attempted on constructing heavy engineering structures on soft ground to very soft ground but they often have their own practical limitations due to the sophistication of the methods and perhaps the cost as well. For these reasons, while there are numerous ground improvement methods available, more new methods or solutions are expected to emerge in the future.

1.2 Background of Study

Bamboo-geotextile buoyant system is one of the inventions by the author's supervisor, Dr. Ir. Low Kaw Sai as a result of the research effort of him and his team in searching method to overcome the problems of constructing heavy structures safely and economically over soft to deep even very soft ground without attracting excessive total and differential settlements. These by far are the major problems related to construction over soft ground. It is hoped that it can be solved through innovative use of bamboo, which is natural material widely available locally, in conjunction with geotextile as in the current Bamboo-Geotextile Composite System.

As a matter of fact, bamboo is one of the oldest building materials used by mankind. The bamboo culms or stems have been made into various kinds of products but most noticeably in the industrial applications, where bamboos are deployed in the construction for bridges, scaffolding and houses in countries like China, Hong Kong, India and elsewhere where bamboos are found abundantly and used extensively in daily life. This being the inspiration for this invention, and of course Malaysia is fortunately to be one of the countries where bamboos are acclimated to grow. Then, this would be green, practical and innovative of this invention for usefulness of this versatile plant that benefits mankind in so many ways for so long.

1.3 Objectives of Study

The objectives of this study are:

1. To investigate using a scaled down bamboo-geotextile composite system model in the laboratory.
2. To examine the various available soil-structure interaction theories that may be suitable in the prediction of the behaviour of bamboo-geotextile model so developed.
3. To produce and compare theoretically predicted results with those observed in the laboratory.

4. To produce useful prediction tool for the settlement of soft subgrade based on a reliable soil modelling theory.

1.4 Significance of Study

The significances of this study are as follows:

1. To develop a reliable prediction model for the soil-bamboo-geotextile interaction system in order to facilitate engineering design work.
2. To reveal the potential of the bamboo-geotextile composite system in solving real life civil engineering problems.

1.5 Layout of this Report

In general, this thesis is divided into 5 chapters. Chapter 1 will present an introduction on the study, background and objectives of the research and then finally the significance of the research.

Chapter 2 gives a review on the application of various theories related to the subject of this study.

Chapter 3 shall focus on the methodologies adopted for this study. However, the materials and apparatus preparation will also be covered in this chapter. Besides, the detailed methods of testing to obtain the necessary experimental data shall also be discussed in this chapter.

Chapter 4 will concentrate mainly on the discussion of the results of this study before the experimental and theoretical results will be compared. Nevertheless, the techniques employed to produce the predicted results will also be examined in this chapter.

Chapter 5 shall make a conclusion of the study conducted. Nevertheless, a number of recommendations for future investigation will be included in this chapter.

CHAPTER 2

LITERATURE REVIEW

2.1 Introduction

This chapter will discuss about some insights into the soft ground problem which are significant to a geotechnical engineer in Malaysia. Various ground improvement methods widely used in Malaysia are to be discussed. Nevertheless, the development of approaches used for the analysis and design for foundation, where Winkler method is specially highlighted will also be explained.

2.2 Soft Soil

Although soft soil generally comprises of clayey soil and loose sandy soil but soft clay is by far the most worrying in civil engineering. Clay deposits which have a high rate of sedimentation and it has been around since the period between 12,000 and 5,000 years ago (Leroueil et al., 1990). Soft clay, organic and inorganic alike, nearly always presents challenges to geotechnical engineers mainly in the settlement and stability problems in soft ground when construction takes place on this type of soil. Terzaghi and Peck (1967) stated that “very soft” clay have very low shear strength which is less than 25 kPa, and for the “soft clay” shear strength was between 25 kPa to 50 kPa.

2.2.1 Problems of Soft Clay

It is a well-known fact to geotechnical engineers that soft clay is highly susceptible to large settlement due to structural loadings and this may take place over hundreds of years if left unconsolidated. It is usually the direct weight of the structure that causes settlement of the cohesive soil. However, secondary influences such as the lowering of the groundwater table can also lead to settlement of cohesive soils. The soil parameters normally employed and characterized in soft soil problems are:

i. Classification and Index Properties, and Natural Moisture Content
ii. Undrained Shear Strength (S_u)
iii. Pre-Consolidation Pressure (P_o)
iv. Compression Index (Cc) and the Coefficient of Volume Change (m_v)
v. Coefficient of Consolidation (C_v)

These parameters are very important in analysing the behaviour of soft soil so that it can carry extra loads subjected to the soils. These natural features of soft ground are widely found in Malaysia along the coastal plains area and with the increasing economic development over the soil; studies were performed to determine the typical properties of soils that can contribute to the failure of the soil structure. (Hasnita, 2009).

For the soft marine clay in Malaysia, it was reported by Broms (1990) that typical moisture contents range from 60% to 80%. This is different to what Ting et al. (1988) and Chen et al. (2003) reported; where the moisture content is typically about 80% to 130% in Penang area and 50% to 100% in Klang area respectively. Brand et al. (1989) reported that the Muar clay has the natural water content as high as 100% and generally exceeds the liquid limit. It is also very common that the moisture content of the soft clay especially near to the ground level to be higher than the liquid limit.

The in-situ undrained shear strength, S_u of soft clay can be measured directly using field vane shear test. The S_u generally increases with depth. Typically the vane

shear test results for clay at Klang areas are about 5 kPa at depth 2 m to 50 kPa at depth 18m (Chen et al., 2003). This is similar to Muar Clay and Juru Clay where the S_u ranges between 10 kPa at depth of 2 m to 35 kPa at depth 18 m, and 10 kPa to 30 kPa at depth of 12 m respectively.

Soil is assumed to be compressing elastically under light loads as shifts and rearrangement of soil particles allow increasing amounts of settlement. This stage of settlement is attributed to primary consolidation, where the rate of settlement is controlled by the time required to allow dissipation of pore water pressure. The most useful parameters to monitor the consolidation process are compression index (C_c), recompression index (C_r) and coefficient of consolidation (C_v).

The compressibility of the soft layers can also be represented using the compression ratio ($C_c/l+e_o$). In the study of Juru Trial Embankment (Huat et al., 1995), it was found that the compression ratio ranges from 0.4 to 0.6 and Ting et al., (1988) reported that the coastal plain areas of Sarawak and Sabah has the average values of $Cc/l + e_o$ vary within a narrow range from about 0.3 in the upper layers to about 0.1 in the lower layers. Terzaghi and Peck (1967) proposed an empirical correlation between C_C and Liquid Limit, w_L for clays of low to medium sensitivity and w_L up to 100% as follow:

$$C_c = 0.009\ (w_L - 10) \tag{2.1}$$

As for clay from Klang areas, Huat et al. (1995) proposed the following relationship for Klang Clay.

$$C_c = 0.005\ (w_L + 71.8) \tag{2.2}$$

The proposed equation 2.2 was made because of the sensitivity of Klang Clay and it is usually ranged around 3 to 8 and higher C_c values are expected. Another important parameter is the coefficient of consolidation, C_v, where it represents time taken for a soil to consolidate. Values of C_v, are different with types of soft clay. Rowe, 1972 stated that laboratory determined C_v value underestimates the rate of settlement, since the laboratory permeability is much lower than the field values

because it is very difficult to reproduce the same soil in the field without having disturbance to the sample. Hence, it is a common practice in design where C_v values are multiplied by 3 to 10 of those measured in oedometer tests. (Brend et al, 1989)

2.3 Embankment

2.3.1 Introduction

Embankment construction is an essential element of any highway and railway construction. The problem arises when the embankment passes through soft ground condition such as soft clay. In that case the soil is subjected to settlement or stability problem due to lack of bearing capacity of the soft soil. Traditionally, there are methods for stabilizing the soft soil which are for example, by driving deep foundations through the unsuitable soils thereby avoiding them altogether, excavate and replace the soft soils with suitable soils, stabilize the soft soils with injected additives or wait until natural consolidation occur. Details of some other soil improvement methods are mentioned in Section 2.3. The methods mentioned are very costly and require a long time to strengthen the soft foundation soil. To overcome these difficulties, soil reinforcement was introduced as one of alternative way in embankment construction over soft clay that proud to be more efficient than other method. Soil reinforcement is a technique where soil been strengthened by tensile elements such as metal rods or strips, non-biodegradable fabrics (geotextile or geogrid), granular materials and bamboo (Das, 2004 and 2006). According to Ochiai et al. (1996), bamboo sheet reinforcements are able to mobilize reaction forces within the ground due to their flexural rigidity. In techniques such as “rope sheet” reinforcement, the geosynthetic generally requires anchorage to adjacent stable ground to support the tensile loads generated in the reinforcement. However, geotextile or geonet reinforcement may work fairly well without anchorage if the ground conditions are better.

The beneficial effects of reinforced soil may be considered in terms of both technical and economic benefits. Technically, the presence of reinforcement in the

soil helps to reduce the forces in the soil which mobilize failure and also provides additional forces in the soil to resist failure, meanwhile with reinforcement the construction time can be shortened because only the reinforcing materials are need be sent to the site and this technique is relatively easy to be done compared to other soil improvement techniques. Another major application for reinforced soil is to improve the short term stability of embankments constructed over soft foundation soils, as shown in Figure 2.1. The purpose of the reinforcement is to maintain equilibrium until consolidation can occur in the soft foundation soil. The foundations strengthen with time during consolidation and finally support the embankment loading without need for the reinforcement.

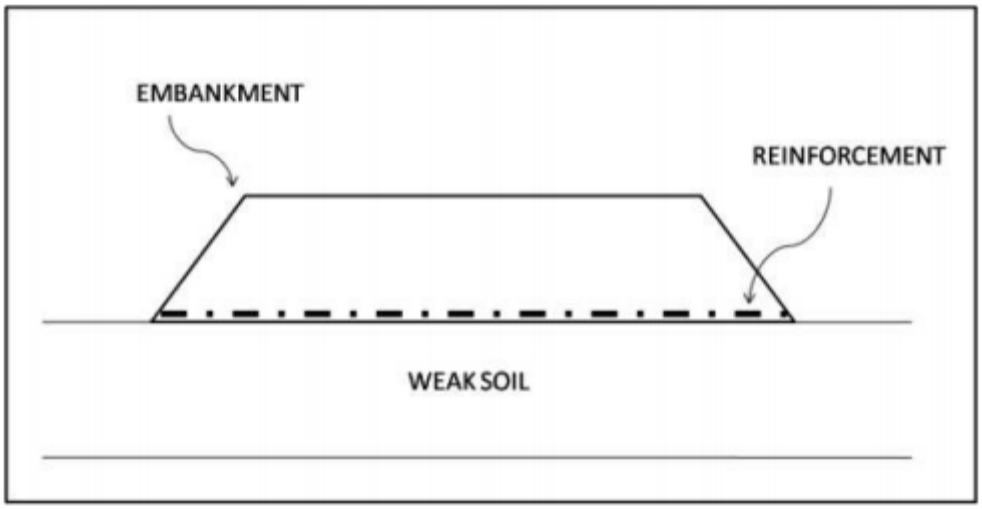

Figure 2.1: Simple Construction of Embankment over Weak Soil with Reinforcement (Holtz, 2001)

2.4.2 Design Consideration of Embankment on Soft Soil

The design and construction of embankments on soft subgrade is a very daunting geotechnical problem. Without adequate geotechnical knowledge and competency, embankments designed will undoubtedly fail as soft subgrade is a very delicate soil problem and without adequate soil reinforcement, the embankment may fail during or after construction such as deep seated sliding wedge, or circular failure, lateral spreading or bearing capacity failure. The conventional design approach for a

reinforced embankment is to design against failure. There are three possible modes of failure for embankments constructed over soft subgrade, which are bearing capacity failure, rotational failure and side displacement failure (Terzaghi et al., 1996 and Holtz, 2001).

2.4.2.1 Bearing Capacity Failure

Bearing capacity is the capacity of soil to support the loads applied to the ground. Soft subgrades supporting embankments may fail in bearing capacity during or soon after construction when applied load from lay embankment exceeds the capacity of foundation subgrade. Method of applying soil reinforcement is one of the possible solutions to this problem. Reinforced soil placed beneath the embankment improves stability by increasing the forces resisting against failure and help to hold the embankment together while the foundation strength increases through consolidation. Figure 2.2 illustrates bearing capacity failure.

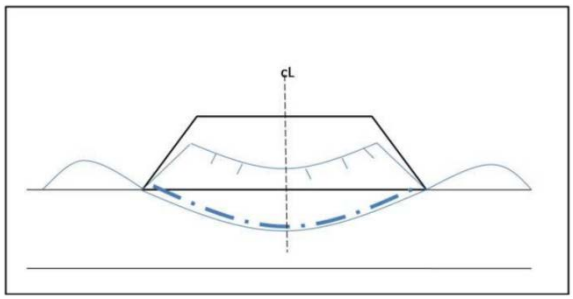

Figure 2.2: Simple Illustration of Bearing Capacity Failure (Ochiai et al, 1996)

2.3.2.2 Rotational Failure

Rotational failure, also known as circular slip failure, normally occurs at the edge of embankment and this is due to the driving forces being greater than the resisting forces. Rotational slope failures can be resisted by the use of reinforcement with

adequate tensile strength and embankment fill with adequate shear strength. Thus, it is important for the tensile strength of the reinforcement to be sufficiently high to control the large unbalanced rotational moment because failure can occur through the embankment, foundation layer and the reinforcement. Figure 2.3 illustrates circular slip failure.

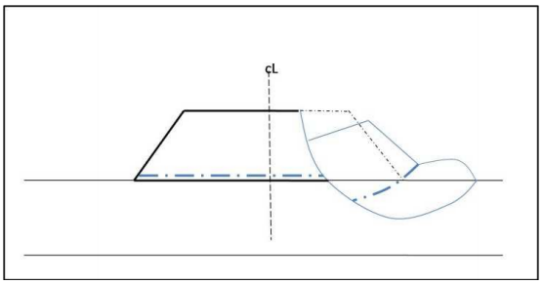

Figure 2.3: Simple Illustration of Circular Slip Failure (Ochiai et al, 1996)

2.3.2.3 Side Displacement Failure

Excessive horizontal sliding of embankments and foundation soils may occur from large lateral earth pressures caused by embankment soils. These forces are derived from the physical properties of the structure such as embankment height, slopes and fill material properties. During construction, the embankment would resist these modes of failure through shear forces developed along the embankment-foundation interface. When reinforcements are used between the soft soil and the embankment, the reinforcement will increase the resisting forces of the equilibrium. Reinforced soil may fail by fill material sliding off the reinforcement surface. These failures can be prevented by specifying the soil reinforcement that meets the required tensile strength. Figure 2.4 illustrates side displacement failure.

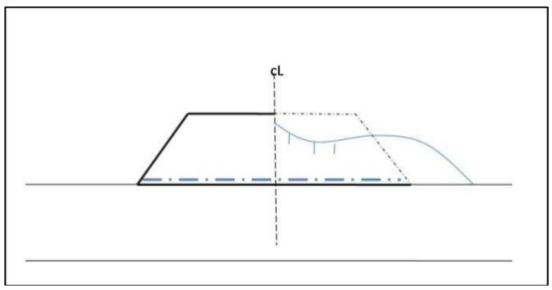

Figure 2.4: Simple illustration of side displacement failure (Ochiai et al, 1996)

2.3.3 Soft Soil Behaviour under Embankment

2.3.3.1 Settlement

The settlement of foundation soil (clay soil) that occurred during and after construction of embankment is due to the applied loads with time. In the first phase, the foundation soil is in over-consolidated condition and has high rate of consolidation. Therefore, the settlement is small and increases linearly with the increase of embankment load (OP'). The clay soils becomes normally-consolidated when height of embankment is greater than critical height ($H>H_{nc}$) and start to respond in undrained condition. As illustrated in Figure 2.5, settlement of P'A' occurs when the rate of consolidation decreases. Finally, after the end of construction, the consolidation settlement decreases at lower rate with time (A'D'). However, it was observed that settlement under the middle of the embankment does not indicate an impending failure condition. The reason for this is considered to be that in most cases the settlement monitoring point under the centre of the embankment is not located within the failure zone (Hunter and Fell, 2003).

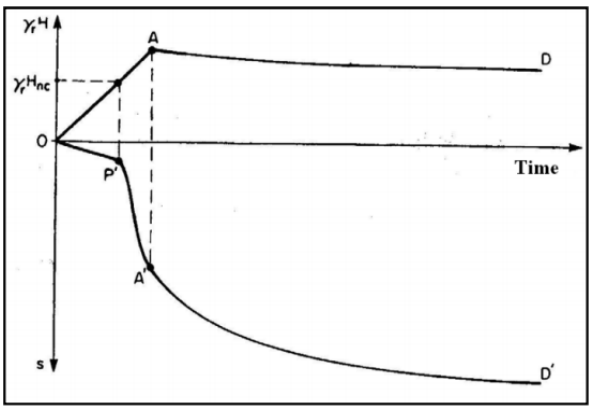

Figure 2.5: Typical Variations in Embankment Load and Settlement with Time (Lerouiel et al., 1990)

Research conducted by Hunter and Fell (2003) shows the vertical deformation at the toe of the embankment versus the relative embankment height, as shown in Figure 2.6. Meanwhile, Figure 2.7 presents the vertical deformation

behaviour beyond the embankment toe (approximately 5 m distance beyond the toe). In all cases the monitoring point beyond the toe was located within the eventual failure zone. The vertical displacement at and particularly beyond the toe of the embankment is a good indicator of an impending failure condition. For measurement points beyond the toe, negligible vertical deformations were usually observed during the initial period of embankment construction, and the impending failure condition was identifiable by heave movements or large increases in the rate of heave movement with increasing embankment height. These observations apply to a wide variety of soil types from low sensitivity, ductile high plasticity clays to highly sensitive, low plasticity clays and silts. Works by Hunter and Fell (2003) show that for the highly sensitive and low plasticity clay foundations (St. Alban and James Bay) the amount of vertical deformation is relatively small (up to 10–15 mm) up to approximately 90% of the eventual embankment failure height.

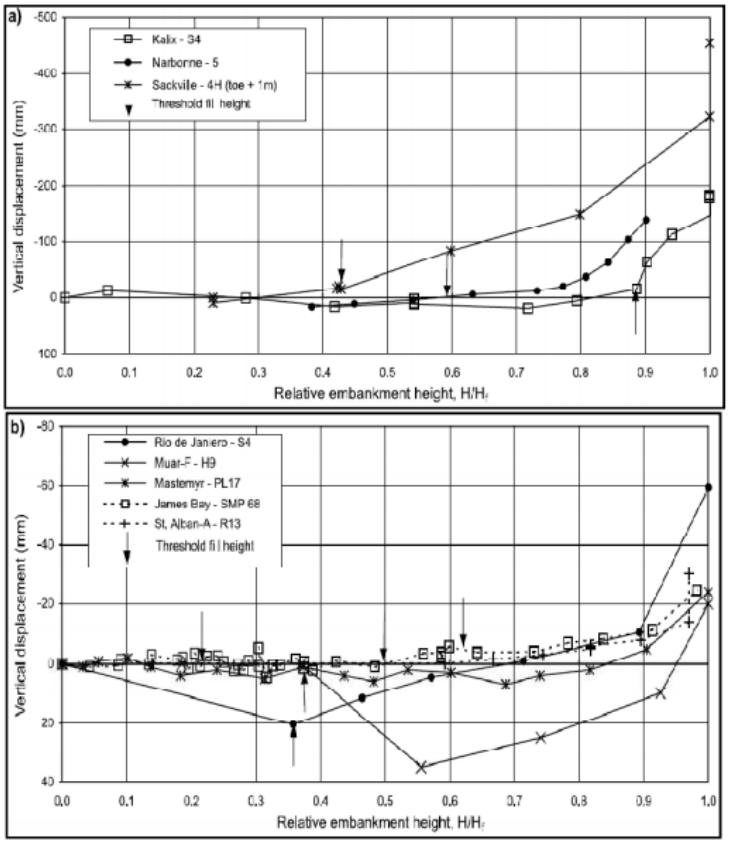

Figure 2.6: Vertical Displacement at the Embankment Toe versus Relative Embankment Height (Hunter and Fell, 2003)

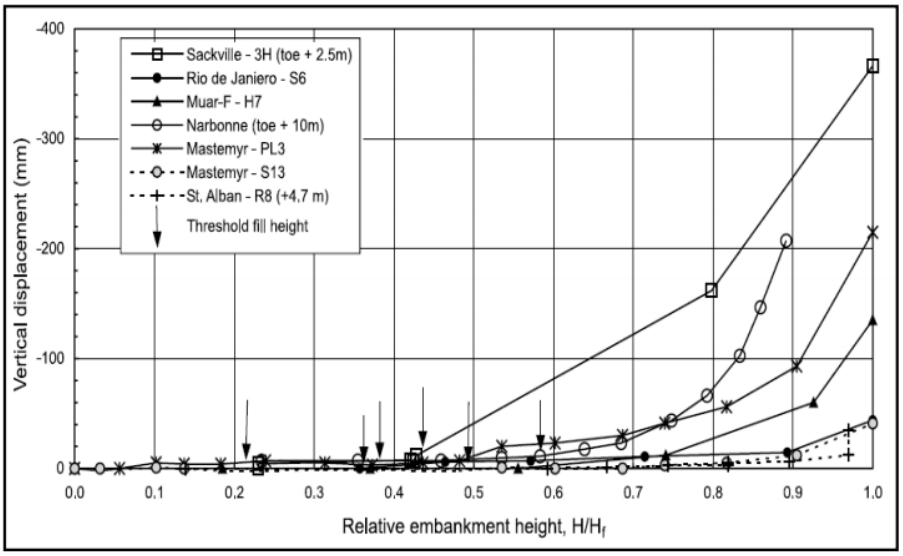

Figure 2.7: Vertical Displacement beyond Toe versus Relative Embankment Height (Hunter and Fell, 2003)

2.3.3.2 Excess Pore Water Pressure Response

The pore water pressure response during construction of embankment is in accordance with the increasing vertical total of the embankment, as shown in Figure 2.8. In the early stage, change in pore pressure, Δu is less than change in stress, $\Delta\sigma_v$ and the values of pore pressure coefficient, $\bar{B}_1 = \Delta u/\Delta\sigma_v$ varies with depth in the clay due to isochrones relation as illustrated in Figure 2.8. At some stage in the construction process, it was observed that the pore pressure at certain increases to an incremental $\bar{B}_1$ value of roughly 1. According to Hunter and Fell (2003), the interpretation by Leroueil et al. (1978) explains that this location of piezometer is where the critical vertical stress is equivalent to the pre-consolidation pressure (P' in Figure 2.8). The embankment height at which this condition happens was termed the "threshold embankment height" or critical embankment height, H_{nc}. Equation (2.3) defines the threshold height.

$$H_{nc} = \frac{\sigma'_p - \sigma'_{vo}}{I\gamma_r(1-\bar{B}_1)} \qquad (2.3)$$

Where at a given depth below the central portion of the embankment σ_p' is the preconsolidation pressure; σ_{vo}' is the initial effective stress; γ_r is the saturated unit weight of the embankment soil, If is the stress influence factor (for the applied load, defined using Osterberg Chart); and $\bar{B}_1$ is the observed initial pore pressure response (determined from Figure 2.9).

With further loading, in undrained condition with the clay in a normally consolidated condition, the excess pore pressure response is typically at an incremental $\bar{B}_1$ value of approximately 1 (B_2 in Figure 2.8) or $\Delta u = \Delta\sigma_v$. In this stage of the loading, the clay is characterized by its high compressibility and a low coefficient of consolidation, *Cv* resulting in low rates of excess pore pressure dissipation. Leroueil et al. (1978) (in Hunter and Fell, 2003) analysed that in most of the cases the rate of construction was sufficiently high that negligible excess pore pressure dissipation occurred. As a result, at the end of construction under stable embankment (A' in Figure 2.8) the pore pressure is given by

$$\Delta u_c = I\gamma_r H_r - (\sigma'_p - \sigma'_{vo}) \tag{2.4}$$

As loading increases, the soil will eventually reach a localized failure condition, and $\bar{B}_f > 1$ is observed (Figure 2.8). A localized failure occurs when the effective stress in a part of the foundation reaches the failure surface (it is generally initiated at a zone in the foundation below the embankment slope and toe). Complete failure of the embankment does not necessarily occur once a localized failure condition is reached as the localized failure zone is supported by the surrounding soil that has not failed.

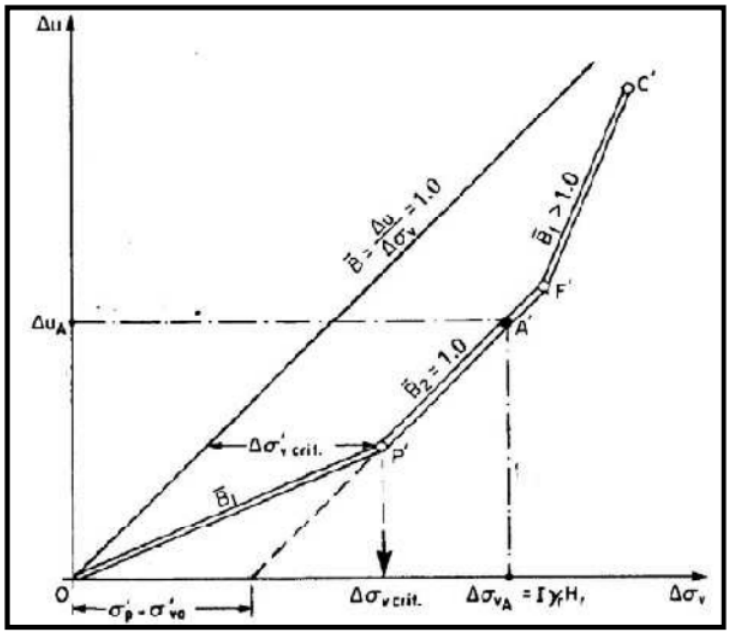

Figure 2.8: Relation between Pore Pressure and Vertical Total Stress Caused by an Embankment (after Tavenas and Leroueil, 1980)

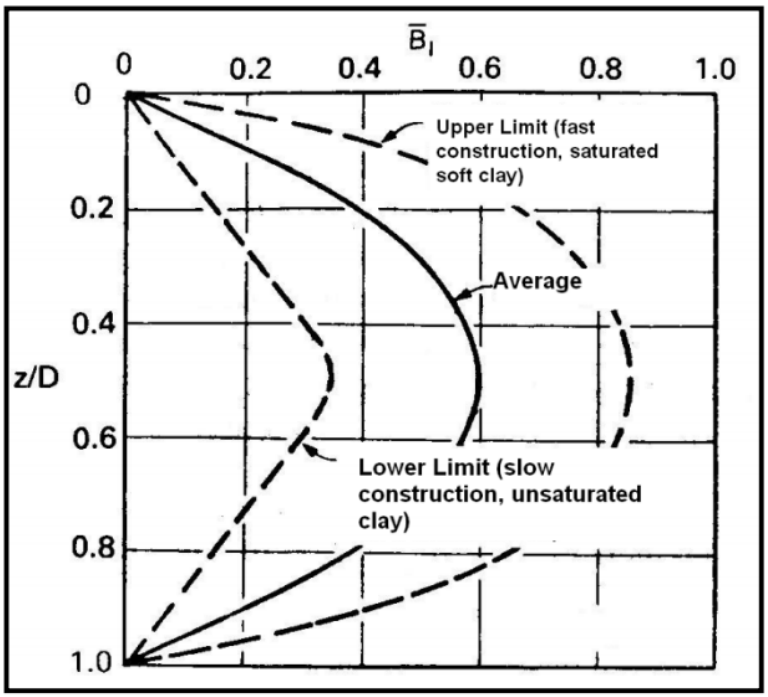

Figure 2.9: Relation between Depth and Coefficient of Pore Pressure, (Leroueil et al., 1990)

2.4 Geotextile

Geotextile is one of the geosynthetic groups and it has been used since the early 1970's by civil engineer to perform several major functions in geotechnical (soil) structures (Holtz, 2001). ASTM defines geotextile as a permeable geosynthetic comprised solely of textiles. Geotextiles perform several functions in geotechnical engineering applications. The major characteristic of geotextiles is that they are porous to liquid flow across their manufactured planes and also within their thickness, but to widely varying degrees. According to Koerner (1990), geotextile can perform as a filter, drainage, separation, erosion control, sediment control, reinforcement and moisture barrier (when impregnated with asphalt).

2.4.1 Manufacture of Geotextile

Geotextiles are made from one or more polypropylene, polyester, polyethylene, polyamide (nylon), polyvinylidene chloride and fibre glass. About 65% geotextile made by polypropylene, 32% made by polyester, 2% made by polyamide and polyethylene 1% (Salfaiza, 2009). Polypropylene is one of the polyolefin groups and it is a synthetic polymer that is lighter than water with specific gravity of 0.9, pH 2 to 13, strong and very durable. The main advantage of Polypropylene usage in geotextile manufacture is because it is an economical material. Polyester a.k.a. polyethylene terephthalate, a category of polymers that contain ester functional group in their main chain with pH greater than nine which is susceptible to degradation. Polyamide is a polymer containing monomers of amides joined by peptide bonds and polyethylene is a thermoplastic polymer consisting of long chains of monomer ethylene.

Woven geotextiles are made from weaving monofilament, multifilament, or slit film yarns and tapes. The weaving techniques are similar to the production of clothing textile. Commonly woven geotextile is plain woven, but sometimes made by twill weave. The physical properties of geotextile are varied by the composition and by the method to form the molten material to filaments. Woven monofilament

geotextiles are generally preferred for engineering applications where both strength and filtration are a concern such as drainage and erosion control. This type of geotextiles is primarily used in reinforcement applications but it is costly. Woven slit-film geotextiles are preferred for applications where high strength properties are needed and filtration requirements are less critical. These fabrics reduce localized shear failure in weak subsoil conditions and aid construction over soft subsoil.

Nonwoven geotextiles were formed by a process other than weaving and they are generally thicker than woven geotextile. Manufacturing of nonwoven geotextile is a more modern method compared to woven method. Nonwoven geotextile is usually manufactured either from continuous filaments or from staple fibres. The fibres are then connected using needle punching or heat bonding technique. Nonwoven geotextiles are highly desirable for subsurface drainage and erosion control applications as well as for road stabilization over wet moisture sensitive soils because it becomes stronger due to the increased thickness of geotextile and the fabrics have high rate of permeability.

Table 2.1: Comparison between Properties of Woven and Nonwoven Geotextile (Ghosh et al., 2006).

Properties	Woven	Nonwoven
Breaking Strength	Higher	Lower
Breaking Elongation	Lower	Higher
Initial Modulus	Higher	Lower
Absorption	Moderate	Very high
Bursting	High	Low
Thickness	Moderate	High
Opening	Can be regular	Irregular
Filtration	Moderate	Better
Porosity	Disadvantageous	Advantageous
In-plane Flow	Low	Can be high
Friction with Soil	Moderate	High

2.5.2 Functions of Geotextile

Geotextiles and related products such as geonets and geogrids have many applications and currently support many civil engineering applications including roadwork, airfields, retaining structures, reservoirs, canals, dams, bank protection, coastal engineering, construction site silt fences and embankment. Since geotextile is good in its tensile strength, it is usually placed at the tension surface to strengthen the soil as shown in Figure 2.10. Geotextile is a very versatile invention as it can perform as a separation, filter, drainage, reinforcement, erosion and sediment control and moisture barrier when impregnated with asphalt (Koerner, 1990).

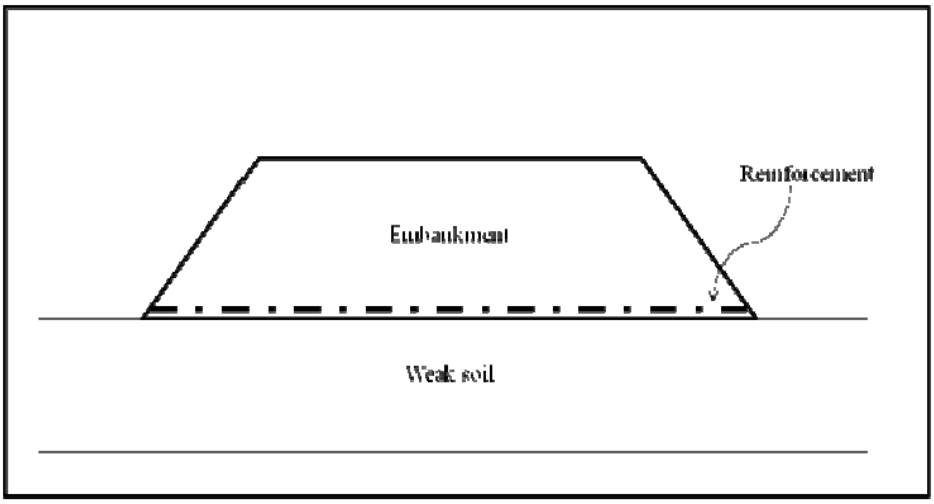

Figure 2.10: Simple Embankment over Weak Soil with Reinforcement (Holtz, 2001)

Separation is a function implying segregation of two or more layers of materials by preventing intermixing of dissimilar materials or similar materials with different grading. The purpose of placement of a flexible porous textile between dissimilar materials is so that the integrity and functions of both materials remain significant or are improved. For example, it is used for stabilization for road construction and railway construction over soft clay foundation.

Geotextile functions as reinforcement when it aims to improve the total system's strength by integrating the tensile strength of a geotextile in a soil which is

good in compression but weak in tension instead. The main advantages of using geotextile acting as reinforcement are increase in height of embankment, acceleration of embankment construction by reducing number of construction phases, reduction in volume of fill material for construction and lastly increase in stability of an embankment.

When geotextile is used for drainage purposes, it acts as a conduit for the movement of liquids or gases through the plane of geotextile. Geotextile can be placed in contact with a material of low permeability where water seeps slowly to escape, so that it acts as a medium to gather the trapped water in such low permeability material, i.e. clayey soil, and conveys the water towards an outlet.

Filtration is a function of geotextile that allows liquid flow with limited soil loss across the plane of the geotextiles over a service lifetime compatible with the application under consideration. It is used for purposes where it is undesired to have leakage of materials, i.e. soil, contaminants, etc. There are three example geotextile acting as filtration: filter for particles suspended in a liquid, filter for removing water from a granular soil and filter associated with armour (for soils exposed to waves).

2.4.3 Durability of Geotextile

The exposure of sunlight can degrade the physical properties of polymers. The rate of degradation is reduced by the addition of carbon black but not eliminated. Polymer materials become brittle in very cold temperatures. Chemicals in the groundwater can react with polymers. High pH water can be harsh on polyesters while low pH water can be harsh on polyamides. All of these factors should be considered in selecting acceptable geotextile materials.

2.5.4 Applications of Geotextile in Embankment Loading

Embankment loading can be determined from the embankment height, slopes and fill material properties. The embankment loading can either be in single stage or multi-stage (Gue, 2000). For single stage loading, it will cause immediate increase in total stress and if the filling is so rapid it can increase pore water pressure because water cannot dissipate from soil. For multi-stage loading, the advantage is that the soil is allowed to consolidate and water can dissipate from soil. The problem with this method is it required longer time of construction. According to Hunter dan Fell (2003), the lowest loading is at embankment toe and then increases to the central line and its variations are dependent on embankment geometry, types and embankment height.

Table 2.2: Comparison of Geotextile and Conventional Methods (Loke, 1998)

Conventional Method	Advantages of Geotextile
Soil replacement	
Removal of soft soil and replace with good soil	Removal of poor subgrade soil may not be required with geotextile reinforced base embankment. If soil replacement is necessary, the used of geotextile allows reduction in volume of soil replaced and therefore, cost savings
Lateral supporting beam	
The berms avoid circular failure by providing counter weight	Lateral supporting berms are not required because geotextiles provides lateral restraint to the embankment and reduces land space requirements.
Step by step construction	
The embankment is built by successive fill layers. Certain degree of consolidation on foundation soil is achieved before construction of the next fill layer.	The number of steps to build the embankment can be reduced using geotextiles to ensure stability. This allows rapid construction of the embankment and reduces consolidation time.
Vertical drains	
Provides drainage to reduce consolidation time of foundation soil	Geotextile reinforcement increases the speed of construction. This allows rapid construction and accelerates the time of consolidation.
Temporary surcharge	
With a temporary surcharge the rate of consolidation increases. When the desired degree of consolidation is achieved, the temporary surcharge is removed.	The geotextile ensures the stability of the embankment during the surcharging. This increases the speed of loading.

2.5 Bamboo

2.5.1 Properties of Bamboo

2.5.1.1 Physical Properties

The amount of moisture in bamboo varies within and between the species, height and age of the living culm. The moisture content has a similar influence on the strength of the bamboo as it has in timber. Generally, in the dry condition the strength is higher than in the green condition. For some Malaysia bamboos, moisture content is about 30% to 130%. However the density of bamboo varies from about 0.5glcms to 0.9gIcm3 with the outer culm having a far higher density than the inner part (Hasnita, 2009). Moisture content and density of selected species of bamboo are tabulated in Table 2.3.

Table 2.3: Physical Properties of some Malaysian Bamboos (FRIM, 1995)

Species	Moisture Content (%)	Density (g/cm^3)
Buluh Duri	57-97	0.43-0.60
Buluh Minyak	79-118	0.27-0.57
Buluh Galak	92-132	0.44-0.58
Buluh Betong	28-105	0.55-0.78
Buluh Semantan	79-108	0.47-0.60
Buluh Benting	30-77	0.65-0.94

2.5.1.2 Mechanical Properties

The strength of bamboo depends on the species and on its age, moisture content, density and culm height. The mechanical properties of bamboo vary with the age of the bamboo and the height of the culm, as mentioned by Chauhan (2000) (in Li, 2004). However, higher moisture content will decrease the strength of bamboo (Prawirohatmodjo 1990) (in Lybeer, 2005). The strength of this material also related to its density. The density of bamboo varies approximately from 0.5 to 0.9 g/cm^3 but

can differ considerably within the culm (increase with the height of the culm) and between species (Siti & Abd. Latif, 1992; Jamaludin et al., 1995; Kabir et al., 1996; Subyakto, 1996) (in Lybeer, 2005).

As bamboo ages, the strength properties will increase. This is probably due to the hardening of the culm walls as the bamboo matures in about 3 to 5 years, by which time it would reached its maximum strength (Lee et al., 1997) (in Khatib, 2009). On the other hand, Wong (1995) states that culms take 2 to 6 years to mature which depends on the species. According to Limaye, (1952) (in FRIM, 1995), young bamboo with higher moisture content shows greater increase in strength on drying than the older culms.

Abang Ali (1984) presented a comparison between bamboo and the more common engineering materials, as tabulated in Table 2.4. It was found that bamboo is very strong in tension, with a few species having tensile strength as high as that for mild steel. The ratio of tensile to compressive strength of bamboo can be as high as seven times. FRIM (1995) has conducted an experiment on selected Malaysian bamboo to evaluate the mechanical properties of bamboo, as shown in Table 2.5. The bending stress at proportional limit was ranged from 21 MPa to 49 MPa and it shows the differences in static bending strengths of specimens (Table 2.5). For the three species of Indonesian bamboos (*Gibantochloa Apus*, *Gigantochloa verticillata* and *Dendrocalamus asper*) where the age of bamboo was more than three years were tested to assess its mechanical properties and Table 2.6 shows the test results (Siopongco and Munandar, 1987). It can be seen that bamboo has more strength in tension compared to bending strength. According to Ghavami (2005), the tensile strength of bamboo is relatively high and can reach 370 MPa. This makes bamboo an attractive alternative to steel in tensile loading applications.

Table 2.4: Typical Material Properties of Bamboo Compared to Mild Steel, Concrete and Timber (Abang Ali, 1984)

Material	Ultimate strength (N/mm^2)		Tensile-Compressive Strength Ratio, σ_t / σ_c	Modulus of Elasticity (kN/mm^2)
	Tension, σ_t	Compression, σ_c		
Mild Steel	480	-	1.0	210
Concrete	2 - 4	25 – 55	0.1	10 – 17
Timber	20 - 110	50 - 100	1.1	8 – 13
Bamboo	180 - 440	38 - 65	4.8 – 7.1	7 - 20

Table 2.5: Strengths of some Malaysian Bamboos (FRIM, 1995)

Species	Compression Parallel to Grain (MPa)	Static Bending		
		Modulus of Rupture (MPa)	Modulus of Elasticity (MPa)	Stress at Proportional Limit (MPa)
Buluh Duri	19.5 – 28.5	43.1 – 156.4	2.6 – 5.6	21.2 – 38.9
Buluh Minyak	20.5 – 30.0	46.1 – 78.4	4.1 – 8.1	28.7 – 42.6
Buluh Betong	28.3 – 34.6	48.9 – 122.4	3.8 – 8.8	32.2 – 46.8
Buluh Semantan	21.6 – 32.3	35.9 – 68.9	3.7 – 5.9	31.1 – 42.2
Buluh Beting	37.3 – 42.8	37.6 – 119.4	3.7 – 6.5	35.7 – 48.7

Table 2.6: Mechanical Properties of Indonesian Bamboos (Gigantochloa apus, Gigantochloa verticillata and Dendrocalamus asper) (Siopongco and Munandar, 1987)

Properties	Range
Tensile strength	118 – 275 MPa
Bending strength	78.5 – 196 MPa
Compressive strength	49.9 – 58.8 MPa
Modulus of elasticity in tension	8.73 – 31.38 GPa
Modulus of elasticity in bending	5.59 – 21.18 GPa
Tensile strain	3.7 – 24.4 kPa

2.5.3 Weakness of Bamboo

Although the bamboo shows a lot of potential in various applications, it is unfortunate that bamboo has a weakness towards pathological attacks. According to Krause and Ghavami (2009), bamboo is easy to be influenced by insect and fungi attack, the degradation of lignin when exposed to UV rays, low shear resistance and has geometric problems since it is a natural material. Once cracking occurs on bamboo, when the compression load is applied, it is highly susceptible to premature flexural compression failure. It is generally seen that bamboo culms crack along their longitudinal fibres due to ambient temperature and humidity.

2.6 The Potential of BGC System

Bamboo-geotextile composite (BGC) system is one of the inventions in using natural materials to solve civil engineering problems. Issues related to the use of bamboo as green materials have been addressed by Irsyam & et al. (2008) and Khatib, A. (2009). It was found that bamboo grids can distribute embankment load uniformly and also it can alter the critical failure surface, besides able to provide upward buoyancy pressure. The use of bamboo has also been experienced by Loke (2000) in which

they claim that it could give saving of up to 45% - 65% compared with using geotextile alone and other conventional methods.

Khatib (2009) studied the bearing capacity of bamboo-geotextile composite with the bamboo laid in parallel and square pattern as shown in Figure 2.10. It was reported that the use of BGC as reinforcement system tend to spread load further so as the stress transferred to the directly underlain soft clay will be much smaller than using geotextile alone or bamboo grid alone. When bamboo is laid in a square grid configuration, they form an interlocking pattern that creates an increase in stiffness of bamboo, which distributes vertical pressure evenly and aims to minimize differential and total settlements. Its central portion supports the embankment against downwards displacement by mobilizing tensile resistance of horizontal ribs and compressive resistance of vertical ribs of bamboo that could prevent a catastrophic failure. For the geotextile, it does not function only as a separator and filter between the backfill material and soft clay layer; it also acts locally as a “tension membrane” between the bamboo interlocks, thereby reducing localised stress in the soft foundation clay.

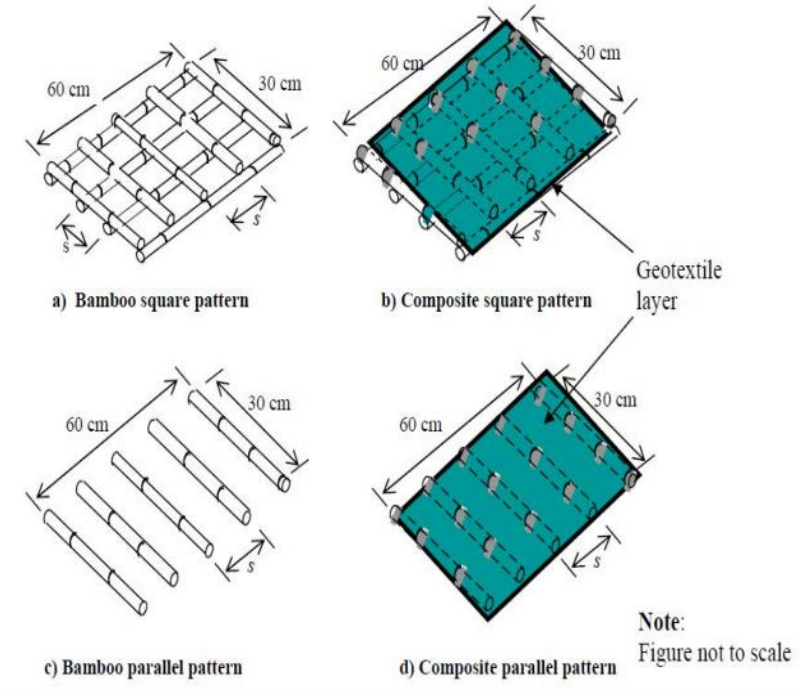

Figure 2.11: Bamboo and Bamboo-Geotextile Composite Reinforcement Model (Khatib, 2009)

According to research done by Marto A. and partners, comparison on the performance of the reinforcement system for Bamboo-Geotextile Composite (BGC) reinforced embankment, High-Strength Geotextile (HSG) reinforced embankment and controlled or unreinforced (UR) embankment were made. (Marto et al., 2010) It was found that by using 2D analysis, the vertical deformation for HSG and UR embankments are the same while BGC embankment shows the lowest value of deformation as shown in Table 2.7. It was proven that bamboo reinforcement had improved the performance of the embankment by reducing probable settlement and increasing the stability of the embankment. These are due to facts that bamboo has both bending and tensile strength, compared to geotextile which only has tensile strength.

Table 2.7: Vertical Deformation for all Embankments (Marto et al., 2010)

	Vertical deformation (mm)			
Embankment	**Phase 1**	**Phase 2**	**Phase 3**	**Phase 4**
HSG	9.83	22.42	32.86	67.92
BGC	9.49	21.38	30.42	63.93
UR	9.83	22.42	32.86	67.92

In another study, trial embankments of the above 3 types constructed on soft clay were monitored for 419 days after start of construction and actual deformation data were taken. (Marto and Othman, 2011) The results are shown in Figures 2.12 and 2.13. The highest settlement occurred at UR embankment, followed by HSG embankment and BGC embankment. For BGC system, it implicates that the bamboo square pattern takes the load from the backfill material and hence, reduced the settlement much better compared to others. On the other hands, the square pattern of bamboo formed an interlock to resist horizontal shear stress and increase the stiffness of bamboo, hence distributing vertical pressure evenly. As a result, low lateral movement was observed. Another contributing factor was due to the hollow section nature of the bamboo. The trapped air inside bamboo gave the buoyancy effect and therefore distribute small embankment load to the soft clay layer.

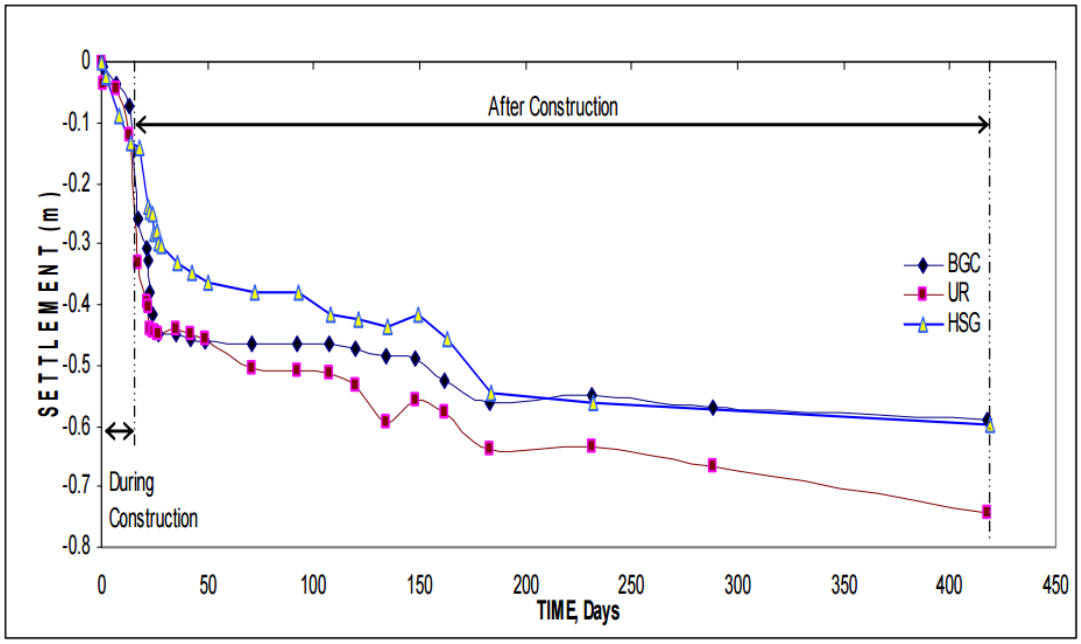

Figure 2.12: Settlement across base of Embankment versus Time (Marto et al., 2010)

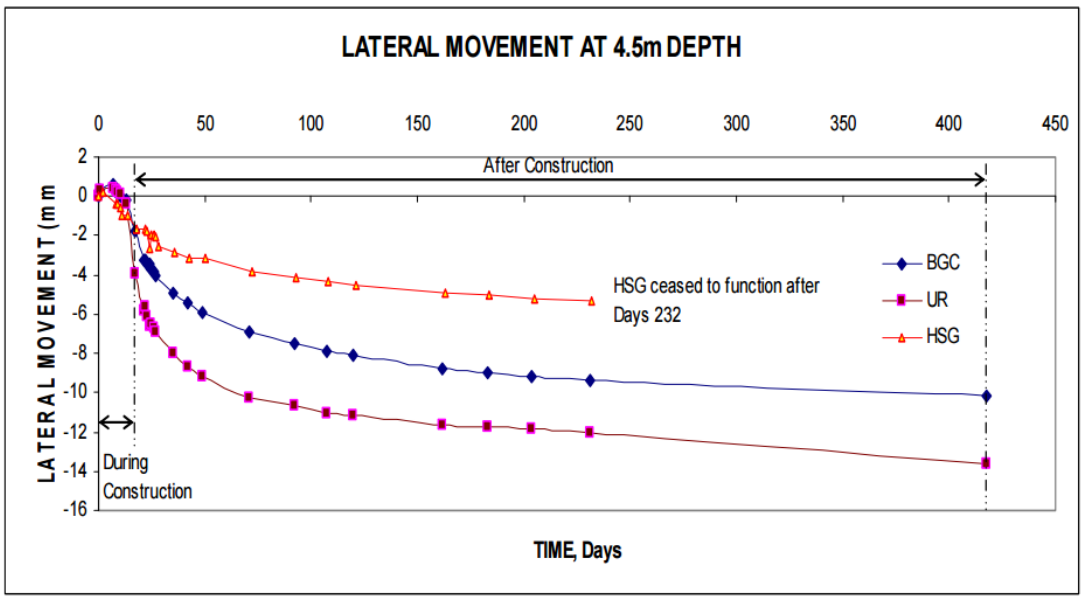

Figure 2.13: Lateral Movement of Embankment at 4.5m depth (Marto et al., 2010)

2.7 Soil-Structure Interaction Theories

The classical Winkler model has been used in many engineering fields. The model originated from “Winkler’s hypothesis”, which stated that the deflection at any point on the surface of an elastic continuum is proportional to the load being applied to any other points on the surface (Winkler, 1867). The vertical deformation characteristics of the foundation are defined by means of identical, independent, closely space, discrete and linearly elastic springs, where the constant of proportionality, *k’* of these springs is known as the modulus of subgrade reaction, k_o.

$$p = k'y \tag{2.5}$$

The Winkler model is very simple but does not accurately represent the characteristics of many practical foundations although it has been widely adopted by practitioners due to its simplicity. One of the most important deficiencies of the Winkler model is that displacement discontinuity appears between the loaded and unloaded part of the foundation surface. In reality, the soil surface does not show any discontinuity as shown in Figure 2.14.

Figure 2.14: Deflections of elastic foundation under uniform pressure: (a) Winkler foundation, (b) practical soil foundation

The physical properties of soils are obviously of a much more complicated nature than that which could be accurately represented by such a simple mathematical relationship as in Equation 2.5 assumed by Winkler. There are however, some important points which can be brought up in supporting the application of this theory to soil foundations. The most debatable part of Winkler’s assumption is that the foundation deforms only along the portion directly under loading, has since August Föppl’s classical experiment, often been found to be true

for a large variety of soil (A. Föppl, 1922). If we take these things into consideration, there is reason to believe that the Winkler theory, in spite of its simplicity, may more accurately represent the actual conditions existing in soil foundations that do some of the more complicated analyses advanced in recent years (Hetenyi, 1946).

Application of Winkler's model involves the solution of a fourth order differential equation which is as follows:

$$EI\frac{d^4y}{dx^2} = -k_oBy + q(x) \tag{2.6}$$

Where
EI = the flexural rigidity of the beam
$k_oB = k$ = the coefficient of subgrade reaction, and
$q(x)$ = the uniformly distributed load on the beam

Derivation of solutions for Equation 2.6 proves to be a difficult task as different loading conditions demand different solutions and the process of solving such equation is long and tedious. Fortunately, the equation has been solved by Hetenyi and solutions of several cases have been reported in his paper (Hetenyi, 1946). Application of Winkler's model has been made easier for practitioners by the discovery in this paper and it has since become a stepping stone for the development of many beams on elastic foundation theories majorly based on the improvement of Winkler's model.

In order to overcome the shortcomings of Winkler's model, a number of researchers have proposed improved or refined models (Filonenko-Borodich, 1940; Pasternak, 1954; Reissner, 1958; Vlasov *et al*., 1960; Kerr, 1964; and Loof, 1965). These are often called two-parameter models because in addition to the first parameter, the modulus of subgrade reaction, they have a second parameter that shows the continuity of adjacent displacements.

2.8 Determination of Coefficient of Subgrade Reaction, *k*

Because of the complexity of soil behaviour, subgrade in soil-structure interaction problems is replaced by a much simpler system called subgrade model. One of the most common models is the Winkler hypothesis. Implementation of this theory has since open eyes for engineers around the world in effort of finding new and innovative ways in solving soil-structure interaction problems.

In additional to the difficulties involved in the solution of general equations of Winkler's model and other improved models, beams on elastic foundation have not been the preferred method by practicing engineers due to the difficulty in determining the value of coefficient of subgrade reaction, *k*. However, Terzaghi (1955) has showed that the coefficient of subgrade reaction depends on the dimensions of the area acted upon by the subgrade reaction, and he incorporated size effects in his equations.

Evaluation of the numerical values of *k* is one of the most complex and sophisticated problems in geotechnical engineering. Even time and widespread use of k_o have not eliminated long-standing disagreement on the determination methods. In general, the methods of determination of k_o can be classified as:

1. Plate load test (Dutta and Roy, 2002; Bowles, 1998)
2. Consolidation test (Dutta and Roy, 2002; Bowles, 1998)
3. Triaxial test (Dutta and Roy, 2002)
4. CBR test (Nascimento and Simoes, 1957)
5. Empirical and theoretical relations proposed by researchers (Bowles, 1998; Elaschachi *et al.*, 2004)

Among these methods, approach 1 and 5 are more widely adopted than the others. Various relations of *k* have been proposed by researchers and some of them are presented in Table 2.8; wherein, E_s = modulus of elasticity of soil, v_s = Poisson's ratio of soil, B = width of footing, EI = flexural rigidity of footing, k_{s1} = the coefficient of subgrade reaction for a plate 1 ft wide and μ = non-dimensional soil mass per unit length.

Table 2.8: Common relations suggested for *k*

No.	Investigator	Suggested expression	
1	Biot	$k = \frac{0.95E_S}{B(1-\nu_S{}^2)}\left[\frac{B^4E_S}{(1-\nu_S{}^2)EI}\right]^{0.108}$	(2.7)
2	Terzaghi	$For\ sands, k = k_{s1}(\frac{B+1}{2B})^2$	(2.8)
		$For\ clays, k = k_{s1}\frac{1}{B}$	(2.9)
3	Vlassov	$k = \frac{E_S(1-\nu_S)}{(1+\nu_S)(1-2\nu_S)}(\frac{\mu}{2B})$	(2.10)
4	Vesic	$k = \frac{0.65E_S}{B(1-\nu_S{}^2)}\sqrt[12]{\frac{E_SB^4}{EI}}$	(2.11)
5	Meyerof and Baike	$k = \frac{E_S}{B(1-\nu_S{}^2)}$	(2.12)
6	Klopple and Glock	$k = \frac{2E_S}{B(1+\nu_S)}$	(2.13)
7	Selvadurai	$k = \frac{0.65}{B}\frac{E_S}{1-\nu_S{}^2}$	(2.14)

The following are some typical values of modulus of subgrade reaction, k_o for different types of soils (Subramanian, 2008).

Table 2.9: Typical values of modulus of subgrade reaction, k_o for different types of soils (Subramanian, 2008)

Type of soil	**k_o (kN/m^3)**
Loose sand	3800 - 16000
Medium dense sand	9600 – 80000
Dense sand	64000 – 128000
Clayey medium dense sand	32000 – 80000
Silty medium dense sand	24000 – 48000
Clayey soil:	
$q_u \leq 200\ N/mm^2$	12000 – 24000
$200 < q_u \leq 400\ N/mm^2$	24000 – 48000
$q_u > 800\ N/mm^2$	> 48000

Note: q_u = Safe bearing capacity

CHAPTER 3

METHODOLOGY

3.1 Introduction

The methodology adopted in this research can be divided into 2 parts where the first part is of laboratory investigation nature (data collection for bamboo-geotextile composite (a.k.a. BGC) system in air) and another one is the theoretical investigation and development of formulation from the results collected. The aim for carrying out these is to develop a reliable prediction tool for the behaviour of BGC system when under simulated embankment loading.

Therefore, it is pertinent to first understand the deflection behaviour of bamboo-geotextile system under uniformly distributed loading (UDL) in air to simulate soft ground at its extreme condition as if there is no soil underneath to support the BGC system, in effort of producing a viable prediction model to portray the viability and reliability of the BGC system. The reason UDL case is chosen for this study is that it closely depicts the application of load on BGC system in practical cases such as embankment over soft ground.

3.2 Fabrication of Steel Frame

A framing system is needed to study the behaviour of the BGC system in air. The steel frame was recycled and reused from the past predecessor’s project of similar

title under Ir. Dr. Low Kaw Sai as well. The previously fabricated steel frame was made using steel angle slotted bars and it was disassembled at its storing location in the previous campus at Setapak before it was transported to the new campus at Sungai Long. The disassembled parts were assembled using pliers and spanners.

In the process of assembling the steel frame, a magnetic level indicator (as shown in Figure 3.1) was used to make sure that the frame fabricated is levelled to the ground, which itself has to be levelled too. This is very important so that the behaviour of the BGC system under UDL can be observed accurately. The dimension of the fabricated steel frame is 1400 mm length x 800 mm height x 700 mm width.

Figure 3.1: Magnetic level indicator

3.3 Fabrication of Bamboo-Geotextile Composite (BGC) Model

The first step to the modelling the BGC system is to prepare materials. The materials required are simply bamboo, geotextile and steel wires. The bamboos used were supplied by the supervisor, Ir. Dr Low Kaw Sai and its species is unknown. Bamboo culms were cut into splints using axe and shaped into desired width using a vertical band saw. Then, the bamboo splints were tied up in a criss-cross manner (grid-like orientation) using steel wires.

The dimension of the bamboo grid as a whole is 1400 mm x 600 mm, comprises of bamboo splints of average 6 mm thickness and 40 mm width with average c/c spacing of 120 mm (longitudinal) and 100 mm (transverse), with short edges fixed onto the fabricated steel frame using steel wires, to simulate a simply supported system as shown in Figure 3.2. A layer of nonwoven geotextile of unknown specification was lay on top of the bamboo grid to act as a separator between the simulated UDL (dry sand) and the bamboo grid as shown in Figure 3.3.

Figure 3.2: Bamboo grid simply supported on steel frame

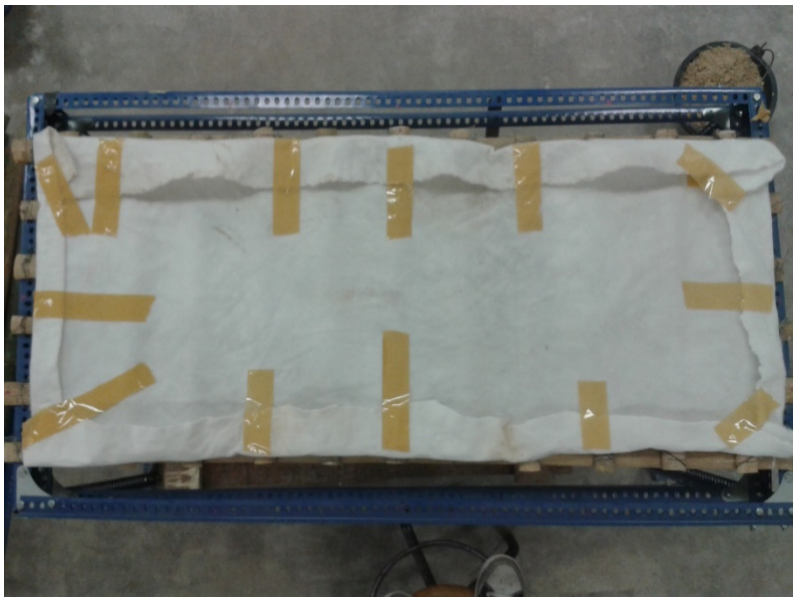

Figure 3.3: Nonwoven geotextile lay over bamboo grid (BGC system)

In Figure 3.3, it can be seen that the nonwoven geotextile was cut into a bigger piece than the area of the bamboo grid and folded at the edges and fixed using tape. This was done purposely to prevent dry sand (simulated UDL) from spilling out from the BGC model as the extra geotextile area provided acts as a wall-like barrier that contains the dry sand within the BGC model. It was later realized that the tape was redundant in the model as the nonwoven geotextile holds the dry sand quite well without it so it was removed in the middle of the experiment.

3.4 Apparatus Set-Up

Deflection of the BGC model under UDL were measured by using dial gauges and rulers set up at 9 different points of the BGC model. The rulers are included as a counter-check for the readings of dial gauges. The locations of points taken are shown in Figure 3.4. The results were then compared with theoretical results.

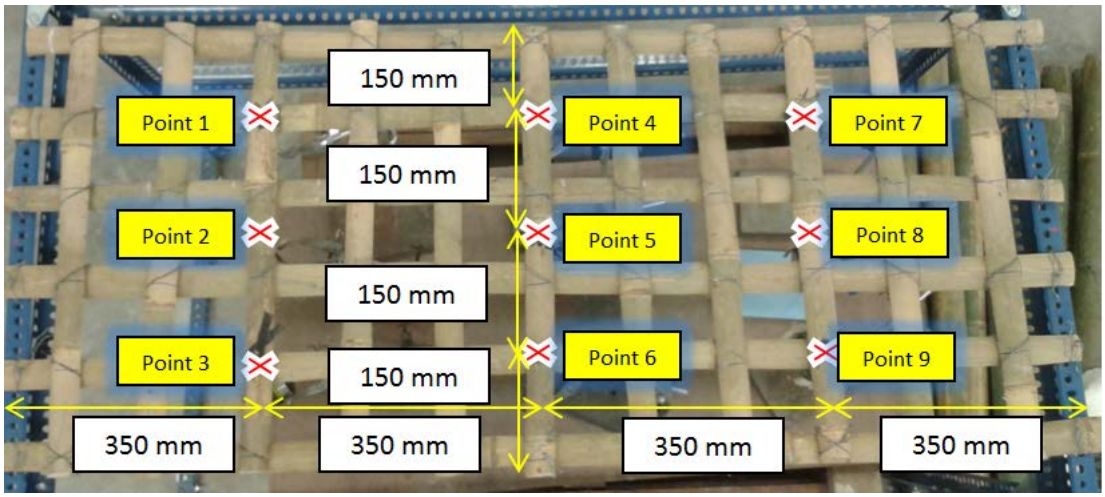

Figure 3.4: Locations of deflection measured

Dial gauges are set up under the BGC model using retort stands and clamps borrowed from the chemistry laboratory. A total of 9 retort stands and clamps were used to hold each dial gauge at their respective points as shown in Figure 3.5.

Figure 3.5: Set-up of dial gauges using retort stands and clamps

It was realized that the retort stands were too short for the steel frame fabricated as the dial gauges could not reach the BGC model if the stands are stood on floor level. So a mini platform of about 200 mm height was proposed to compensate the height difference of retort stands to the desired height so that the dial gauges held are able to make contact with the BGC model. The mini platform was put up together by using some unused wood pieces in the laboratory as shown in Figure 3.6.

Figure 3.6: Mini platform made up of wooden pieces

As for the ruler readings, many efforts have been done to find a suitable way of measuring the deflection at 9 points accurately. It was found that pointers made up of either steel wires or nylon string used for outdoor clothesline is unsatisfactory because they are too stiff in texture and would not free hang naturally, which would affect the results. Eventually, it was decided to use sewing thread and needle tied to the bamboo grid because sewing thread is able to free hang naturally. The needle acts as a pointer to the ruler that is taped to a wooden piece and stood up vertically with ruler pointed perpendicular to the floor, as shown in Figure 3.7. The only downside of using threads is that it will swing with the slightest wind movement so it was made sure that the doors were shut and fans were turned off when deflection readings were being taken.

Figure 3.7: Set-up of rulers

3.5 Experimental Procedure

With all the apparatus, steel frame and BGC model in place, a simulated UDL using dry sand can be applied over the BGC model. Dry sand was prepared by oven-drying it over the night. The reason dry sand is used instead of wet sand is that evaporation of water from wet sand will affect the accuracy of UDL applied, although such evaporation is negligible in short run testing. Successive loading of 5 kg of dry sand was evenly distributed over the geotextile of area 600 mm x 1400 mm = 840000 mm^2.

In order to ensure that the dry sand is spread out evenly over the BGC model, the geotextile surface was divided into 5 equal areas, where each area takes 1 kg of sand spread over it as evenly as possible. So for each successive loading of 5 kg sand, this procedure was repeated to minimize the uneven distribution of loading across the surface. This is simply illustrated in Figure 3.8. Of course, needlessly to say that the dry sand was first weighed using a weighing machine as shown in Figure 3.9.

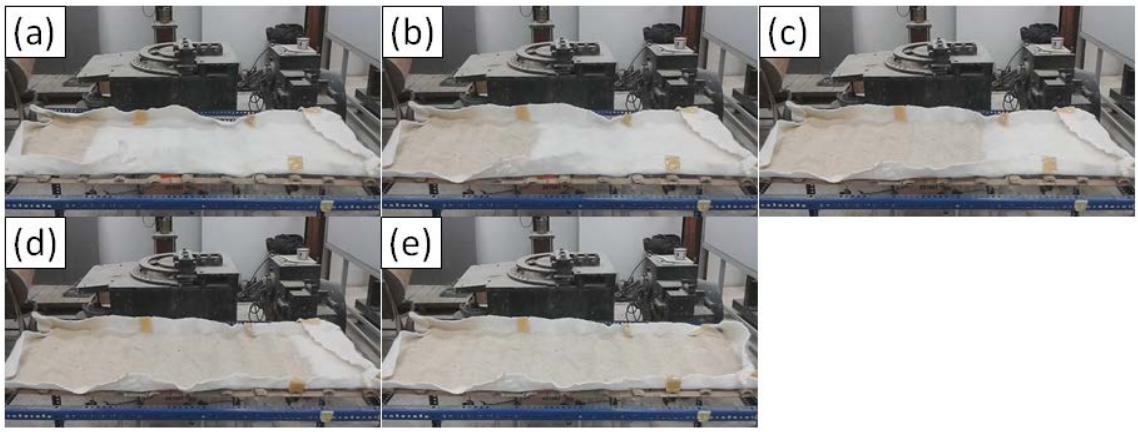

Figure 3.8: Procedure used for distribution of dry sand (a) 1 kg (b) 2kg (c) 3 kg (d) 4 kg (e) 5 kg

Figure 3.9: Weighing of dry sand using a weighing machine

Before the commencement of the experiment, the initial readings were recorded from the dial gauges and rulers. After every successive placing of 5 kg dry sand, dial gauge and ruler readings were recorded again from the 9 designated points as shown in Figure 3.4 previously. This is done until 20 kg of dry sand has been distributed evenly on top of the BCG model. Then the whole process was repeated for another 9 times so that there are 10 sets of observed results.

The dial gauges used are of 25 mm and 10 mm types so there was a flaw when measuring deflection more than the device's limit. These dial gauges had to be reset every 5 kg for the 10 mm ones and every 10 kg for the 25 mm ones by moving the dial gauges down the retort stand to compromise with further deflection, although this may cause some minor error in the results obtained. Another flaw of this set up using retort stands to hold the dial gauges is that there is a limit to which the deflection can be measured as the retort stands will start making contact with the BCG model on top when loaded with 25 kg as shown in Figure 3.10. Lowering the mini platform may seem like a sound idea but it was not practical to do so, which is why readings up to only 20 kg were taken.

3.6 Theoretical Development Based on Observed Results

3.6.1 Euler-Bernoulli Beam Theory

The BGC model built here is similar to a simply supported beam under UDL, so as starter, Euler-Bernoulli beam theory a.k.a. classical beam theory was adopted as the first step in developing a theoretical model. This theory is actually a simplification of the linear theory of elasticity which provides a means of calculating load-carrying and deflection characteristics of beams. The out-of-plane displacement, y of a beam is governed by the Euler-Bernoulli beam equation:

$$\frac{d^2}{dx^2}\left[EI\frac{d^2y}{dx^2}\right] = q(x) \tag{3.1}$$

Where
q(x) = Distributed load along the beam (force per unit length);
E = Young's modulus of the beam
I = Moment of inertia of the beam's cross-section

If *E* and *I* do not vary with x along the length of the beam, then the beam equation simplifies to:

$$\left[EI\frac{d^4y}{dx^4}\right] = q(x) \tag{3.2}$$

Equation 3.2 is the most common equation used to develop beam equations of different cases of loading conditions in most structural analysis references. It should be noted that in the BGC model, *I* value varies along the length of the beam as it is made up of grid-like orientation. It was first assumed that our BGC model has a constant *I* value along the whole span so that Equation 3.2 stands valid and the equations developed from it can be applied.

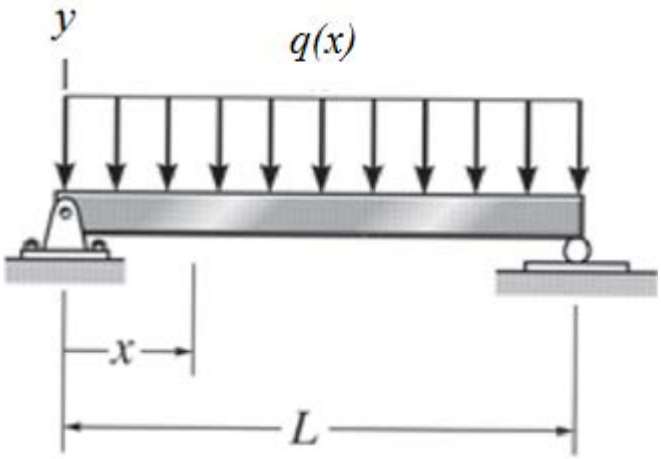

Figure 3.10: Simply supported beam under UDL

Figure 3.10 depicts the case where a simply supported beam is experiencing uniformly distributed loading (UDL). The beam deflection equation for this type of loading condition is as follows (assuming downward y direction to be positive):

$$y = \frac{qx}{24EI}(x^3 - 2Lx^2 + L^3) \tag{3.3}$$

The deflection at its maximum occurs at x = L/2, so Equation 3.3 can be simplified into:

$$y_{max} = \frac{5qL^4}{384EI} \; at \; x = \frac{L}{2} \tag{3.4}$$

Equations 3.3 and 3.4 will be the main equations used to be compared with the observed deflection values of BGC model when loaded with UDL of 5 kg, 10 kg, 15 kg and 20 kg.

It should be noted that *E* and *I* are the only two parameters that cannot be determined directly from the set-up of the experiment. *E* value of the bamboo is unknown and *I* value cannot be calculated directly from the cross-sections as it varies along the length of beam as explained above. Simply speaking, there are two different cross-sections that can be found along BGC model due to the grid orientation of the bamboo. These two parameters will be determined indirectly

through mathematical analysis using the Euler-Bernoulli equations and the observed results. This analysis will be further discussed in details in the following chapter.

Theoretically speaking, the overall *E* value of the BGC system would be the same as if the splints were tested individually, provided that they were made up of the same homogeneous material, but it was not the case because bamboo is a natural material where the *E* value varies slightly across the culm of bamboo due to the anatomical structure of bamboo (presence of nodes and internodes). Therefore, in the BGC system, the *E* value of the system is not the same as the individual *E* value tested in the laboratory.

3.6.2 Soil-Structure Interaction Theories

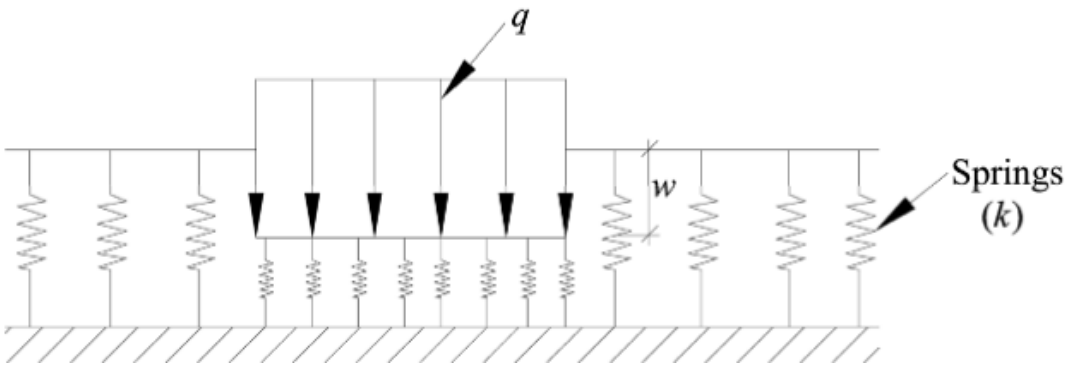

Figure 3.11: Winkler model

The Winkler model (Winkler, 1987), as shown in Figure 3.11 is the pioneer model theory in explaining soil-structure interaction where it was first developed to be used in analysing the deflection and resultant stresses of railroad tracks. The Winkler model is actually originated from “Winkler’s hypothesis” which states that the deflection, *y* at any point on the surface of an elastic continuum is proportional only to the load, *p* being applied to the surface and is independent of the load applied to any other point on the surface (Winkler, 1987).

This theory actually incorporates Hooke's law which is used to explain the behaviour of soil where a series of spring with proportionality constant, *k'* is used to represent the stiffness of the soil under the foundation, into the Euler-Bernoulli theory, which is the reason such soil-structure interaction theories are commonly known as beams on elastic foundation.

$$p = k'y \tag{3.5}$$

Equation 3.5 shows the basic Hooke's law equation or also known as the Winkler's hypothesis in this matter. The proportionality constant, *k'* [Force/Length] when used in beams on elastic foundation theories, is commonly known as the coefficient of subgrade reaction, *k* [Force/Length^2] or the modulus of subgrade reaction, k_o [Force/Length^3], where $k = k_oB$ (*B* is the width of the foundation).

By using Equation 3.2 as the basis (Euler-Bernoulli beam theory), another reaction force representing the soil behaviour by using Equation 3.5 (Hooke's law/Winkler's hypothesis), is added into so that the resultant equation becomes:

$$EI\frac{d^4y}{dx^2} = -k_oBy + q(x) \tag{3.6}$$

It can be noticed that the sign convention used for the applied load, *q(x)* is positive and the reaction force from the soil, k_oBy is negative, which are accurate. Equation 3.6 can be further simplified into a nonhomogeneous fourth order linear differential equation as follows (λ is the characteristic equation which includes the flexural rigidity of the beam as well as the elasticity of the foundation):

$$\frac{d^4y}{dx^4} + 4\lambda^4 y = \frac{q(x)}{EI} \tag{3.7}$$

Where

$$\lambda = \sqrt[4]{\frac{k_oB}{4EI}}$$

3.6.3 Hetenyi's Solutions to Winkler's Model

Solving Equation 3.7 (a 4th order nonhomogeneous linear differential equation) proves to be a tedious and daunting task and it becomes impractical to be applied in engineering practices without a readily-available solution. Fortunately, Hetenyi (1946) had solved this equation and provided the final solutions for several load conditions and various cases (detailed derivation for the solutions should be referred to Hetenyi (1946)). According to Hetenyi (1946), the deflection equation of a UDL over the whole span for a simply supported beam, as shown in Figure 3.12, which is the same as the case under investigation is as follows:

$$y = \frac{q}{k}\left(1 - \frac{\cosh \lambda x \cos \lambda x' + \cosh \lambda x' \cos \lambda x}{\cosh \lambda l + \cos \lambda l}\right) \tag{3.8}$$

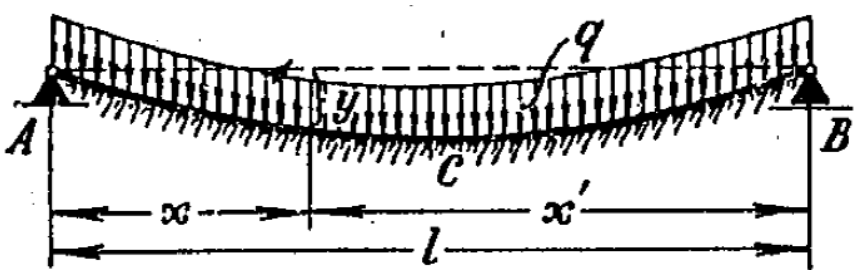

Figure 3.12: UDL over whole span

Equation 3.8 will also be used to compare with the observed results from the experiment by assuming that the coefficient of subgrade reaction, *k* to be very small, i.e. 0.00001 N/mm^2, as if the beam is supported by extremely soft clay (most critical condition).

A more sensible solution which is closer to reality where beam is rested on subgrade without being simply supported has also been proposed by Hetenyi (1946). It should be noted that this solution is for uniformly-distributed loading case on a finite beam. Figure 3.13 shows the diagram of such condition where parameters used in the solution equation are labelled clearly.

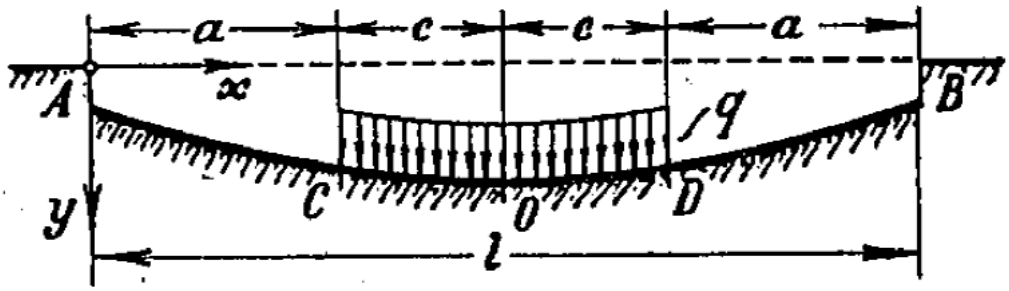

Figure 3.13: Beam rested on subgrade without support for symmetrically placed uniformly distributed loading (finite beam)

The solutions for Figure 3.13 are as follows:

- Deflection line for portion A-C ($x < a$):

$$y_{A-C} = \frac{q}{k}\frac{1}{\sinh \lambda l + \sin \lambda l}\{\cosh \lambda x \cos \lambda x\,[\cosh \lambda a \sin \lambda(l-a) - \sinh \lambda a \cos \lambda(l-a) + \cos \lambda a \sinh \lambda(l-a) - \sin \lambda a \cosh \lambda(l-a)] + (\cosh \lambda x \sin \lambda x + \sinh \lambda x \cos \lambda x)[\sin \lambda a \sinh \lambda(l-a) - \sinh \lambda a \sin \lambda(l-a)\}$$

(3.9)

With the aid of the formula above, the deflection line for the portion C-D can be expressed as:

$$y_{C-D} = [y_{A-C}]_{x>a} + \frac{q}{k}[1 - \cosh \lambda(x-a) \cos \lambda(x-a)] \quad (3.10)$$

- Deflection at the end points:

$$y_A = y_B = \frac{q}{k}\frac{1}{\sinh \lambda l + \sin \lambda l}[\cosh \lambda a \sin \lambda(l-a) - \sinh \lambda a \cos \lambda(l-a) + \cos \lambda a \sinh \lambda(l-a) - \sin \lambda a \cosh \lambda(l-a)]$$

(3.11)

- Deflection at the middle:

$$y_o = \frac{q}{k}[1 - \frac{2\left(\sinh \lambda a \cos \lambda c \cosh \frac{\lambda l}{2} + \sin \lambda a \cosh \lambda c \cos \frac{\lambda l}{2}\right)}{\sinh \lambda l + \sin \lambda l}] \quad (3.12)$$

The solution for UDL case for infinite beam was also derived by Hetenyi (1946). For an infinite beam, the effect of loading is assumed to be localized, meaning that in an infinite distance from the application of the load, the deflection of the beam must approach zero. This solution is useful if it we were to assume that the effect of loading is localized in the case of a long beam.

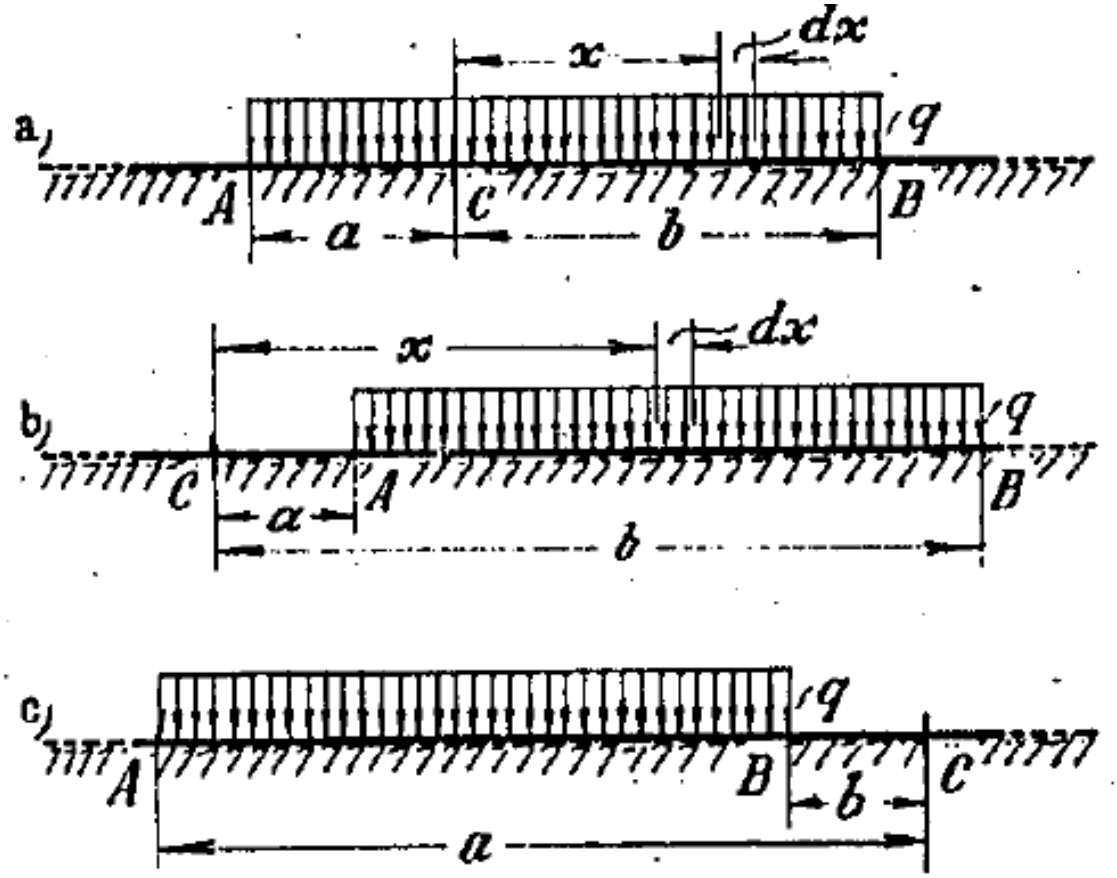

Figure 3.14: UDL on an infinitely long beam (a) When Point C is under the loading (b) When Point C is to the left of the loading (c) When Point C is to the right of the loading

The solutions for deflection profile for Figure 3.4 are as follows:

- When Point C is under the loading (Figure 3.14 (a))

$$y_c = \frac{q}{2k}[(1 - e^{-\lambda a}\cos\lambda a) + (1 - e^{-\lambda b}\cos\lambda b)] \quad (3.13)$$

- When Point C is to the left of the loading (Figure 3.14 (b))

$$y_c = \frac{q}{2k}[(e^{-\lambda a}\cos\lambda a) - (e^{-\lambda b}\cos\lambda b)] \quad (3.14)$$

- When Point C is to the right of the loading (Figure 3.14 (c))

$$y_c = -\frac{q}{2k}[(e^{-\lambda a}\cos\lambda a) - (e^{-\lambda b}\cos\lambda b)] \quad (3.15)$$

3.7 Determination of *I* values from the BGC model

For completeness of the investigation, the moment of inertia, *I* of the bamboo grid at the two cross-sections where one is with top layer of bamboo splints whereas the other one is without top layer of bamboo splints, were determined. It should be noted that *I* values obtained here do not represent *I* value of the overall BGC model. However, these *I* values can be compared with *I* value obtained from the mathematical analysis in Section 4.3 of the following chapter.

The first step would be to obtain the average width and thickness of all the bamboo splints using external callipers as shown in Figure 3.15. It should be assumed that the bamboo splints are of rectangular cross-section. 10 sets of readings were taken for both width and thickness for each bamboo splint so that average readings can be obtained to calculate *I*. The results are tabulated in Table 4.15 and 4.16.

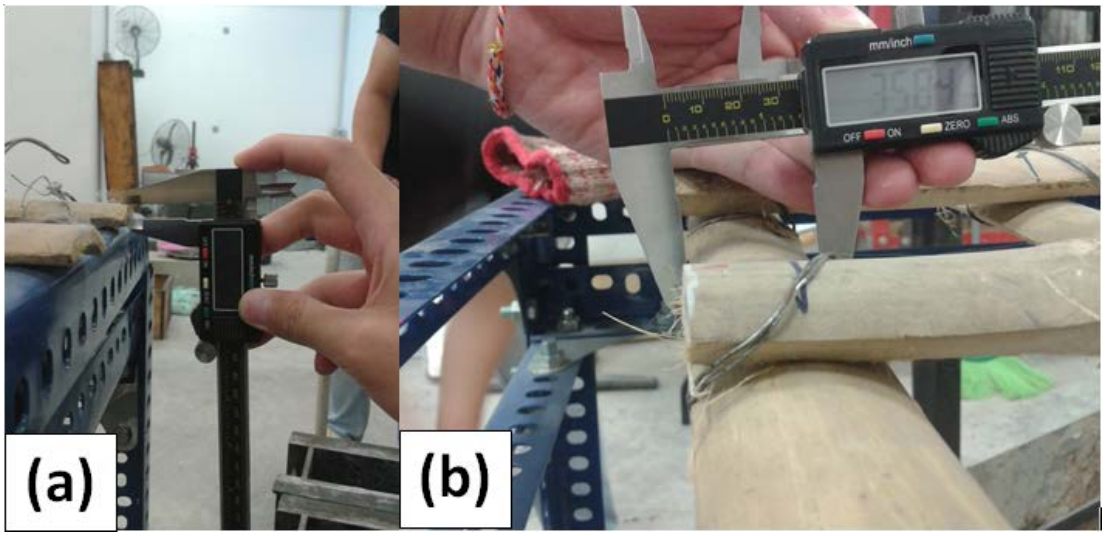

Figure 3.15: Measuring (a) thickness (b) width of bamboo splints

3.8 Set-up using 100 mm LVDT

In order to verify the average flexural rigidity value, EI obtained from the analysis based on the observed results in Section 3.5, for loadings over 20 kg, which was previously limited by the set-up of the dial gauges, another set-up using 100 mm Linear Variable Differential Transformer (LVDT), which is an alternative displacement-measuring method that will display displacement readings on a data logger, was prepared as shown in Figure 3.16. Since this set-up only serves for verification purpose, only one point was chosen to measure its deflection which is Point 5 as shown in Figure 3.4. The reason Point 5 was chosen is that this is usually the point of interest for an engineer as it would give the largest deflection value under UDL. The test was repeated 4 more times to obtain average results.

Figure 3.16: (a) Data logger (b) 100 mm LVDT

The calibration of 100 mm LVDT is presented as follows in Table 3.1 and Figure 3.17:

Table 3.1: Calibration data for 100 mm LVDT

Displayed reading, x	Actual displacement, y (mm)
-76.814	0
-68.157	4
-45.018	14
-23.926	24
0	34
22.037	44
43.444	54
67.527	64
89.721	74
111.916	84
133.638	94
157.091	104

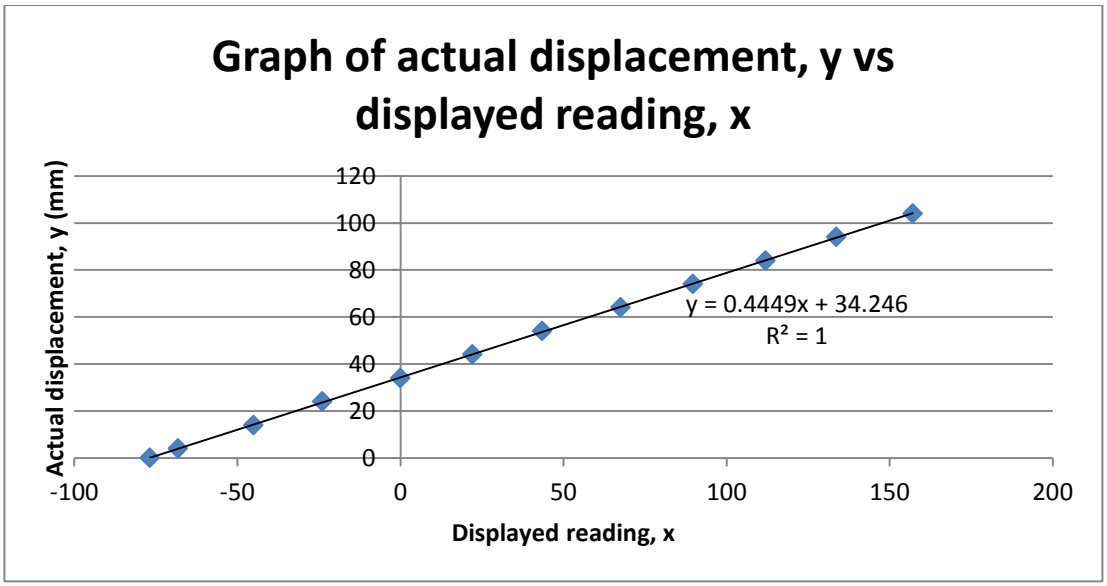

Figure 3.17: Calibration graph for 100 mm LVDT

3.9 Modification of the Steel Frame

It was realized that the steel frame initially assembled is imperfect as the deflection of the BGC model could not be observed clearly from the anterior view as shown in Figure 3.18. The frame was then modified when testing using LVDT which was tested up to 40 kg UDL deflection. The anterior top steel slotted bar was removed and the frame was supported by standing two steel bars at the sides, as shown in Figure 3.19. The modified steel frame clearly shows improvement for the observation of deflection of BGC model.

Figure 3.18: Steel frame before modification (loaded up to 20 kg of sand)

Figure 3.19: Steel frame after modification

CHAPTER 4

RESULTS AND DISCUSSION

4.1 Introduction

As it is described in Chapter 3 of this report, deflection data for successive uniformly distributed loading on the simply supported bamboo-geotextile composite has been recorded in this study. The relevant techniques employed in the data collection process are covered in the previous chapter as well.

As a recap, the deflection profile of the bamboo-geotextile composite (BGC) model was observed using two main instruments which are dial gauges and rulers. The dimension of the bamboo grid as a whole is 1400 mm x 600 mm, comprises of bamboos splints of average 6 mm thickness and 40 mm width with average c/c spacing of 120 mm, with the short ends fixed onto the fabricated steel frame to simulate a simply supported system as shown in Figure 4.1 below. Figure 4.2 indicates the 9 points measured across the bamboo-geotextile composite using dial gauges and rulers.

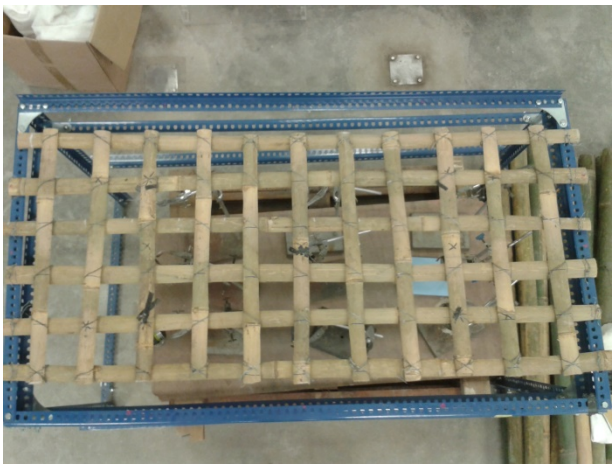

Figure 4.1: BGC model

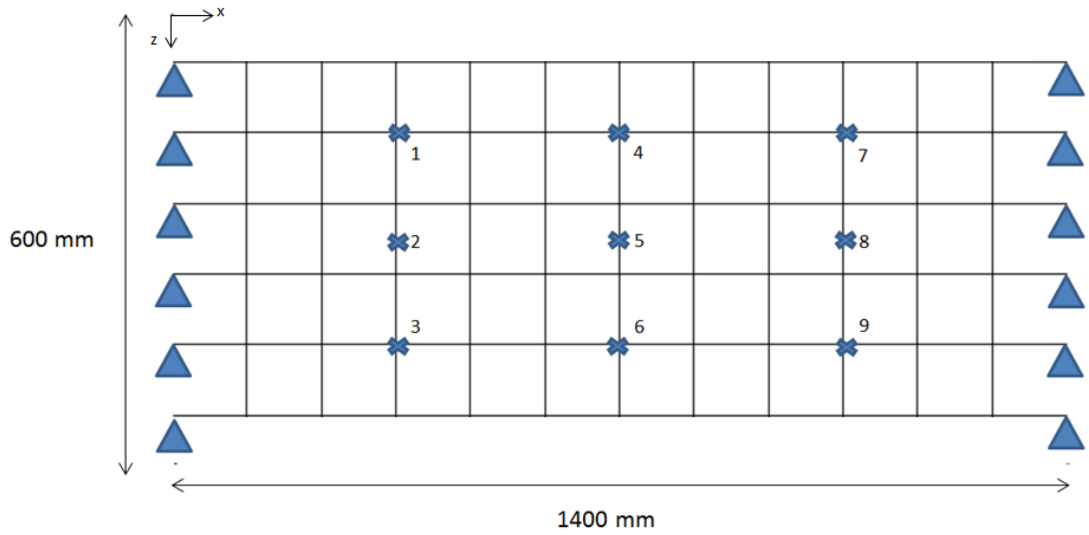

Figure 4.2: 9 points measured on BGC model

It is always the desire of a researcher that the experimental studies can be useful in real life through theoretical formulation or vice versa, so that both experimental and theoretical studies can ultimately be convincing and verified. The only reasonable way of doing this is by comparing the theoretical results of the problem defined which portray the predicted behavioural characteristics of the system under investigation with the actual experimental results observed in the laboratory or in the field. The observed experimental results should always be held as the true results for reference. The degree of discrepancy between the computed results and the experimental results would easily depict the reliability and accuracy of the theoretical model formulated.

Due to time constraints, no effort could be spared to arrange for an on-site field test program to study the behaviour of BGC model on actual soft clay. Efforts to study BGC model only went as far as understanding the properties of the beam itself, i.e. flexural rigidity of the beam, *EI* (an important characteristic parameter in every beams on elastic foundation theory) which represents the structure part of the soil-structure interaction model. In order to understand the deformation behaviour of soil under the BGC system, it is useful to carry out on-site prototype testing, along with obtaining real soil parametric data, i.e. modulus of subgrade reaction, k_o, Poisson's ratio of soil, v_s, modulus of elasticity of soil, E_s, etc., required in various beams on elastic foundation theories such as Pasternak model, Vlasov's model, etc. so that these data can be substituted into these models to obtain theoretical deformation behaviour of soil which can be compared with the observed results.

The following sections in this chapter will demonstrate the results obtained from the experimental testing of BGC model simply supported in air to simulate extremely soft ground condition and methods of analysis which are proposed and recommended for future researches in obtaining the overall *E* and *I* values of the BGC system indirectly from experimental procedure.

4.2 Deflection Results of BGC model

10 sets of deflection results of BGC model were obtained for 5 kg, 10 kg, 15 kg and 20 kg sand loading by using dial gauges and rulers for 9 appointed points as shown in Figure 4.2. The detailed results obtained are tabulated in Appendix A for dial gauges and Appendix B for rulers. The results taken by rulers merely serve as a counter-check device for the dial gauge readings and only dial gauges readings will be used in the analysis, since dial gauge readings are accurate up to 0.01 mm (analogue dial gauge) and 0.001 mm (digital dial gauge).

A total of 8 deflection profiles can be derived from the observed results, which are made up of combinations of points 1-4-7, 2-5-8, 3-6-9, 1-2-3, 4-5-6, 7-8-9,

1-5-9 and 3-5-7. These deflection profiles should be labelled as profiles I, II, III, IV, V, VI, VII and VIII respectively for convenience purpose, as shown in Figure 4.3.

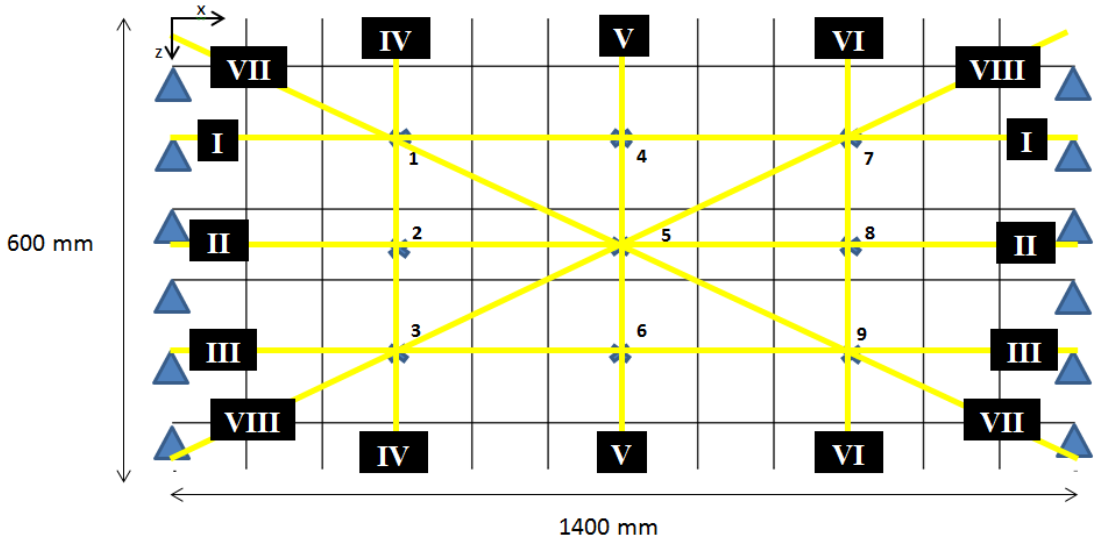

Figure 4.3: Assigned labels for different deflection profiles

4.2.1 Determination of Mean, Standard Deviation and Coefficient of Variation (CV)

Mean, standard deviation and coefficient of variation (CV) are several statistical techniques commonly used by engineers to ensure that the average of repetitive sets of results obtained are adequately consistent for the purpose of study or analysis. The formulas for mean, standard deviation of sample population and CV are as follows:

$$Mean, \bar{X} = \frac{\sum X}{N} \tag{4.1}$$

$$Standard\ Deviation, \sigma = \frac{\sum (X - \bar{X})}{N-1} \tag{4.2}$$

$$Coefficient\ of\ Variation\ (\%) = \frac{\sigma}{\bar{X}} \times 100\% \tag{4.3}$$

Table 4.1: Deflection results for Point 1 (Dial Gauge)

Sand load (kg)	UDL (N/mm)	Cumulative deflection (mm) Trials										Mean (mm)	Standard Deviation (mm)	Coefficient of Variation (%)
		1	2	3	4	5	6	7	8	9	10			
0	0	0	0	0	0	0	0	0	0	0	0	0	0	0
5	0.08175	0.71	6.87	7.02	6.3	5.59	5.85	5.87	5.24	5.82	5.87	6.893	0.527	7.64
10	0.1635	11.52	13.58	13.63	13.36	11.08	11.64	12.85	10.71	12.15	11.2	15.22	1.101	7.24
15	0.24525	14.18	16.01	19.76	17.82	19.78	17.66	15.52	12.91	17.85	15.45	20.87	2.343	11.23
20	0.327	15.36	16.97	24.89	19.5	25.16	23.7	16.51	14.59	19.55	17.72	24.24	3.983	16.43

Table 4.2: Deflection results for Point 2 (Dial Gauge)

Sand load (kg)	UDL (N/mm)	Cumulative deflection (mm) Trials										Mean (mm)	Standard Deviation (mm)	Coefficient of Variation (%)
		1	2	3	4	5	6	7	8	9	10			
0	0	0	0	0	0	0	0	0	0	0	0	0	0	0
5	0.08175	0.86	6.3	7.62	6.73	6.02	5.99	6.64	5.91	7.86	5.64	7.446	0.822	11.04
10	0.1635	10.87	13.65	13.55	13.86	12.8	13.86	14.05	14.52	14	13.05	16.78	0.560	3.334
15	0.24525	13.63	17.27	20.5	18.81	21.32	20.62	18.07	16.98	20.3	18.17	23.21	1.543	6.647
20	0.327	15.25	18.86	25.25	22.15	27.72	27.22	20.45	20.69	22.87	21.97	27.8	2.840	10.21

77

Table 4.3: Deflection results for Point 3 (Dial Gauge)

Sand load (kg)	UDL (N/mm)	Cumulative deflection (mm) Trials										Mean (mm)	Standard Deviation (mm)	Coefficient of Variation (%)
		1	2	3	4	5	6	7	8	9	10			
0	0	0	0	0	0	0	0	0	0	0	0	0	0	0
5	0.08175	5.46	7.972	8.192	8.077	6.964	6.068	7.304	7.785	6.566	6.518	8.863	0.785	8.852
10	0.1635	11.787	13.389	15.56	13.606	11.681	14.058	13.356	14.34	12.985	13.043	16.73	1.136	6.789
15	0.24525	13.486	17.885	20.347	19.19	18.702	20.624	18.375	17.936	19.991	18.904	23.18	0.968	4.175
20	0.327	13.487	22.299	25.517	24.454	24.619	27.247	21.723	21.536	22.829	22.937	28.33	1.965	6.936

Table 4.4: Deflection results for Point 4 (Dial Gauge)

Sand load (kg)	UDL (N/mm)	Cumulative deflection (mm) Trials										Mean (mm)	Standard Deviation (mm)	Coefficient of Variation (%)
		1	2	3	4	5	6	7	8	9	10			
0	0	0	0	0	0	0	0	0	0	0	0	0	0	0
5	0.08175	8.821	9.49	9.45	8.74	8.35	8.87	9.16	8.33	8.95	9.12	11.16	0.391	3.5
10	0.1635	16.324	18.5	18.53	18.67	17.38	19.31	19.04	18.46	17.87	18.92	22.88	0.633	2.77
15	0.24525	18.988	22.24	25.81	23.37	27.53	29.26	22.67	19.8	24.75	27.57	30.25	3.092	10.22
20	0.327	19.67	22.75	32.59	24.05	36.8	38.29	24.74	21.2	26.5	30.12	34.59	6.215	17.97

78

Table 4.5: Deflection results for Point 5 (Dial Gauge)

Sand load (kg)	UDL (N/mm)	Cumulative deflection (mm)										Mean (mm)	Standard Deviation (mm)	Coefficient of Variation (%)
		Trials												
		1	2	3	4	5	6	7	8	9	10			
0	0	0	0	0	0	0	0	0	0	0	0	0	0	0
5	0.08175	0.83	9.787	10.187	9.579	9.431	9.799	9.889	9.842	11.445	9.236	11.25	0.681	6.05
10	0.1635	17.48	18.836	20.181	19.705	17.274	19.695	20.681	19.288	19.724	18.981	23.98	1.016	4.24
15	0.24525	19.22	23.355	24.786	24.051	27.626	28.815	25.875	22.806	28.763	27.015	31.54	2.215	7.02
20	0.327	22.68	26.281	31.341	27.576	37.085	38.156	28.586	25.93	32.538	30.862	37.63	4.341	11.54

Table 4.6: Deflection results for Point 6 (Dial Gauge)

Sand load (kg)	UDL (N/mm)	Cumulative deflection (mm)										Mean (mm)	Standard Deviation (mm)	Coefficient of Variation (%)
		Trials												
		1	2	3	4	5	6	7	8	9	10			
0	0	0	0	0	0	0	0	0	0	0	0	0	0	0
5	0.08175	7.849	10.637	10.787	10.338	10.263	11.131	10.542	10.473	10.508	9.528	12.76	0.461	3.61
10	0.1635	14.161	19.569	21.315	20.512	16.241	21.393	22.136	20.127	20.367	19.89	24.46	1.785	7.30
15	0.24525	17.058	26.464	27.217	28.109	25.692	30.641	28.875	25.341	30.484	28.406	33.54	1.965	5.86
20	0.327	17.06	32.507	33.726	35.438	35.056	40.347	33.653	30.807	35.267	34.328	41.02	2.675	6.52

Table 4.7: Deflection results for Point 7 (Dial Gauge)

Sand load (kg)	UDL (N/mm)	Cumulative deflection (mm) Trials										Mean (mm)	Standard Deviation (mm)	Coefficient of Variation (%)
		1	2	3	4	5	6	7	8	9	10			
0	0	0	0	0	0	0	0	0	0	0	0	0	0	0
5	0.08175	0.16	5.49	6.38	5.46	5.05	6.18	6.02	6.17	6.72	6.98	6.826	0.628	9.21
10	0.1635	7.89	10.92	12.23	11.85	11.28	13.64	12.24	17.39	18.05	13	16.06	2.580	16.06
15	0.24525	9.25	12.81	16.94	15.6	17.618	20.09	14.64	19.13	23.55	17.56	20.9	2.798	13.39
20	0.327	14.56	20.89	20.94	20.58	24.068	26.21	16.74	27.27	27.28	18.12	27.08	4.143	15.3

Table 4.8: Deflection results for Point 8 (Dial Gauge)

Sand load (kg)	UDL (N/mm)	Cumulative deflection (mm) Trials										Mean (mm)	Standard Deviation (mm)	Coefficient of Variation (%)
		1	2	3	4	5	6	7	8	9	10			
0	0	0	0	0	0	0	0	0	0	0	0	0	0	0
5	0.08175	0.89	5.49	7.2	5.89	6.79	6.89	7.04	6.18	7.63	5.8	7.475	0.655	8.768
10	0.1635	1.85	11.74	13.61	11.56	11.9	14.33	13.76	12.71	13.65	12.15	14.66	1.015	6.928
15	0.24525	12.15	15.55	17.93	15.78	19.3	20.71	17.42	16.37	19.85	18.1	21.65	1.696	7.834
20	0.327	12.26	19.56	22.35	18.42	25.52	27.03	19.24	19.12	23.35	21.24	26.01	3.138	12.06

80

Table 4.9: Deflection results for Point 9 (Dial Gauge)

Sand load (kg)	UDL (N/mm)	Cumulative deflection (mm)										Mean (mm)	Standard Deviation (mm)	Coefficient of Variation (%)
		Trials												
		1	2	3	4	5	6	7	8	9	10			
0	0	0	0	0	0	0	0	0	0	0	0	0	0	0
5	0.08175	6.003	7.161	7.231	7.011	6.36	6.706	6.136	6.297	6.819	5.767	8.186	0.487	5.94
10	0.1635	12.549	12.576	13.926	12.028	10.524	12.662	12.97	12.108	12.767	11.172	15.41	1.068	6.92
15	0.24525	13.463	17.112	18.88	16.797	16.474	18.084	17.053	15.183	18.887	16.432	21.05	1.299	6.17
20	0.327	13.463	21.08	23.834	21.566	21.674	23.583	19.833	18.15	21.948	19.988	25.64	1.929	7.52

Tables 4.1 to 4.9 above demonstrate the consistency of observed deflection results obtained for Points 1 to 9. It can be seen that the coefficient of variation (CV) of all 9 points ranges from about 2 % to 17 %, which is a fairly acceptable outcome for indicating the mean values obtained are of reliable consistency. Since CV is of such reliable range, discrepancy with ruler's results can be neglected and only dial gauge results are adopted in the analysis since it is a more accurate displacement measuring device. A researcher can only be confident to proceed with the analysis with sets of results for a system that are consistent and reliable. By using the mean values calculated from Table 4.1 to 4.9, a true mean results can only be obtained to represent the entire system, which are tabulated in Table 4.10. Based on these results, 8 deflection profiles can be plotted as shown in Figure 4.4 to 4.11.

Table 4.10: Overall mean deflection results (dial gauge)

z-axis	**150**	**300**	**450**	**150**	**300**	**450**	**150**	**300**	**450**
x-axis	**350**	**350**	**350**	**700**	**700**	**700**	**1050**	**1050**	**1050**
Sand load (kg)	**Cumulative deflection (mm)**								
	Points								
	1	**2**	**3**	**4**	**5**	**6**	**7**	**8**	**9**
0	0	0	0	0	0	0	0	0	0
5	6.893	7.446	8.863	11.16	11.25	12.76	6.826	7.475	8.186
10	15.22	16.78	16.73	22.88	23.98	24.46	16.06	14.66	15.41
15	20.87	23.21	23.18	30.25	31.54	33.54	20.9	21.65	21.05
20	24.24	27.8	28.33	34.59	37.63	41.02	27.08	26.01	25.64

Table 4.11: Overall mean deflection results (ruler)

z-axis	**150**	**300**	**450**	**150**	**300**	**450**	**150**	**300**	**450**
x-axis	**350**	**350**	**350**	**700**	**700**	**700**	**1050**	**1050**	**1050**
Sand load (kg)	**Cumulative deflection (mm)**								
	Points								
	1	**2**	**3**	**4**	**5**	**6**	**7**	**8**	**9**
0	0	0	0	0	0	0	0	0	0
5	7.0	7.3	8.8	11.6	11.0	12.0	6.8	7.3	8.5
10	15.4	16.0	15.6	23.1	24.5	23.8	14.1	14.5	16.8
15	21.1	22.3	23.0	31.9	35.1	34.4	19.8	22.1	24.3
20	25.2	27.3	28.4	37.5	42.4	42.8	26.9	27.8	30.3

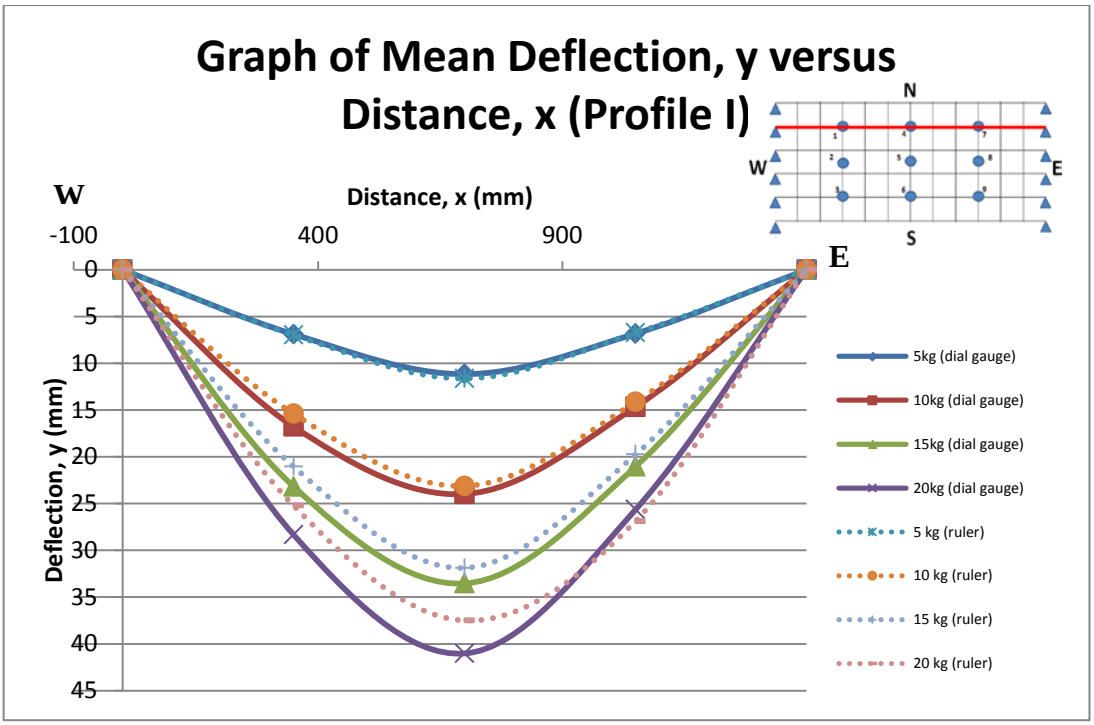

Figure 4.4: Mean deflection profile I

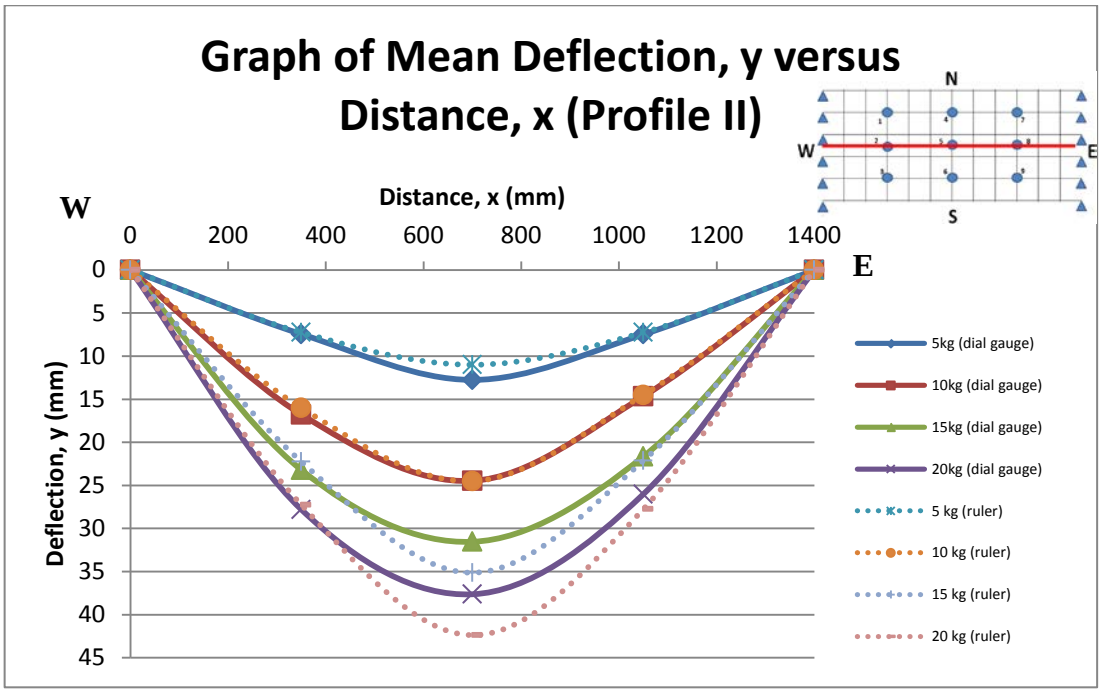

Figure 4.5: Mean deflection profile II

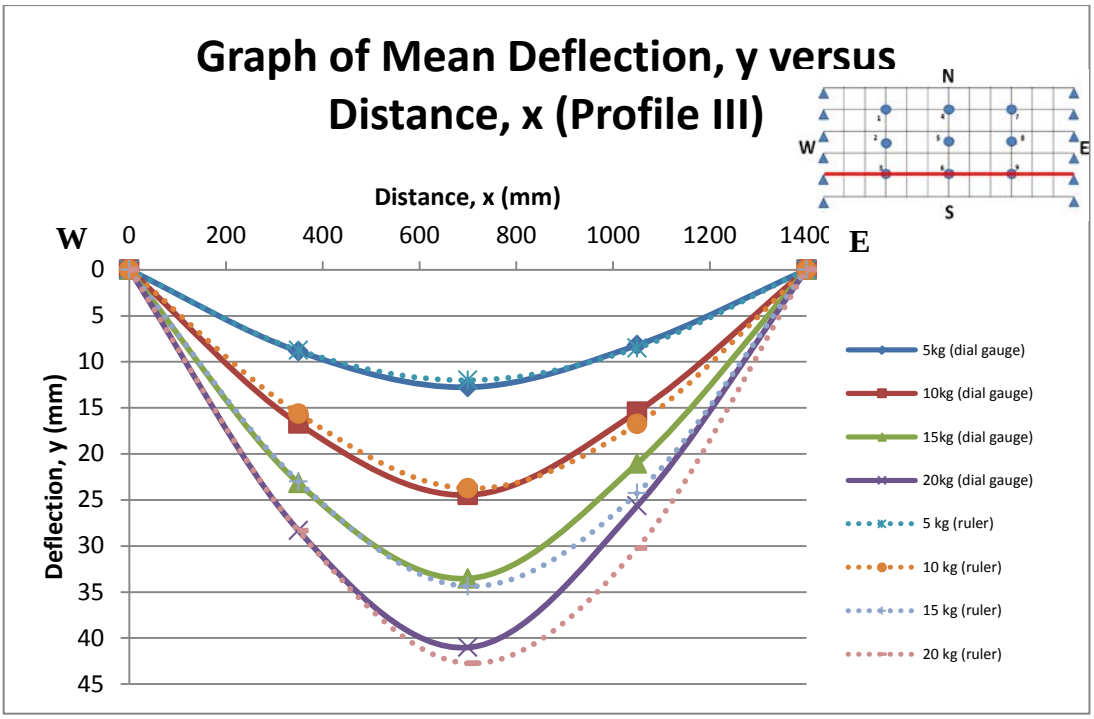

Figure 4.6: Mean deflection profile III

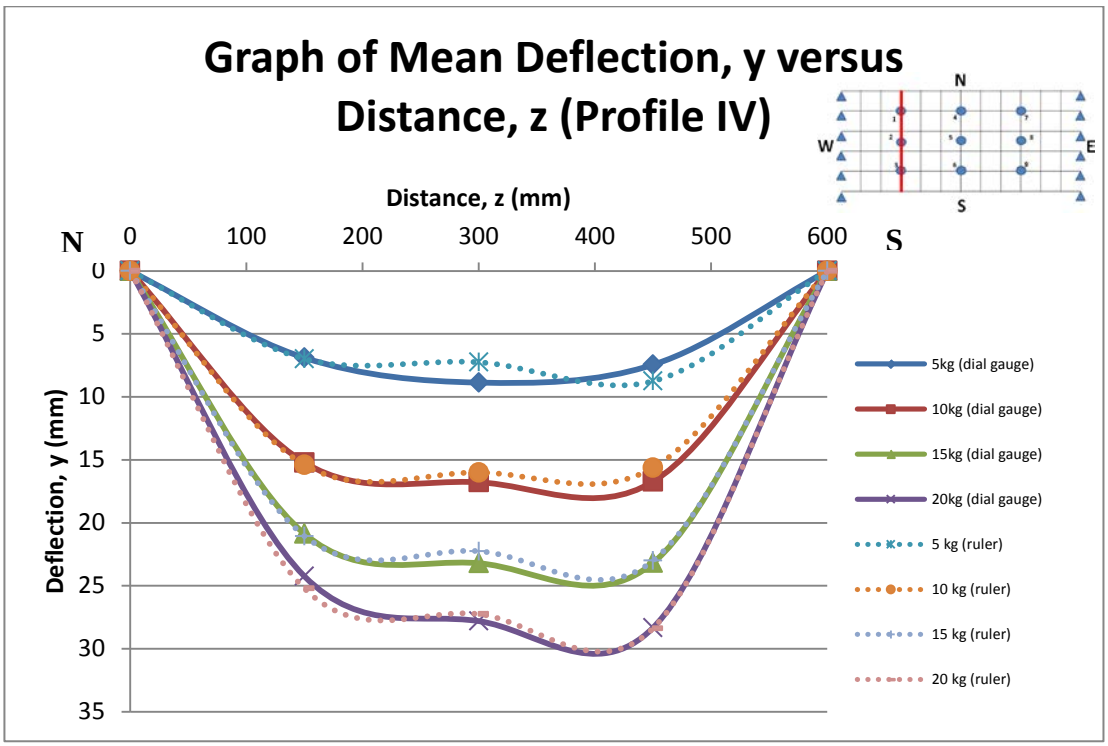

Figure 4.7: Mean deflection profile IV

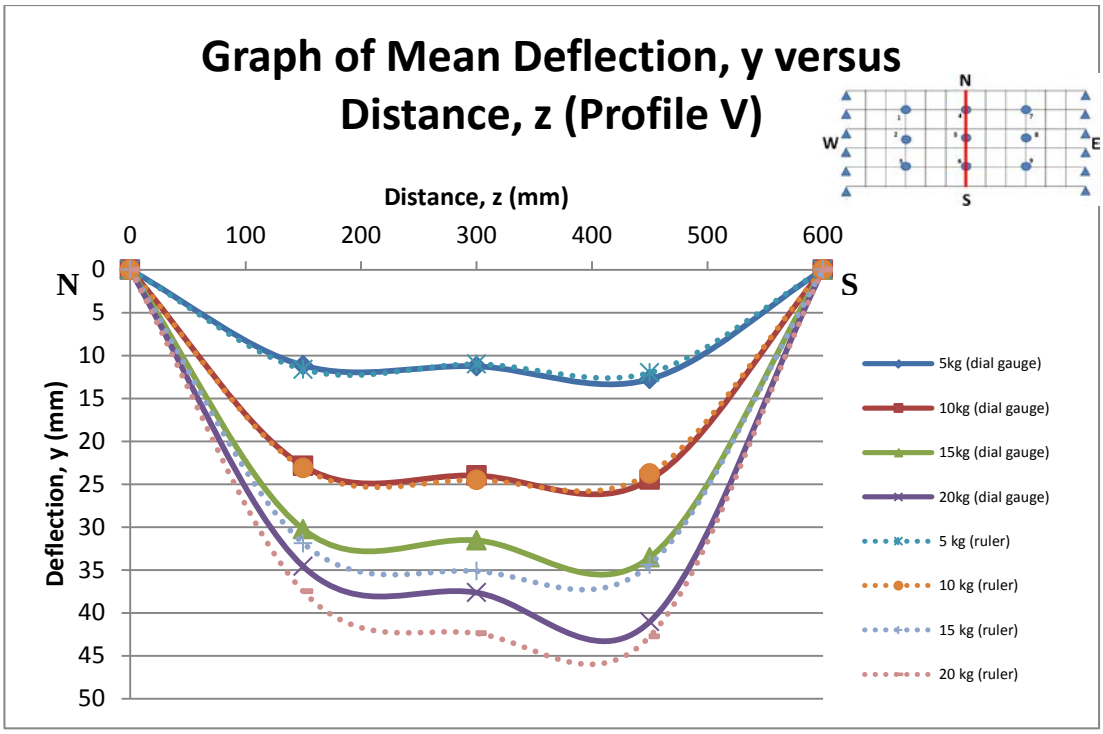

Figure 4.8: Mean deflection profile V

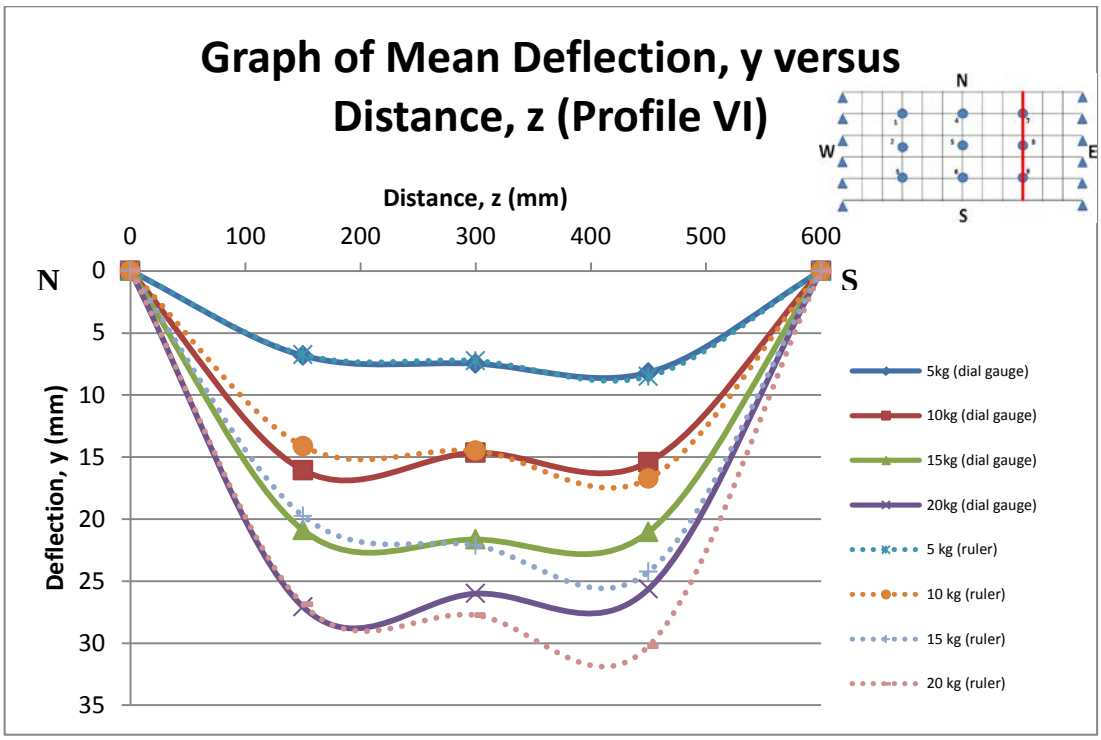

Figure 4.9: Mean deflection profile VI

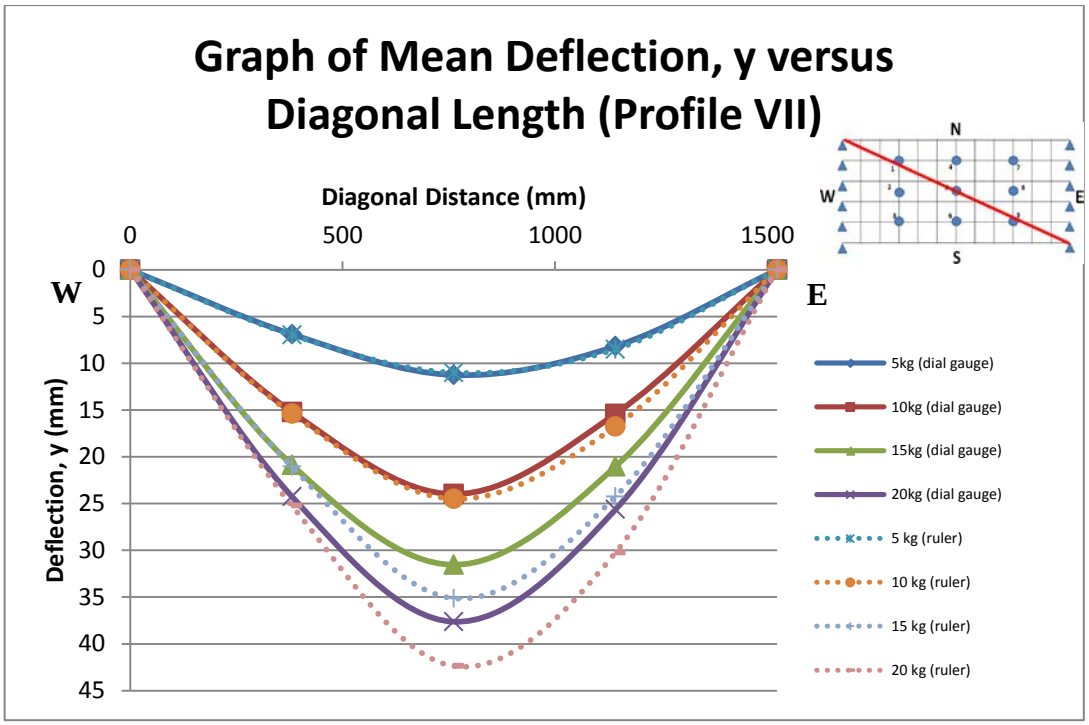

Figure 4.10: Mean deflection profile VII

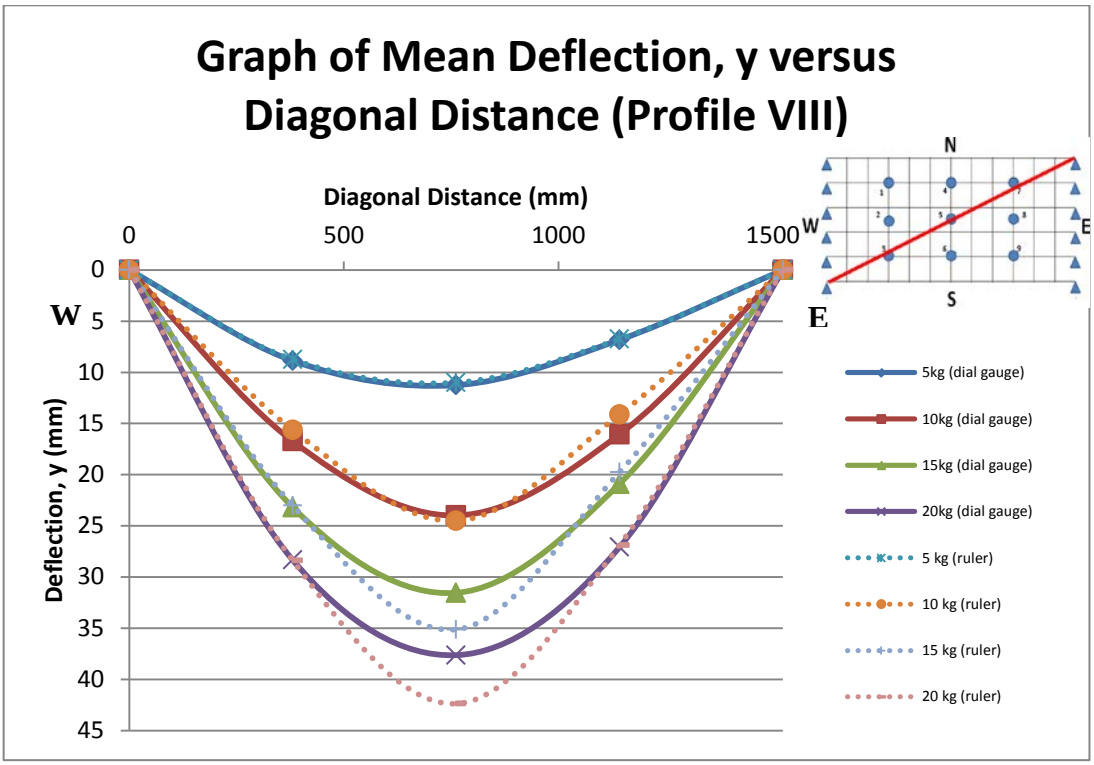

Figure 4.11: Mean deflection profile VIII

To break it down simply, Figures 4.4, 4.5 and 4.6 show the mean deflection profiles of BGC model along its longitudinal axis or x-axis as defined in Figure 4.3. These 3 profiles are actually the results of interest for the analysis which is discussed in Section 4.2.2.

Figures 4.7, 4.8 and 4.9 show the mean deflection profiles of BGC model along its transverse axis or z-axis as defined above whereas Figure 4.10 and 4.11 show the deflection profiles along both lines cutting through BGC model diagonally. These 5 profiles demonstrate how homogeneous it is of the BGC model.

From profiles I, II, III, VII and VIII, it can be seen that the BGC model has a smooth deflection curve which verifies the case of uniformly-distributed loading in a simply supported beam. However, the deflection profiles along the transverse axis/z-axis are not as smooth as it should be, as shown in profiles IV, V and VI. This could be due to the irregular uniformity of loading across the surface area as volume of sand may be more at the gaps of bamboo grid than the areas where the splints are as geotextile is soft enough to form shallow cavity at the gaps to allow more sand to sink in. Another reason is that the method proposed for sand distribution is simply flawed, causing uneven distribution of sand. It could also be due to the BGC model itself is inhomogeneous as bamboo is a natural material which is hardly perfectly homogeneous in most cases.

The discrepancy between dial gauge's and ruler's results may be due to the difference in degree of sensitivity to displacement readings. All the deflection profiles above have shown agreeable consistency in results as the deflection lines between dial gauge's and ruler's readings are relatively close to each other.

4.2.2 Determination of Overall Mean Deflection Profile along the x-axis

Since it is known that the longitudinal axis is the point of interest in this study as it is the axis where the system deflects the most, which is also the interested deflection profile explained in the Euler-Bernoulli's theory, an overall mean deflection profile

comprises of the average of Profile I, II and III is obtained to represent the BGC model. A way of doing this is calculating the overall mean deflections based on Profile IV, V and VI sets and obtaining the overall mean deflection representing the x-axis, i.e. mean of profile IV represents overall mean deflection at x = 350 mm, mean of profile V represents overall mean deflection at x = 700 mm and mean of profile VI represents overall mean deflection at x = 1050 mm.

Table 4.12: Overall mean for Points 1, 2, 3 (from Profile IV)

Sand load (kg)	Mean deflection (mm) Points			Overall Mean (mm)	Standard deviation, σ (mm)	Coefficient of Variation (%)
	1	2	3			
0	0	0	0	0	0	0
5	6.8925	7.44625	8.86325	7.734	1.0163975	13.1419
10	15.215	16.7763	16.7256	16.239	0.8871351	5.46301
15	20.8675	23.2088	23.18	22.4188	1.3434988	5.99275
20	24.2438	27.8038	28.331	26.7928	2.2232561	8.29795

Table 4.13: Overall mean for Points 4, 5, 6 (from Profile V)

Sand load (kg)	Mean deflection (mm) Points			Overall Mean (mm)	Standard deviation, σ (mm)	Coefficient of Variation (%)
	4	5	6			
0	0	0	0	0	0	0
5	11.1601	11.2531	12.757	11.7234	0.8963164	7.64552
10	22.8755	23.9806	24.4639	23.7733	0.8142243	3.42495
15	30.2485	31.539	33.5359	31.7745	1.6562877	5.21264
20	34.5888	37.6294	41.0236	37.7473	3.2190565	8.52792

Table 4.14: Overall mean for Points 7, 8, 9 (from Profile VI)

Sand load (kg)	Mean deflection (mm) Points			Overall Mean (mm)	Standard deviation, σ (mm)	Coefficient of Variation (%)
	7	8	9			
0	0	0	0	0	0	0
5	6.82625	7.475	8.18638	7.49588	0.6803027	9.07569
10	16.0613	14.6575	15.4103	15.3763	0.7024893	4.56864
15	20.8985	21.645	21.0456	21.1964	0.3954235	1.86552
20	27.0823	26.0113	25.6399	26.2445	0.7489332	2.85368

Table 4.15: Overall mean deflection along x-axis

Sand load (kg)	UDL (N/mm)	Overall mean deflection (mm)				
		x-coordinates (mm)				
		0	350	700	1050	1400
0	0	0	0	0	0	0
5	0.08175	0	7.734	11.7234	7.49588	0
10	0.1635	0	16.239	23.7733	15.3763	0
15	0.24525	0	22.4188	31.7745	21.1964	0
20	0.327	0	26.7928	37.7473	26.2445	0

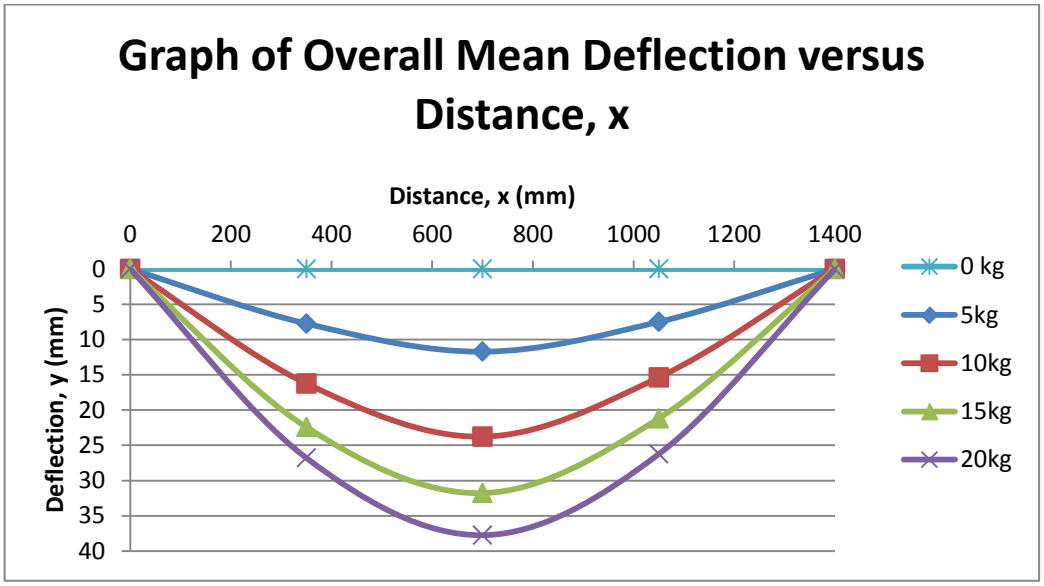

Figure 4.12: Overall mean deflection profile along the x-axis

4.3 Determining the Unknown Parameters, *E* and *I*

4.3.1 Introduction

In any equation that governs beam behaviour, two characteristic parameters of the beam which are the Young modulus, *E* and the moment of inertia, *I*, are always incorporated so that the properties of the beam are accounted for. These two parameters if put together, i.e. *EI* which they always are in equations where beam theory is involved, is known as the flexural rigidity of the beam, which indicates how rigid or stiff the beam is if subjected to flexural stress. There is no difference in the

case at hand as both Euler-Bernoulli beam equation and Winkler model which incorporated the Euler-Bernoulli beam theory, always include these two parameters to acknowledge the presence and importance of the subjected beam.

Say, even if the bamboo has been tested for its properties such as the Young modulus, *E* in the laboratory, there is no way that this individual tested material can represent the bamboo grid in the BGC model because bamboo is a natural material which has varying *E* value along its culm due to the presence of nodes and internodes. Theoretically, the *E* value should be a constant for a material but since bamboo itself can hardly be called a homogeneous material, even so it has been cut into splints and the fibres in the bamboo in its natural orientation or arrangement has been interrupted, thus causing varying *E* value along the splint. Due to reasons above, the overall *E* of the BGC system needs to be determined through unconventional methods.

The moment of inertia, *I* of any continuous solid body can be easily interpreted through available standard equations. However, a discontinuous body will pose difficulty in determining its moment of inertia (not to be confused with cross-sections with discontinuous parts such as I-beam). Since the BGC model bends about z-z axis (as defined in Figure 4.2), moment of inertia, I_{zz} of only this axis is interested in this study. It should be noted that the I_{zz} of the bottom splints can be easily calculated as it is continuous along the x-axis, whereas the top splints are arranged in a discontinuous manner to form a grid (as shown in Figure 4.14) so I_{zz} for the top splints cannot be determined normally using the conventional method.

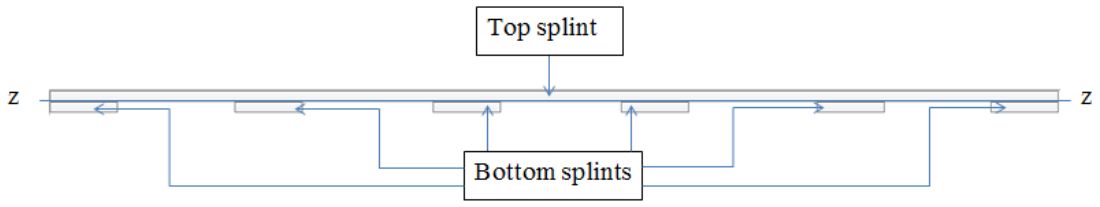

Figure 4.13: Lateral view of bamboo grid (z-z axis)

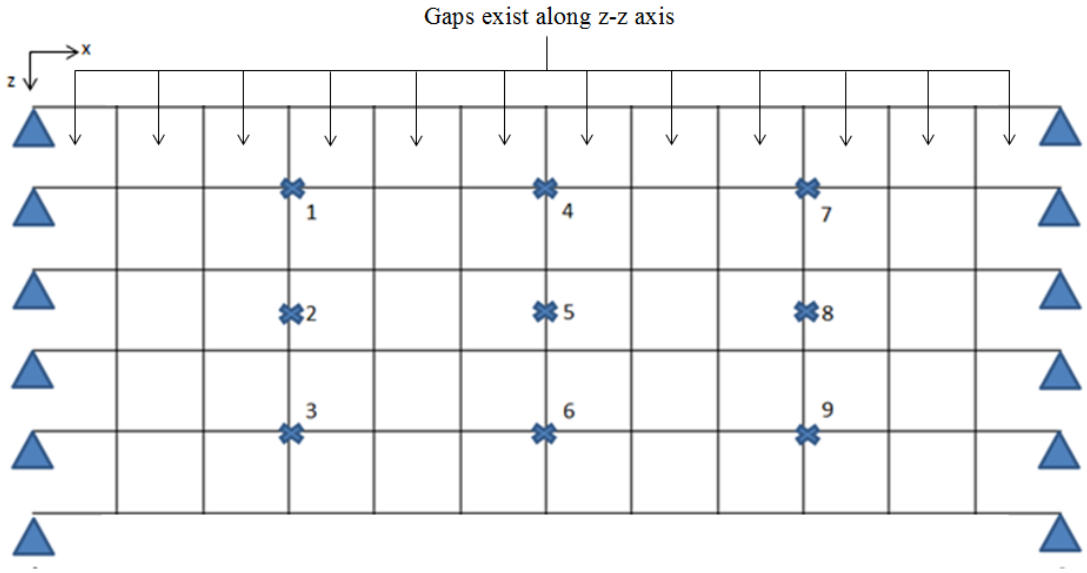

Figure 4.14: Demonstrating that top splints from lateral view are discontinuous

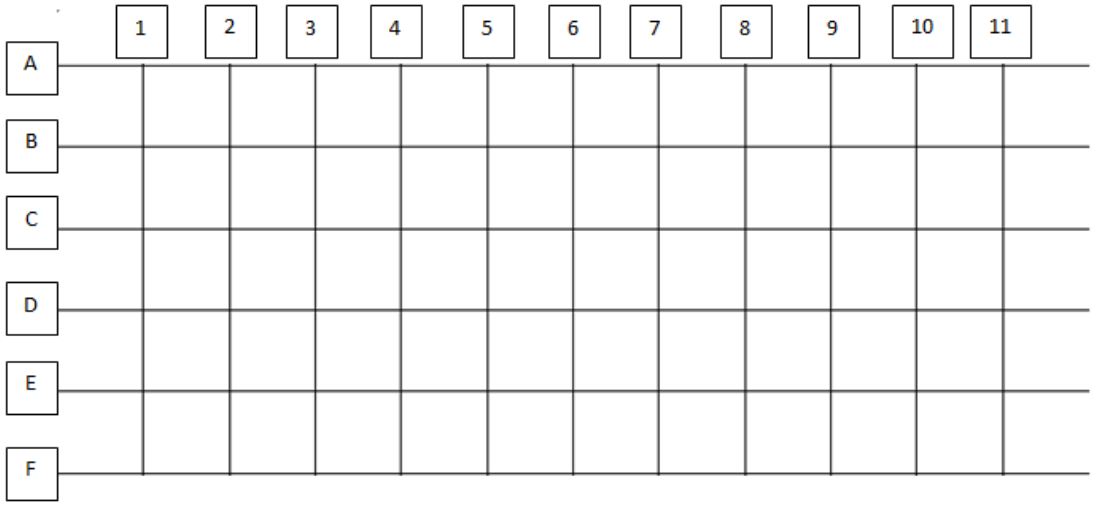

Figure 4.15: Labels for bamboo splints

Table 4.16: Measured thickness of bamboo splints

Bamboo splints	Bamboo thickness (mm)										Average (mm)
	Trials										
	1	2	3	4	5	6	7	8	9	10	
A	6.97	6.81	7.04	6.50	7.05	6.96	6.61	6.26	7.95	7.25	6.94
B	5.37	5.10	5.87	4.71	5.19	5.27	4.96	7.38	7.23	8.54	5.96
C	5.13	5.70	4.95	5.78	5.43	5.90	6.52	6.06	6.22	6.12	5.78
D	6.60	7.01	6.91	6.59	6.67	6.64	5.23	6.26	7.60	7.00	6.65
E	6.57	5.95	6.09	7.77	6.24	7.11	6.11	7.06	7.33	6.57	6.68
F	5.33	5.38	5.22	5.02	5.95	6.95	7.30	6.21	8.32	7.89	6.36
1	35.73	35.19	34.74	34.90	36.08	32.09	32.46	33.01	31.80	30.72	33.67
2	39.48	36.80	36.88	39.85	36.28	36.38	38.02	37.52	38.81	38.80	37.88
3	36.00	36.65	36.28	33.81	34.24	36.08	37.98	36.17	32.42	31.59	35.12
4	34.91	35.49	37.05	34.79	35.29	36.96	36.21	34.48	39.22	34.85	35.93
5	38.44	38.64	36.28	35.76	35.57	36.26	35.15	37.60	34.92	34.89	36.35
6	38.31	34.02	37.03	36.75	35.77	40.00	38.63	36.54	38.54	40.66	37.63
7	36.61	34.75	37.10	37.69	37.59	35.86	34.13	37.27	35.32	33.80	36.01
8	38.90	37.76	38.00	40.82	37.82	37.48	37.94	39.19	42.14	41.72	39.18
9	38.44	40.00	40.49	39.74	39.54	43.30	40.64	39.61	39.72	40.26	40.17
10	36.16	35.96	36.34	36.49	35.19	32.92	34.92	37.23	35.39	34.05	35.47
11	41.30	39.09	40.28	39.71	39.57	40.09	40.39	40.32	37.15	37.86	39.58

92

Table 4.17: Measured width of bamboo splints

Bamboo splints	Bamboo width (mm)										Average (mm)
	Trials										
	1	2	3	4	5	6	7	8	9	10	
A	36.77	30.98	31.89	28.34	31.82	39.48	40.42	41.41	42.81	41.71	36.56
B	37.47	44.16	41.51	43.09	40.65	37.82	37.22	37.92	37.63	37.28	39.48
C	43.20	43.01	41.54	41.65	44.12	42.01	41.24	44.05	43.27	43.05	42.71
D	37.15	38.33	37.26	38.22	37.42	34.19	38.51	39.26	34.31	31.87	36.65
E	43.20	43.01	41.54	41.65	44.12	42.01	41.24	44.05	43.27	43.98	42.81
F	38.32	38.12	36.48	36.49	36.36	36.97	36.31	36.59	36.02	31.61	36.33
1	9.12	7.63	8.62	7.85	9.48	11.26	12.19	11.35	12.29	11.56	10.14
2	9.83	8.57	8.90	8.04	9.26	14.23	16.10	18.27	11.13	12.05	11.64
3	10.17	10.97	10.16	9.63	9.95	8.91	9.84	10.08	8.98	9.54	9.82
4	11.17	9.60	10.14	9.35	8.76	8.06	8.39	8.40	8.17	7.86	8.99
5	9.73	8.03	9.72	7.18	9.21	6.33	7.54	8.15	7.51	7.83	8.12
6	10.36	12.81	13.44	13.29	12.30	14.99	15.15	15.35	15.29	15.09	13.81
7	7.36	7.37	7.01	6.77	7.10	7.06	7.36	7.94	7.06	6.40	7.14
8	15.24	15.76	14.89	14.76	13.61	10.05	9.63	10.87	9.76	10.37	12.49
9	14.70	15.42	15.28	14.85	15.42	9.44	10.44	9.75	9.97	10.94	12.62
10	8.22	7.96	7.90	7.99	7.81	7.11	8.14	7.34	7.94	8.53	7.89
11	8.43	8.40	9.12	9.52	9.02	8.40	8.11	6.83	6.65	6.57	8.11

93

First of all, it is useful to compute the I_{zz} of the cross-section as shown in Figure 4.13. It gives a rough figure of what the I_{zz} of the whole system could be if the top splints were continuous. Table 4.16 and 4.17 recorded 10 repetitive sets of results of each bamboo splint's thickness and width so that an average value can be obtained for computational purposes. The computation of I_{zz} is simplified by assuming that the cross-sections of bamboo splints are of rectangular shape as depicted in Figure 4.13. Centroid of the cross-section was calculated using equations 4.3 and 4.4 whereas I_{zz} was calculated using Equation 4.5 as follows:

$$\bar{z} = \frac{\sum_{i=1}^{n} z_i A_i}{\sum_{i=1}^{n} A_i} \tag{4.3}$$

$$\bar{y} = \frac{\sum_{i=1}^{n} y_i A_i}{\sum_{i=1}^{n} A_i} \tag{4.4}$$

$$I_{zz} = I_{\bar{z}} + Ay^2 \tag{4.5}$$

The calculations of centroid and I_{zz} are simplified in Table 4.18 below:

Table 4.18: Centroid and I_{zz} calculations

Bamboo Splints	**Average Thickness, *h* (mm)**	**Average Width, *b* (mm)**	**Area, A (mm^2)**	**I_z (mm^4)**	**I_{zz} (mm^4)**
A	6.94	36.563	253.747	1018.45	12991.93
B	5.962	39.475	235.35	697.13	5206.52
C	5.781	42.714	246.93	687.70	5818.32
D	6.651	36.652	243.772	898.62	4214.71
E	6.68	42.807	285.951	1063.32	4892.24
F	6.357	36.327	230.931	777.69	4439.87
Top layer	10.07 (average)	600	6042	51057.4	51495.4
Total I_{zz} with top layer included					89058.98
Total I_{zz} without top layer assuming same centroid					37563.58

Note: Centroid z = 300 mm from left/right edge (middle), y = 10.34 mm from bottom edge

It should be clarified again that the I_{zz} obtained in Table 4.18 is not the I_{zz} representing the overall BGC model. The two I_{zz} values are merely presented to give an idea that the actual overall BCG model is expected to have a value in between these two, i.e. 37563.58 mm^4 < $I_{zz,actual}$ < 89058.98 mm^4, theoretically. The excess of $I_{zz,actual}$ compared to the lower limit will be the I_{zz} provided by the discontinuous top splints.

4.3.2 Analysis of Results to Derive *E* and *I* Parameters

Overall mean deflection results tabulated in Table 4.15 were used as the observed results to be coupled with Euler-Bernoulli beam theory (Equation 3.3) to produce a derived back-substitution analysis for determining *E* and *I* parameters, assuming that the BGC model follows Euler-Bernoulli beam theory, which is widely renowned and reliable.

From literature review, it is known that the Young modulus, *E* of bamboo is approximately 10% of steel's which is 200 to 210 GPa, so any value in the range of less than 10 to slightly more than 20 GPa is expected for a bamboo. Using results from Table 4.14 as the basis for comparison, dummy *E* values ranging from 5 GPa to 30 GPa were substituted into Equation 3.3 to obtain the deflection value closest to the observed overall mean values from Table 4.15 by varying dummy *I* values through trials and errors. For convenience in carrying out trials and errors using spreadsheet, the dummy *I* value is expressed as 89059/factor mm^4.

As an example, Table 4.19 to 4.21 are presented to demonstrate the trials and errors process in determining dummy *I* values by fixing an *E* value.

Table 4.19: Fixed E = 20 GPa, factor = 4.51 (I = 19747.01 mm^4)

x-axis (mm)		350			700			1050		
Load (kg)	UDL, q (N/mm)	Deflection, y (mm)		%	Deflection, y (mm)		%	Deflection, y (mm)		%
		Observed	Calculated	Difference	Observed	Calculated	Difference	Observed	Calculated	Difference
5	0.08175	7.734	7.377	4.613	11.723	10.354	11.681	7.496	7.377	1.583
10	0.1635	16.239	14.754	9.142	23.773	20.708	12.894	15.376	14.754	4.045
15	0.24525	22.419	22.132	1.281	31.774	31.062	2.242	21.196	22.132	4.412
20	0.327	26.793	29.509	10.137	37.747	41.416	9.719	26.244	29.509	12.438

Table 4.20: Fixed E = 20 GPa, factor = 4.52 (I = 19703.32 mm^4)

x-axis (mm)		350			700			1050		
Load (kg)	UDL, q (N/mm)	Deflection, y (mm)		%	Deflection, y (mm)		%	Deflection, y (mm)		%
		Observed	Calculated	Difference	Observed	Calculated	Difference	Observed	Calculated	Difference
5	0.08175	7.734	7.394	4.402	11.723	10.377	11.485	7.496	7.394	1.365
10	0.1635	16.239	14.787	8.940	23.773	20.754	12.701	15.376	14.787	3.832
15	0.24525	22.419	22.181	1.062	31.774	31.131	2.026	21.196	22.181	4.644
20	0.327	26.793	29.574	10.381	37.747	41.508	9.962	26.244	29.574	12.688

96

Table 4.21: Fixed E = 20 GPa, factor = 4.53 (I = 19659.82 mm^4)

x-axis (mm)		350			700			1050		
Load (kg)	UDL, q (N/mm)	Deflection, y (mm)		%	Deflection, y (mm)		%	Deflection, y (mm)		%
		Observed	Calculated	Difference	Observed	Calculated	Difference	Observed	Calculated	Difference
5	0.08175	7.734	7.410	4.190	11.723	10.400	11.290	7.496	7.410	1.147
10	0.1635	16.239	14.820	8.739	23.773	20.800	12.508	15.376	14.820	3.619
15	0.24525	22.419	22.230	0.843	31.774	31.200	1.809	21.196	22.230	4.875
20	0.327	26.793	29.640	10.626	37.747	41.600	10.206	26.244	29.640	12.937

From Tables 4.19 to 4.21, highest % difference of each dummy *I* (as shown highlighted) is recorded to be compared with results from other sets of dummy *I* for a fixed *E* = 20 GPa in this example. After trials and errors, the lowest % difference recorded for the set of dummy *I* which is of factor 4.51 in this case is determined to be the *I* value most accurate to the fixed *E*. For higher accuracy, up to 3 or more decimal places should be used for the factor during trials and errors. Such process was repeated by fixing different values of *E* and the results are tabulated in Table 4.22.

Table 4.22: *E* and *I* values from trials and errors

Fixed *E* (N/mm^2)	Factor	*I* (mm^4)	*EI* (N mm^2)	log *E*	log *I*
5000	1.13	78813.274	394066371.681	3.69897	4.8966
7500	1.69	52697.633	395232248.521	3.87506	4.72179
10000	2.26	39406.637	394066371.681	4	4.59557
12000	2.71	32863.100	394357195.572	4.07918	4.51671
14000	3.16	28183.228	394565189.873	4.14613	4.44999
16000	3.62	24601.934	393630939.227	4.20412	4.39097
18000	4.07	21881.818	393872727.273	4.25527	4.34008
20000	4.52	19703.319	394066371.681	4.30103	4.29454
22000	4.97	17919.316	394224949.698	4.34242	4.25332
24000	5.42	16431.550	394357195.572	4.38021	4.21568
26000	5.88	15146.088	393798299.320	4.41497	4.1803
28000	6.33	14069.352	393941864.139	4.44716	4.14827
30000	6.78	13135.546	394066371.681	4.47712	4.11845

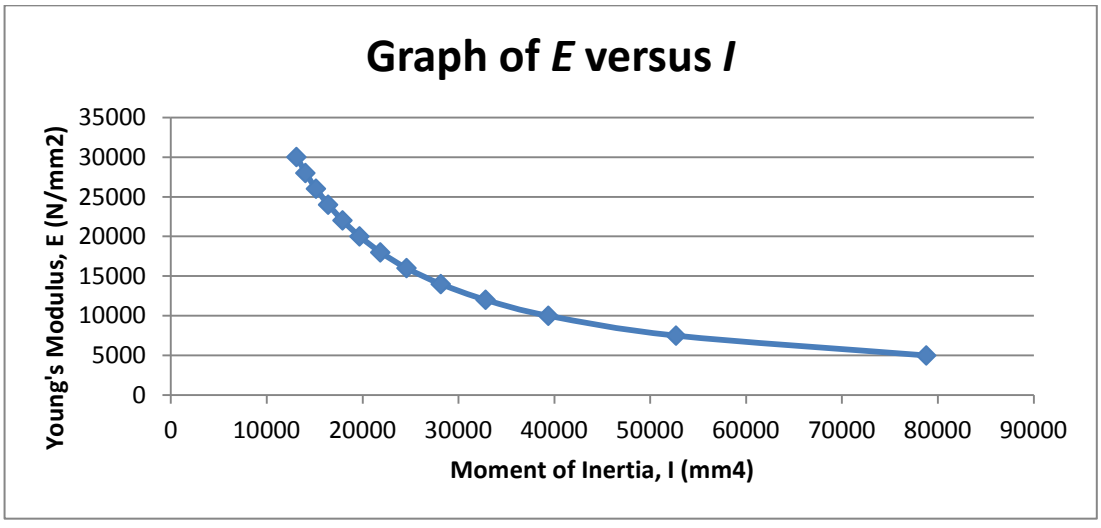

Figure 4.16: E vs I graph from trials and errors

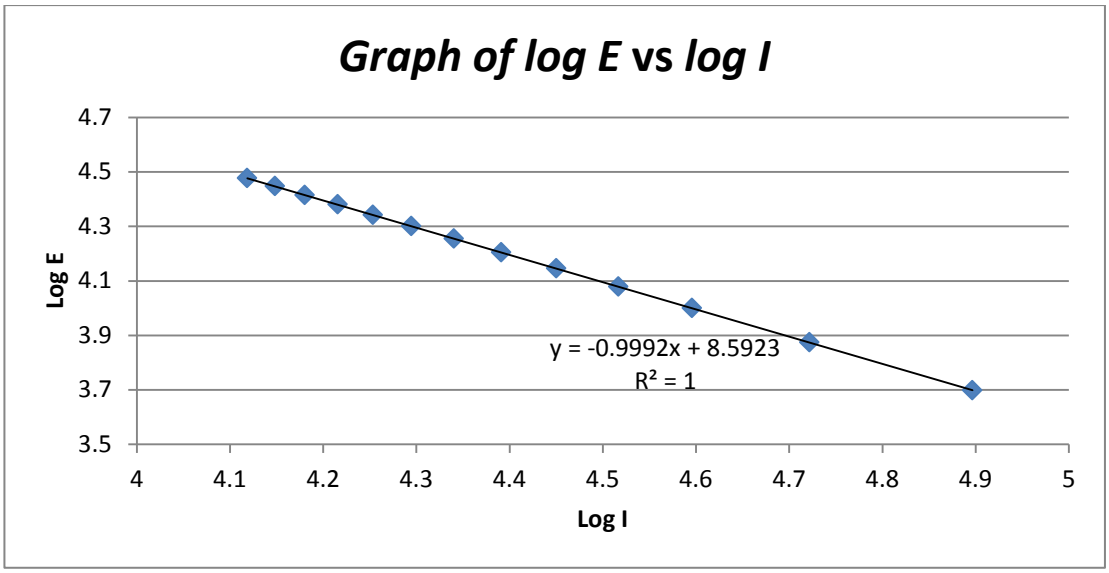

Figure 4.17: Graph of log E vs log I

Since the graph of *E* vs *I* (Figure 4.16) is not in linear form which does not give a representative simple equation of their relationship, graph of *log E* vs *log I* was plotted as shown in Figure 4.17 to present a linear correlation between E and I parameters so that a linear equation which is useful in the coming analysis can be obtained as follows:

$$\log E = -0.9992\ logI + 8.5923 \tag{4.6}$$

From Table 4.22, another equation representing the BGC model can be obtained by getting the mean of the sets of EI tabulated which gives:

$$EI = 394172777\ Nmm^2 \tag{4.7}$$

By having two equation and two unknowns, one may solve the two equations simultaneously. The proper steps are shown as follows:

$$I = \frac{394172777}{E} \tag{4.8}$$

By substituting Equation 4.8 into Equation 4.6, the problem is simplified into as follows:

$$E = (394172777^{-0.9992} \times 10^{8.5923})^{\left(\frac{1}{1-0.9992}\right)} = 23035.8\ MPa \quad (4.9)$$

$$I = \frac{394172777}{23035.8} = 17111.3127\ mm^4 \quad (4.10)$$

Therefore, the unknown *E* and *I* of the BGC model have been solved using the method as shown above. It is noticed that the Young modulus, *E* of the overall system is about 23 GPa, which matches the assumption made that *E* of bamboo is about 10% of steel's.

However, the overall *I* value obtained which gives 17111.3127 mm^4 is lower than the expected range (37563.58 mm^4 < $I_{zz,actual}$ < 89058.98 mm^4) which was predicted in Section 4.3.1. This could be due to errors in assumptions made during the analysis such as in the process of trials and errors where the *EI* pairs are not accurate enough which gives a slight deviation from the results. But the most probable source of error is that the bamboo splints were not cut smoothly enough to its intended width which is 40 mm, and that the thickness of bamboo varies throughout the splints due to its natural making, which causes the average of 10 sets of measurement for each splint lost its significance as these 10 sets of measured dimensions could not capture well enough to represent the natural dimensions of the bamboo splints. This adds to the point that the moment of inertia of bamboo grid system cannot be calculated directly based on measured natural dimensions of bamboo due to many uncertainties. Nevertheless, it can be estimated that the *I* value of a unit of strip as shown in Figure 4.18 for the BGC model to be approximately one-fifth of the value obtained from the analysis, i.e. 17111.3127/5 = 2566 mm^4. This value would seem to give a conservative approach for design as it is smaller than the calculated *I* value based on measured dimensions of the splints.

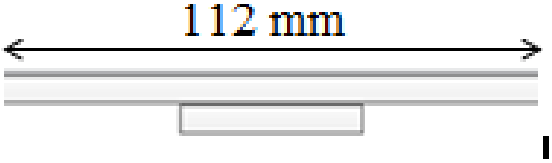

Figure 4.18: A unit of bamboo strip

4.4 Verification of *EI* Obtained Through Analysis

Since EI = 39417277 N mm^2 derived in Section 4.3.2 is based on loading data up to only 20 kg of sand due to reasons stated before, there is a need to verify whether the results stand true for loading beyond that so in effort of this, another 5 sets of experiments were carried out on Point 5 using 100 mm LVDT for loading up 40 kg of sand and results are presented in the Tables 4.23 to 4.27 below.

Table 4.23: Set 1 observed results using 100 mm LVDT @ Point 5

1	2	3	4	5	6	7	8	9	10
UDL (N/mm)	**Sand load (kg)**	**Displayed reading @ point 5**	**Calibrated reading (mm)**	**Calibrated reading minus initial reading (mm)**	**Ruler reading (mm)**	**Ruler reading minus initial reading (mm)**	**Theoretical displacement (mm)**	**% difference (LVDT) [(5)-(8)]/(5)*100**	**% difference (ruler) [(7)-(8)]/(7)*100**
0	**0**	-40.926	16.038	0.000	20	0	0.000	0.00	0.00
0.08175	**5**	-17.472	26.473	10.435	30	10	10.374	0.58	-3.74
0.1635	**10**	10.704	39.008	22.970	43	23	20.748	9.67	9.79
0.24525	**15**	36.046	50.283	34.245	54	34	31.122	9.12	8.46
0.327	**20**	57.925	60.017	43.979	64	44	41.497	5.64	5.69
0.40875	**25**	82.323	70.872	54.833	75	55	51.871	5.40	5.69
0.4905	**30**	106.407	81.586	65.548	84	64	62.245	5.04	2.74
0.57225	**35**	131.119	92.581	76.543	97	77	72.619	5.13	5.69
0.654	**40**	149.378	100.704	84.666	105	85	82.993	1.98	2.36

102

Table 4.24: Set 2 observed results using 100 mm LVDT @ Point 5

1	2	3	4	5	6	7	8	9	10
UDL (N/mm)	**Sand load (kg)**	**Displayed reading @ point 5**	**Calibrated reading (mm)**	**Calibrated reading minus initial reading (mm)**	**Ruler reading (mm)**	**Ruler reading minus initial reading (mm)**	**Theoretical displacement (mm)**	**% difference (LVDT) [(5)-(8)]/(5)*100**	**% difference (ruler) [(7)-(8)]/(7)*100**
0	**0**	-39.217	16.798	0.000	21	0	0.000	0.00	0.00
0.08175	**5**	-15.783	27.224	10.426	31	10	10.374	0.50	-3.74
0.1635	**10**	9.832	38.620	21.822	43	22	20.748	4.92	5.69
0.24525	**15**	34.228	49.474	32.676	54	33	31.122	4.75	5.69
0.327	**20**	56.713	59.478	42.679	64	43	41.497	2.77	3.50
0.40875	**25**	79.756	69.729	52.931	74	53	51.871	2.00	2.13
0.4905	**30**	103.224	80.170	63.372	85	64	62.245	1.78	2.74
0.57225	**35**	128.776	91.538	74.740	96	75	72.619	2.84	3.17
0.654	**40**	151.719	101.746	84.947	106	85	82.993	2.30	2.36

103

Table 4.25: Set 3 observed results using 100 mm LVDT @ Point 5

1	2	3	4	5	6	7	8	9	10
UDL (N/mm)	**Sand load (kg)**	**Displayed reading @ point 5**	**Calibrated reading (mm)**	**Calibrated reading minus initial reading (mm)**	**Ruler reading (mm)**	**Ruler reading minus initial reading (mm)**	**Theoretical displacement (mm)**	**% difference (LVDT) [(5)-(8)]/(5)*100**	**% difference (ruler) [(7)-(8)]/(7)*100**
0	**0**	-43.716	14.797	0.000	17	0	0.000	0.00	0.00
0.08175	**5**	-19.221	25.695	10.898	28	11	10.374	4.81	5.69
0.1635	**10**	5.818	36.834	22.038	39	22	20.748	5.85	5.69
0.24525	**15**	31.911	48.443	33.646	51	34	31.122	7.50	8.46
0.327	**20**	52.702	57.693	42.896	60	43	41.497	3.26	3.50
0.40875	**25**	78.132	69.007	54.210	72	55	51.871	4.32	5.69
0.4905	**30**	102.978	80.061	65.264	83	66	62.245	4.63	5.69
0.57225	**35**	127.115	90.799	76.003	93	76	72.619	4.45	4.45
0.654	**40**	146.373	99.367	84.571	102	85	82.993	1.87	2.36

104

Table 4.26: Set 4 observed results using 100 mm LVDT @ Point 5

1	2	3	4	5	6	7	8	9	10
UDL (N/mm)	**Sand load (kg)**	**Displayed reading @ point 5**	**Calibrated reading (mm)**	**Calibrated reading minus initial reading (mm)**	**Ruler reading (mm)**	**Ruler reading minus initial reading (mm)**	**Theoretical displacement (mm)**	**% difference (LVDT) [(5)-(8)]/(5)*100**	**% difference (ruler) [(7)-(8)]/(7)*100**
0	**0**	-49.243	12.338	0.000	11	0	0.000	0.00	0.00
0.08175	**5**	-24.731	23.243	10.905	22	11	10.374	4.87	5.69
0.1635	**10**	1.608	34.961	22.624	34	23	20.748	8.29	9.79
0.24525	**15**	26.973	46.246	33.908	45	34	31.122	8.22	8.46
0.327	**20**	50.234	56.595	44.257	55	44	41.497	6.24	5.69
0.40875	**25**	73.643	67.010	54.672	66	55	51.871	5.12	5.69
0.4905	**30**	99.207	78.383	66.045	77	66	62.245	5.75	5.69
0.57225	**35**	121.482	88.293	75.956	87	76	72.619	4.39	4.45
0.654	**40**	142.562	97.672	85.334	97	86	82.993	2.74	3.50

105

Table 4.27: Set 5 observed results using 100 mm LVDT @ Point 5

1	2	3	4	5	6	7	8	9	10
UDL (N/mm)	**Sand load (kg)**	**Displayed reading @ point 5**	**Calibrated reading (mm)**	**Calibrated reading minus initial reading (mm)**	**Ruler reading (mm)**	**Ruler reading minus initial reading (mm)**	**Theoretical displacement (mm)**	**% difference (LVDT) [(5)-(8)]/(5)*100**	**% difference (ruler) [(7)-(8)]/(7)*100**
0	**0**	-45.324	14.081	0.000	15	0	0.000	0.00	0.00
0.08175	**5**	-21.036	24.887	10.806	26	11	10.374	3.99	5.69
0.1635	**10**	5.427	36.660	22.579	38	23	20.748	8.11	9.79
0.24525	**15**	25.401	45.547	31.466	47	32	31.122	1.09	2.74
0.327	**20**	53.297	57.958	43.876	59	44	41.497	5.42	5.69
0.40875	**25**	77.202	68.593	54.512	70	55	51.871	4.85	5.69
0.4905	**30**	99.014	78.297	64.216	80	65	62.245	3.07	4.24
0.57225	**35**	125.232	89.962	75.880	91	76	72.619	4.30	4.45
0.654	**40**	142.903	97.824	83.742	99	84	82.993	0.89	1.20

106

Table 4.28: Mean results compared to theoretical results (LVDT)

1	2	3					4	5	6	7	8
UDL (N/mm)	**Sand Load (kg)**	**Deflection @ Point 5 measured by LVDT (mm)**					**Mean (mm)**	**Standard deviation, σ (mm)**	**Coefficient of Variation (%)**	**Theoretical deflection (mm)**	**% Difference [(4)-(7)]/(4)*100**
		Set 1	**Set 2**	**Set 3**	**Set 4**	**Set 5**					
0.08175	**5**	10.435	10.426	10.898	10.905	10.806	10.694	0.244	2.28	10.374	2.99
0.1635	**10**	22.970	21.822	22.038	22.624	22.579	22.407	0.467	2.08	20.748	7.40
0.24525	**15**	34.245	32.676	33.647	33.909	31.466	33.188	1.126	3.39	31.122	6.22
0.327	**20**	43.979	42.679	42.896	44.257	43.877	43.538	0.703	1.61	41.497	4.69
0.40875	**25**	54.834	52.931	54.210	54.672	54.512	54.232	0.763	1.41	51.871	4.35
0.4905	**30**	65.549	63.372	65.264	66.045	64.216	64.889	1.080	1.66	62.245	4.08
0.57225	**35**	76.543	74.740	76.003	75.956	75.880	75.824	0.660	0.87	72.619	4.23
0.654	**40**	84.666	84.947	84.571	85.334	83.742	84.652	0.589	0.70	82.993	1.96

107

Table 4.29: Mean results compared to theoretical results (ruler)

1	2	3					4	5	6	7	8
UDL (N/mm)	**Sand Load (kg)**	**Deflection @ Point 5 measured by LVDT (mm)**					**Mean (mm)**	**Standard deviation, σ (mm)**	**Coefficient of Variation (%)**	**Theoretical deflection (mm)**	**% Difference [(4)-(7)]/(4)*100**
		Set 1	**Set 2**	**Set 3**	**Set 4**	**Set 5**					
0.08175	**5**	10	10	11	11	11	10.6	0.5	5.17	10.374	2.13
0.1635	**10**	23	22	22	23	23	22.6	0.5	2.42	20.748	8.19
0.24525	**15**	34	33	34	34	32	33.4	0.9	2.68	31.122	6.82
0.327	**20**	44	43	43	44	44	43.6	0.5	1.26	41.497	4.82
0.40875	**25**	55	53	55	55	55	54.6	0.9	1.64	51.871	5.00
0.4905	**30**	64	64	66	66	65	65	1.0	1.54	62.245	4.24
0.57225	**35**	77	75	76	76	76	76	0.7	0.93	72.619	4.45
0.654	**40**	85	85	85	86	84	85	0.7	0.83	82.993	2.36

108

Table 4.28 and 4.29 represent the summary of mean observed deflection results at Point 5 compared to theoretical results using *EI* value obtained from the analysis in Section 4.3.2. It can be seen that both the coefficient of variation and percentage difference between the mean observed deflection for Point 5 and the theoretical deflection are relatively small. This has proven that the flexural rigidity, *EI* obtained through the analysis stands valid. Since *E* and *I* are always grouped together, there is really no point in distinguishing them out individually when applied in Winkler model equations if the same BGC model is used.

4.5 Comparison between Hetenyi's Model (simply-supported beam solution), Euler-Bernoulli Beam Theory and Observed Results

This paper studies the behaviour of BGC model in air which simulates the most critical soft ground condition as if nothing is supporting it underneath except air. Hetenyi's equation of solving the same simply supported case but with soil underneath the beam supporting it as shown in Equation 3.8 is used to compare with theoretical deflection results based on Euler-Bernoulli's beam theory. The reaction force, k_o from soil is called the modulus of subgrade reaction which idealizes soils as a series of springs of spring constant, *k'*. In the case where the beam is supported in air, for Equation 3.8 to represent the situation, the *k* value substituted has to be very small. Table 4.30 tabulated results calculated from Bernoulli-Euler deflection equation (Equation 3.3) and from Hetenyi's equation (Equation 3.8). Figure 4.18 shows the relationship of *k* with deflection results, compared with theoretical results from usual classical beam theory together with overall mean observed deflection for 5 kg sand load. The flexural rigidity, *EI* substituted was from the analysis.

Table 4.30: Comparison of deflection between observed, Bernoulli-Euler and Hetenyi (simply-supported beam solution) of different k when load = 5kg

x (mm)			0	100	300	500	700	900	1100	1300	1400
x' (mm)			1400	1300	1100	900	700	500	300	100	0
Observed y (mm)			0	-	7.734	-	11.723	-	7.496	-	0
y (Euler-Bernoulli) (mm)			0	2.3479	6.53039	9.37172	10.3741	9.37172	6.53039	2.3479	0
	k (N/mm2)	λ									
y (Hetenyi) (mm)	1	0.005018	0	0.0383	0.0803	0.0873	0.0863	0.0873	0.0803	0.0383	0
	0.1	0.002822	0	0.2381	0.6230	0.8426	0.9109	0.8426	0.6230	0.2381	0
	0.01	0.001587	0	1.1886	3.2825	4.6792	5.1662	4.6792	3.2825	1.1886	0
	0.001	0.000892	0	2.1371	5.9398	8.5183	9.4270	8.5183	5.9398	2.1371	0
	0.0001	0.000502	0	2.3249	6.4661	9.2788	10.2710	9.2788	6.4661	2.3249	0
	0.00001	0.000282	0	2.3456	6.5239	9.3623	10.3637	9.3623	6.5239	2.3456	0

110

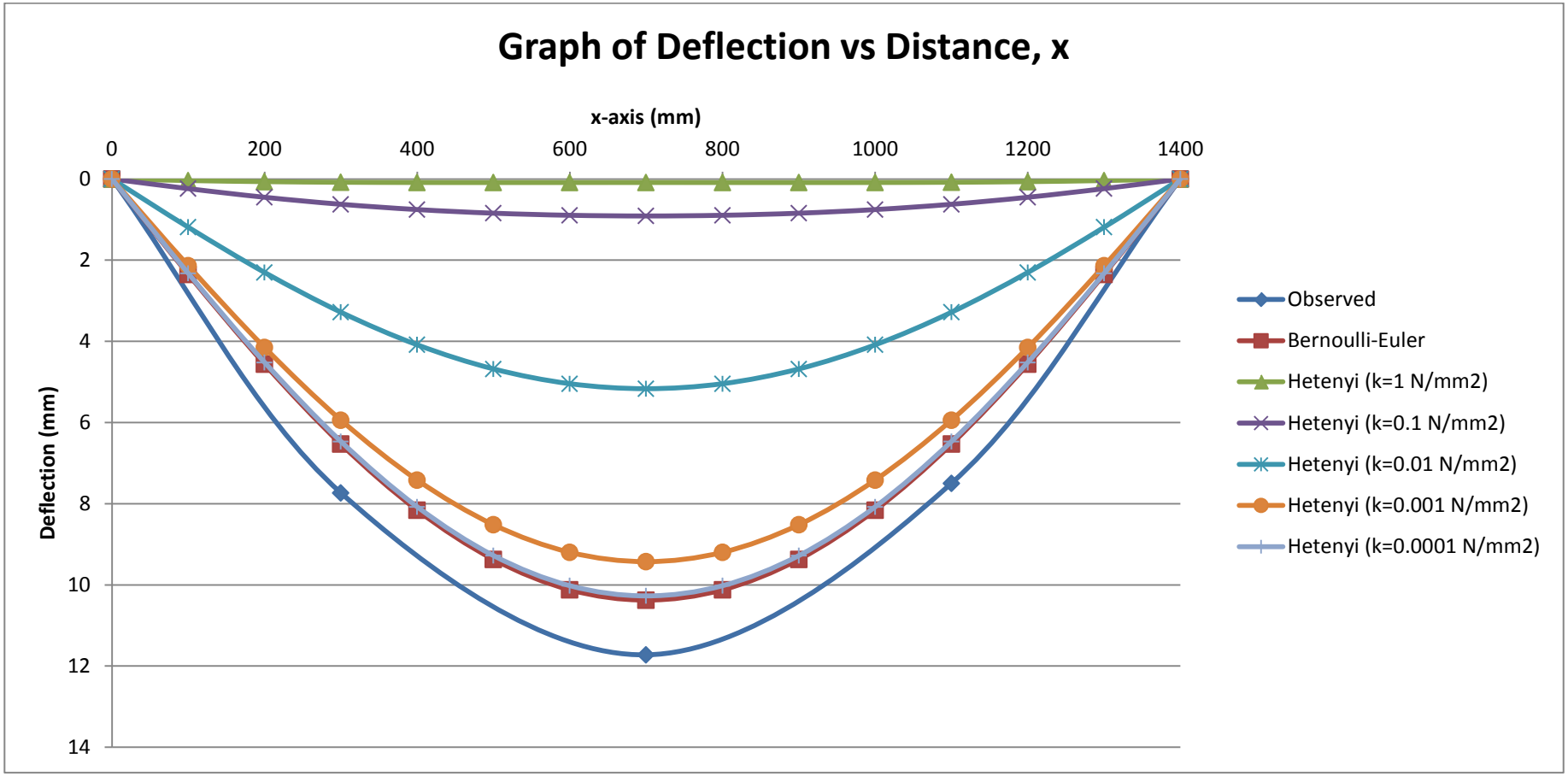

Figure 4.19: Comparison of deflection between observed and theoretical results for simply-supported condition under UDL

111

From Figure 4.19, it can be seen that as the coefficient of subgrade reaction, *k* decreases, Hetenyi's solution becomes closer and closer to Euler-Bernoulli's solution until they overlap with each other at k = 0.0001 N/mm^2. When the value of coefficient of subgrade reaction, *k* is zero or near to zero, then the structure is equivalent to an ordinary beam. By comparison, Hetenyi's solution is found to be in good agreement with the exact values. This validates that the Hetenyi's solution converges to become the same as Euler-Bernoulli's solution when *k* becomes small enough (cannot be zero since it will produce an undefined result) as if the soil provides as little resistance as air which is the most critical case assumed.

4.6 Hetenyi's Solutions for Cases without Support (Simply Rested on Subgrade)

As explained in Section 3.6, Hetenyi (1946) had solved the Winkler's one parameter equation for several load cases and supporting conditions. The solutions provided were used to predict the behaviour of BGC model on soft subgrade. The parameters substituted are as derived in previous sections, such as the flexural rigidity, *EI* value and the dimensions used is the same as the fabricated BGC model. The coefficient of subgrade reaction, *k* is assumed to be 0.01 N/mm^2.

There are two types of solutions provided for UDL case for beam supported by subgrade as explained in Section 3.63, where one is for beams of finite length whereas the other one is for beams of infinite length where the effects of load is localized. The results of several deflection profiles for the relevant solutions are compared as shown in Figure 4.20 and tabulated in Table 4.31.

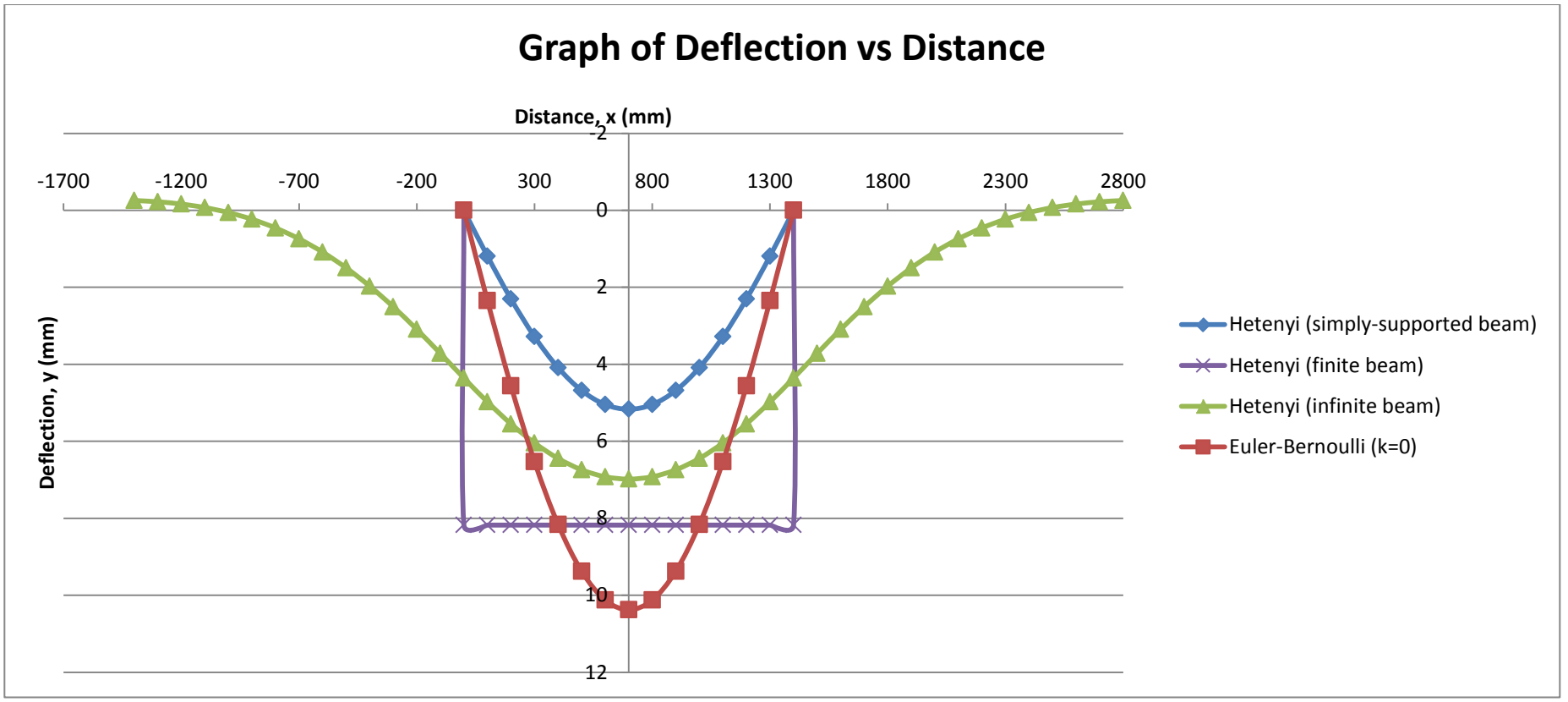

Figure 4.20: Comparison of several solutions of deflection profiles of BGC model on subgrade (k = 0.01 N/mm^2) under 5kg of uniformly-distributed load over 1400 mm (whole span length except for infinite beam solution)

113

Table 4.31: Tabulation of Hetenyi's theoretical results (k = 0.01 N/mm2)

Distance, x (mm)	Deflection, *y* (mm)												
	-1400	**-700**	**0**	**100**	**300**	**500**	**700**	**900**	**1100**	**1300**	**1400**	**2100**	**2800**
Hetenyi (simply-supported beam)	-	-	0.0	1.2	3.3	4.7	5.2	4.7	3.3	1.2	0.0	-	-
Hetenyi (finite beam)	0.0	0.0	8.2	8.2	8.2	8.2	8.2	8.2	8.2	8.2	8.2	0.0	0.0
Hetenyi (infinite beam)	-0.3	0.7	4.4	5.0	6.0	6.7	7.0	6.7	6.0	5.0	4.4	0.7	-0.3
Euler-Bernoulli	-	-	0.0	2.3	6.5	9.4	10.4	9.4	6.5	2.3	0.0	-	-

114

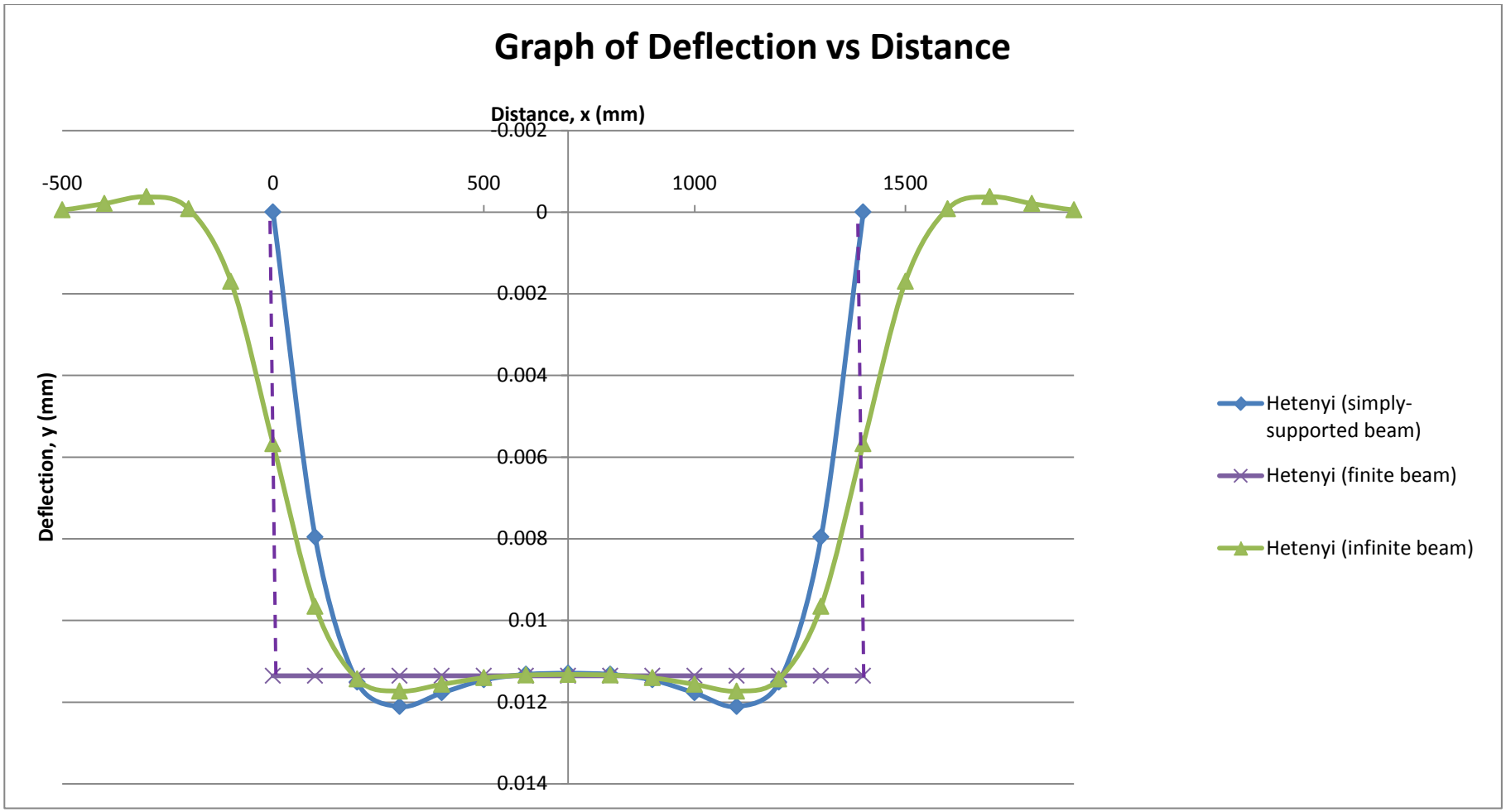

Figure 4.21: Comparison of several Hetenyi's solutions of deflection profile when k_o = 12000 kN/m^3

115

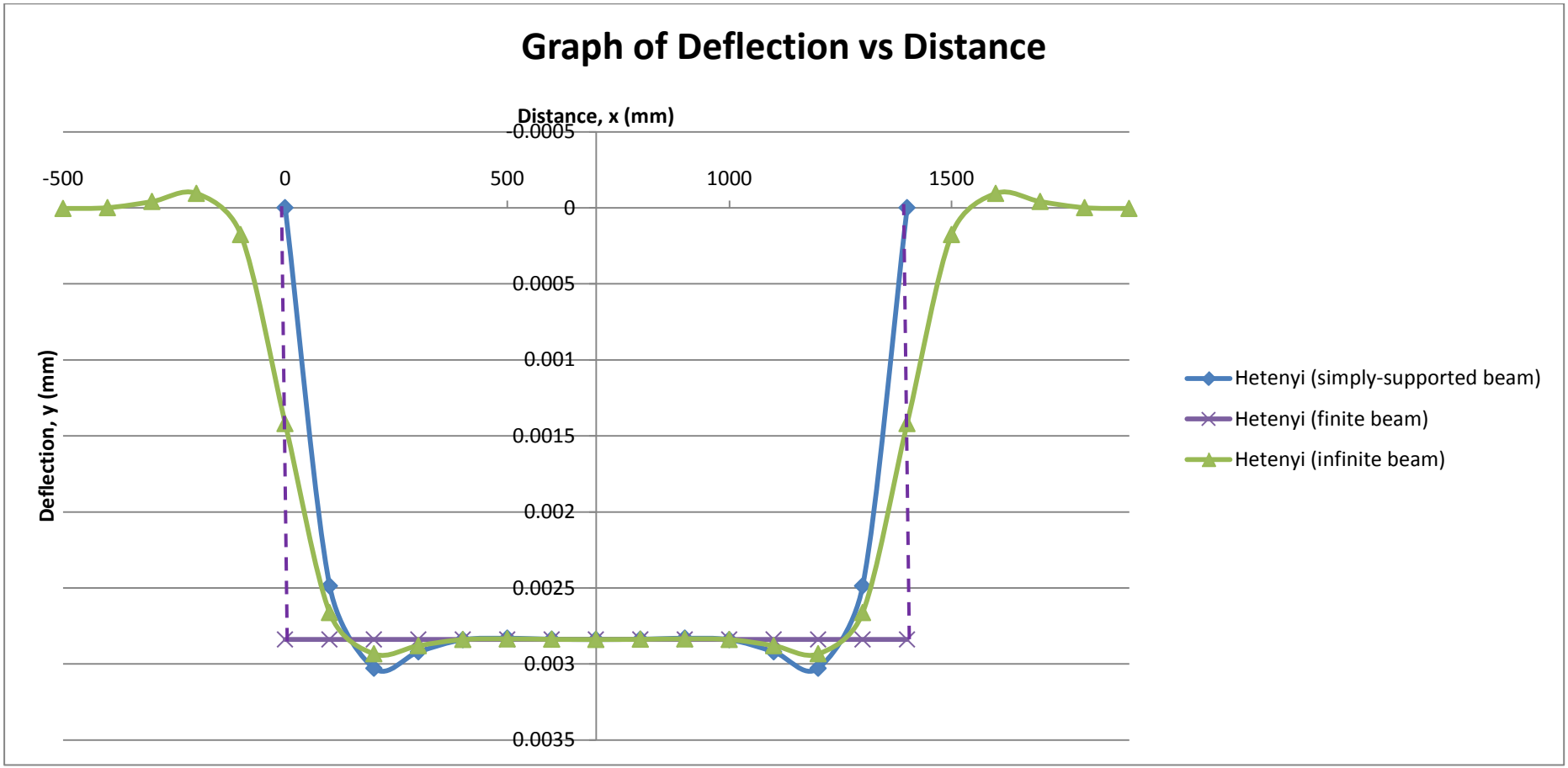

Figure 4.22: Comparison of several Hetenyi's solutions of deflection profile when k_o = 48000 kN/m^3

The comparison between Hetenyi's solutions of simply-supported beam on subgrade, beam rested on subgrade for finite and infinite beam length, and Euler-Bernoulli's solution is shown in Figure 4.20. The cases discussed above are all under the effect of uniformly-distributed loading (UDL) of 5 kg sand or 0.08175 N/mm along full span length of 1400 mm which is similar to the case under investigation. It should be noted that here is no effect of magnitude of UDL on shapes of deflection profiles as it will result in the same shapes of deflection profiles except that there is change in overall deflection magnitude. Euler-Bernoulli's solution is included for the sake of comparison for the case of $k = 0$ (in air). The value of coefficient of subgrade reaction of 0.01 N/mm^2 was selected so that all 4 deflection profiles can be fitted clearly in the graph for comparison. Spreadsheet for this graph has been developed so that the cases here can be used for design purposes where the dimensions and properties of the BGC model as well as the modulus of subgrade reaction, k_o and magnitude of UDL can be modified.

In Figures 4.20, it can be seen that the deflection profile for Hetenyi's finite beam solution is the typical deflection profile used to explain Winkler's model, where the edge shear force is not considered. This might not be the case in reality as stresses of soils outside the area of application of load is affected as well, thus it is expected that the soil outside of the beam deforms along as well, which should be similar to the deflection profile for Hetenyi's infinite beam solution where same loading was applied over the length of 1400 mm which is the same as BGC model for comparison purpose. Euler-Bernoulli's deflection profile has the highest maximum deflection accounted in this figure, followed by Hetenyi's finite beam's solution, Hetenyi's infinite beam's solution and lastly Hetenyi's simply-supported case's solution. This is to be expected since in Euler-Bernoulli's solution, there is no resistance force from below the BGC system, i.e. $k = 0$, whereas k exists for the other 3 cases.

If the value of modulus of subgrade reaction of 12000 kN/m^3 for typical clayey soil with q_u < 200 N/mm^2 (adopted from Table 2.9) is adopted in this case

assuming very weak soft clay condition as expected in the application of BCG system, then the coefficient of subgrade reaction would be k = 12000000 N/m^3 x 10^{-9} m^3/mm^3 x 600 mm width = 7.2 N/mm^2. It should be reminded that the values of the coefficient of subgrade reaction, k is a case-specific value and it should be carefully derived by an experienced engineer using methods as explained in Section 2.8. The resultant deflection profile is shown in Figure 4.21. Interestingly, the 3 deflection profiles coincide at mid-span and gives the same deflection value from x = 600 mm to 800 mm. This observation was compared with other k values such as in Figure 4.22 and it was found that the 3 Hetenyi's solutions gave similar observation of deflection profile as in Figure 4.21 as long as k > 1. It can be safely conclude that the deflection profiles at mid-span for UDL case for 3 observed Hetenyi's solution converge as long as k > 1.

The difference in deflection profiles at mid-span shown in Figure 4.20 might not hold truth in reality as the k value used, i.e. k = 0.01 N/mm^2 was too small to be in existent. Since the modulus of subgrade reaction, k_o of real soft clay is assumed to be at least 12000 kN/m^3 (refer to Table 2.9), the deflection profiles shown in Figure 4.21 (k_o = 12000 kN/m^3) are more likely to be closer to the case in reality since the same deflection profile is observed for all cases of k more than 1 N/mm^2. Thus, it is safe to conclude that the solution for Hetenyi's simply-supported beam case (simplest solution) is as good as Hetenyi's solutions for finite and infinite beam length cases in predicting the maximum deflection at mid-span of BGC system on soft subgrade.

4.7 Problems Encountered During the Practical Session

Dry sand has been chosen as a suitable material to simulate a uniformly distributed loading on the bamboo-geotextile composite because it will not hinder the deflection of bamboo grid as it is able to deform following the deflection profile. A bad

example would be using a material that is too rigid as simulated loading such as thick wooden boards as its stiffness would be too high to deflect along with bamboo grid, thus exerting loading not uniformly distributed, and possibly will exert 2 points loading near the edges as it rests on the bamboo grid which is undesirable for the purpose of the investigation. This is the reason the Perspex box which is a rigid material, fabricated by the predecessors to allow for more apparent observation of the bamboo grid deflection profile was discarded in this study. The downside of using dry sand is that the sand will not be able to be perfectly distributed uniformly across the bamboo-geotextile surface. The sand distribution method proposed as described in Chapter 3 would be able to minimize uneven distribution of loading across the surface.

Another method of measuring deflection/displacement would be using the Linear Variable Differential Transformer (LVDT) along with data logger but it was unfortunate that the laboratory is not sufficiently equipped with 100 mm or larger LVDT as only one 100 mm LVDT was available for the purpose of this experiment, although there are plenty of 10 mm and 25 mm LVDTs around but they are not viable as the deflection for each successive loading for each point measured is easily over the capacity the 10 mm LVDT can measure and also the cable connecting the LVDTs to the data logger is too short for practical purpose. Nevertheless, applying this method would undoubtedly make a more distinct and novelty of the current study.

Also, due to time constraint, investigation of BGC system on soft subgrade could not be carried out. This has resulted in lack of experimental data to be compared with the theoretical results as discussed in the section above, thus verification of the theoretical results could not be carried out.

CHAPTER 5

CONCLUSION AND RECOMMENDATIONS

5.1 Conclusion

The following itemized list represents brief summaries of the more important conclusions reached as a result of this research.

1. A sound experimental approach is developed for understanding the behaviour of Bamboo-Geotextile Composite (BGC) model when simply supported to simulate extreme soft ground condition and analysis approach is proposed to determine the model's *E* and *I* values.

2. The analysis approach has been verified and checked by back-substituting the results into theoretical equations for comparison with the observed results.

3. The behaviour of BGC model agrees well with the Euler-Bernoulli's beam theory which governs the structure/beam part of beam on elastic foundation theories.

4. An insight to the *E* and *I* values of bamboo grid to be substituted into beam on elastic foundation theories is developed.

5. Certain deflection profiles deviate from what it should be such as along the z-axis (Profiles IV, V and VI) which may be due to inhomogeneous nature of bamboo itself, besides the probability of uneven distribution of load, however, overall deflection profiles agree quite well theoretically.

6. Hetenyi's model of beams on elastic foundation theory was applied in predicting the deflection of the BGC model and the results are identical to those obtained using the classical beam theory when coefficient of subgrade reaction, *k* used is small enough to represent a soil-less or extremely soft soil condition.

7. Hetenyi's solutions of three cases of simply-supported beam, finite beam solely supported by soil and infinite beam solely supported by soil were demonstrated and it was found that the solution of simply-supported beam is as good as the solutions for finite beam and infinite beam solely supported by soil in estimating the maximum deflection at mid-span of BCG system.

5.2 Recommendations

There were certain assumptions made in the experimental approach that could be modified or improved to strengthen this work. In addition, further efforts should be considered to enhance the theoretical background. Furthermore, other loading conditions could be considered to expand the application of this research.

The following represents a more specific itemized listing of these categories of future work that could enhance and expand the application of this research.

1. To ensure a consistent uniformly-distributed load (UDL) to be applied over the BGC model, rubber mats or materials of such would work better than dry sand as flexible mat-like material works more homogeneously than dry sand.

2. Effects of different spacing of bamboo grid on the deflection and moment of inertia, *I* value of the BGC system should be further investigated so that optimum spacing of bamboo grid can be designed practically for application of BGC system.

3. Prototype testing should be carried out in the field to test the behaviour of BGC system along with on-site soil data and deformation results so that a more accurate theoretical approach can be developed as a simply supported BGC model cannot essentially be used to predict its exact behaviour on soil.

4. Individual bamboo testing should be carried out to find out the properties of bamboo used in the study so that laboratory *E* value found can be compared with the one derived from proposed analysis procedure.

5. A more precise instrument for measuring deflection should be used such as 100 mm LVDTs for all 9 designated points because adjusting dial gauges manually due to insufficient capacity will undoubtedly incur errors in the results obtained.

6. Theoretical solutions of other loading types and support conditions should be further studied and enhanced to provide a more holistic insight for the application of BGC system.

REFERENCES

Abang Abdullah, A.A. & Aband Abdul Rahim, A.A. (1984). Basic strength properties of a few selected Malaysian bamboos. Journal of Institution of Engineers, Malaysia. Vol. 34 June, 68-71.

Aband Abdullah, A.A. (1984). Development of basic mechanical test for Malaysian bamboos. PERTANIKA Vol. 7. No. 2. August.

Abang Ali A.A. (1984). *Use of Bamboo as Scaffolding Material*. University Pertanian Malaysia, Malaysia.

Bergado, D.T., Anderson, L.R., Miura, N., Balasubramaniam, A.S. *Soft Ground Improvement in Lowland and Other Environments*, ASCE, 1996.

Bergado, D.T., Long, P. V. and Murthy, S. (2002). *A case study of geotextilereinforced embankment on soft ground.*

Biot M. A., "Bending of infinite beams on an elastic foundation", Journal of Applied Mechanics, 59 (1937) A1-A7.

Bowles, J.E. (1968). Foundation Analysis and Design. McGraw-Hill Book Co., New York.

Brand, E. W. and Premchitt, J. (1989). Moderator's Report for the Predicted Performance of the Muar Test Embankment. Proceedings of the *International Symposium on Trial Embankments on Malaysian Marine Clays*. November 6-8, Kuala Lumpur, pp. 32-49.

Broms, B. B. (1990). Soil Improvement Methods for Malaysia Soft Soil. *Symposium on Recent Advances in Geotechnical Engineering II.* November 1, Kuala Lumpur.

Chen, C. S. and Tan, S. M. (2003). Some Engineering Properties of Soft Clay from Klang area. *Proceedings of 2nd International Conference on Advances in Soft Soil Engineering and Technology*. July 2-4, Malaysia, pp. 79-87.

Das, B.M. (2004). Principles of Foundation Engineering. (5th Edition). Thomson Brooks/Cole Publishing Company. Forest Research Institute Malaysia (1995).

Dutta S.C. and Roy R. A., "Critical Review on Idealization and Modeling for Interaction among Soil Foundation-Structure System", Computers and Structures, 80 (2002) 1579-1594.

Essler, R. and Yoshida, H. "Jet Grounting", *Ground Improvement*, Spon Press, New York, NY, 2004

Filonenko-Borodich, M.M. (1940). Some approximate theories of the elastic foundation (in Russian), Uchenyie Zapiski Moskovskogo Gosudarstvennogo Universiteta Mekhanica.

Forest Research Institute Malaysia (1995). Planting and Utilization of Bamboo in Peninsular Malaysia. FRIM, Malaysia

Ghavami K, Allameh S.M., Sanchez C.M.L. and Soboyejo W.O. (2003). *Multiscale Study of Bamboo Phyllostachys Edulis*.

Ghavami, K. (2005). *Bamboo as reinforcement in structural concrete elements*. Cement & Concrete Composites 27. pp. 637-649.

Hasnita Bt. Hirman (2009), Performance Of Full Scale Embankment On Soft Clay Reinforced With Bamboo-Geotextile Composite At The Interface, Masters of Civil Engineering (Geotechnics) Tesis, Universiti Teknologi Malaysia.

Hetényi, M. *Beams on elastic foundation*. Univ. Michigan Press, Ann Arbor, 1946.

Hirman, H. (2009). *Performance of Full Scale Embankment on Soft Clay Reinforced with Bamboo-Geotextile Composite at the Interface*. Master Project Report of Faculty of Civil Engineering, Universiti Teknologi Malaysia, Malaysia.

Holtz, R.D. and Kovacs, W.D. (1981). *An Introduction to Geotechnical Engineering*. New York: Prentice-Hall, Inc.

Holtz, R.D. (2001). *Geosynthetics For Soil Reinforcement. 9th Spencer J. Buchanan Lecture.*

Huat, B.B.K., Othman, K., and Jaffar, A.A. (1995). Geotechnical Properties of Malaysian Marine Clays. *Journals of Institute engineers Malaysia*. Vo1.56, pp. 23-33.

Hunter, G. dan Fell, R. (2003). *Prediction of impending failure of embankments on soft ground*. Canada Geotechnical Journal Vol. 40, pp. 209–220.

Irsyam, M., Krisnanto.,S. and Wardhani., S.P.R. (2008). *Instrumented Full Scale Test and Numerical Analysis to Investigate the Performance of Bamboo Pile-Mattress System as Soil Reinforcement for Coastal Embankment on Soft Clay*. Liu,

Deng and Chu (eds) 2008 Science Press Beijing and Springer-Verlag GmbH Berlin Heidelberg, Geotechnical Engineering for Disaster Mitigation and Rehabilitation.

Kamon, M. and Bergado D. T. “Ground Improvement Techniques”, 9th Asian Region Conf. on Soil Mechanics and Foundation Engieering., Bangkok, Vol. 2, pp. 526-546, 1991.

Kerr, A.D. (1964, September). Elastic and viscoelastic foundation models. Journal of Applied Mechanics. Transactionss of the ASME, 491-498.

Khatib, A. (2009). *Bearing Capacity Of Granular Soil Overlying Soft Clay Reinforced with Bamboo-Geotextile Composite at the Interface*. PhD. Thesis, Department of Geotechnics and Transportation, Faculty of Civil Engineering, Universiti Teknologi Malaysia, Malaysia.

Krause, Q. and Ghavami, K. (2009). Transversal Reinforcement in Bamboo Culms. *Proceedings of the 11th International Conference on Non-conventional Materials and Technologies (NOCMT 2009)*. 6-9 September 2009, Bath, UK.

Leroueil, S., Magnan, J.P. dan Tavenas, F. (1990). *Embankments on soft ground*. West Sussex, England. Ellis Horwood.

Loke, K. H. (2000). “Geosynthetic-Proven and Innovative Method for Soft Soil Stabilization”. Seminar on Ground Improvement-Soft Clay. August, 23-24. Kuala Lumpur, 34-42.

Lybeer, B. (2005). *Age-related anatomical aspects of some temperate and tropical bamboo culms*. Faculteit Wetenschappen, Universiteit Gent.

Marto, A., Othman, B. A., Mohd Hanipiah, M. Z., & Hirman, H. (2010). *Performance of bamboo-geotextile composite reinforced embankment on soft clay*. Paper presented at the Conference on Engineering and Technology Education, World Engineering Congress, Kuching, Sarawak, Malaysia.

Marto, A., Ismail, B. N., Bakar, I. and Othman, B. A. *2D Finite Element Analysis of Bamboo Reinforced Embankment*. International Conference on Geotechnical and Transportation Engineering (GEOTROPIKA 2010), 1-3 December 2010, Kota Kinabalu, Sabah, Malaysia.

Marto, A. and Othman, B. A. *The Potential Use of Bamboo as Green Material for Soft Clay Reinforcement System*. 2011 International Conference on Environment Science and Engineering (ICESE 2011), 1-3 April 2011, Bali, Indonesia. Published at IPCBEE vol.8 (2011) © (2011) IACSIT Press, Singapore.

Ochiai, H., Watari, Y., and Tsukamoto, Y. (1996). Soil Reinforcement Practice for Fills Over Soft Ground in Japan. *Geosynthetics International*, Vol.3, No.1, pp. 31-48.

Pasternak, P.L. (1954). On a new method of analysis of an elastic foundation by means of two foundation constants (in Russian), Gosudarstvennoe Izdatelstvo Literaturi po Stroitelsvu I Arkhitekture. Moscow, Russia.

Reissner E., *Notes on Deflection of Plates on a Viscoelastic Foundation*, J. of Appl. Mech., **25,** 144-155 (1958)

Sadrekarimi, J., Akbarzad, M. "Comparative Study of Methods of Determination of Coefficient of Subgrade Reaction" EJGE volume 14, Bundle E, 2008.

Salfaiza.N (2009). *Effect of geotextile reinforcement of embankment in stability analysis*. *Masters thesis*.

Semprich, S. and Stakler, G. "Grouting", *Geotechnical Engineering*, Geotechnical Handbook, Ernst & Sohn, Berlin.

Siopongco, J.O. and Munandar M. (1987). *Technology Manual on Bamboo as Building Material*. Regional Network in Asia for Low-Cost Building Materials Technologies and Construction System. Forest Products Research and Development Institute, Phillipine.

Sondermann W. and Wehr, W. "Deep Vibro Techniques", *Ground Improvement*, Spon Press, New York, NY, 2004.

Subramanian, Narayanan. *Design of Steel Structures*. Oxford University Press, 2008.

Tavenas, F., Mieussens, C. and Bourges, F. (1979). *Lateral Displacements in Clay Foundations Under Embankments*. Canadian Geotechnical Journal. Vol. 16, No. 3, pp. 532-550.

Terzaghi, K. (1955). Evaluation of coefficients of subgrade reaction, Geotechnique. Vol. 5, 297-326.

Terzaghi, K., and Peck, R.B (1967). Soil Mechanics in Engineering Practice. John Wiley and Sons, New York.

Ting, W.H., Wong, T.F. and Toh, C.T. (1988). *Design Parameters for Soft Ground in Malaysia*. Journal of Southeast Asian Geotechnical Society. Vol. 19 No.1.

Topolnicki, M. "In Situ Soil Mixing", *Ground Improvement*, Spon Press, New York, NY, 2004.

Vesic A.S., “Bending of beams resting on isotropic solids”, Journal of the engineering Mechanics division, ASCE, 87(EM2) (1961) 35-53.

Vlasov. V. Z., & Leont’ev, N. N. (1966). Beams, plates and shells on elasic foundations. Translated from Russian. Isreal Program for Scientific Translation. Jerusalem.

Winkler E., “Die Lehre von Elastizitat und Festigkeit (on elasticity and fixity)”, Dominicus, Prague (1867).

Wong, K.M. (1995). *The Bamboos of Peninsular Malaysia*. Forest Research Institute Malaysia (FRIM) in Collaboration with Forest research Centre, Forestry Department, Sabah, Malaysia. Malayan Forest Records, No. 41.

APPENDICES

APPENDIX A: Tables for Observed Deflection Results Measured with Dial Gauges

Table A1: Trial 1 observed results using dial gauges

Axis	z (mm)	0	150	300	450	150	300	450	150	300	450	600
	x (mm)	0	350	350	350	700	700	700	1050	1050	1050	1400
Sand load (kg)	UDL (N/mm)	Cumulative deflection (mm)										
		Points										
		edge	1	2	3	4	5	6	7	8	9	edge
0	0	0	0	0	0	0	0	0	0	0	0	0
5	0.08175	0	0.71	0.86	5.46	8.821	0.83	7.849	0.16	0.89	6.003	0
10	0.1635	0	11.52	10.87	11.787	16.324	17.48	14.161	7.89	1.85	12.549	0
15	0.24525	0	14.18	13.63	13.486	18.988	19.22	17.058	9.25	12.15	13.463	0
20	0.327	0	15.36	15.25	13.487	19.67	22.68	17.06	14.56	12.26	13.463	0

Table A2: Trial 2 observed results using dial gauges

Axis	z (mm)	0	150	300	450	150	300	450	150	300	450	600
	x (mm)	0	350	350	350	700	700	700	1050	1050	1050	1400
Sand load (kg)	UDL (N/mm)	Cumulative deflection (mm)										
		Points										
		edge	1	2	3	4	5	6	7	8	9	edge
0	0	0	0	0	0	0	0	0	0	0	0	0
5	0.08175	0	6.87	6.3	7.972	9.49	9.787	10.637	5.49	5.49	7.161	0
10	0.1635	0	13.58	13.65	13.389	18.5	18.836	19.569	10.92	11.74	12.576	0
15	0.24525	0	16.01	17.27	17.885	22.24	23.355	26.464	12.81	15.55	17.112	0
20	0.327	0	16.97	18.86	22.299	22.75	26.281	32.507	20.89	19.56	21.08	0

129

Table A3: Trial 3 observed results using dial gauges

Axis	z (mm)	0	150	300	450	150	300	450	150	300	450	600
	x (mm)	0	350	350	350	700	700	700	1050	1050	1050	1400
Sand load (kg)	UDL (N/mm)	Cumulative deflection (mm)										
		Points										
		edge	1	2	3	4	5	6	7	8	9	edge
0	0	0	0	0	0	0	0	0	0	0	0	0
5	0.08175	0	7.02	7.62	8.192	9.45	10.187	10.787	6.38	7.2	7.231	0
10	0.1635	0	13.63	13.55	15.56	18.53	20.181	21.315	12.23	13.61	13.926	0
15	0.24525	0	19.76	20.5	20.347	25.81	24.786	27.217	16.94	17.93	18.88	0
20	0.327	0	24.89	25.25	25.517	32.59	31.341	33.726	20.94	22.35	23.834	0

Table A4: Trial 4 observed results using dial gauges

Axis	z (mm)	0	150	300	450	150	300	450	150	300	450	600
	x (mm)	0	350	350	350	700	700	700	1050	1050	1050	1400
Sand load (kg)	UDL (N/mm)	Cumulative deflection (mm)										
		Points										
		edge	1	2	3	4	5	6	7	8	9	edge
0	0	0	0	0	0	0	0	0	0	0	0	0
5	0.08175	0	6.3	6.73	8.077	8.74	9.579	10.338	5.46	5.89	7.011	0
10	0.1635	0	13.36	13.86	13.606	18.67	19.705	20.512	11.85	11.56	12.028	0
15	0.24525	0	17.82	18.81	19.19	23.37	24.051	28.109	15.6	15.78	16.797	0
20	0.327	0	19.5	22.15	24.454	24.05	27.576	35.438	20.58	18.42	21.566	0

130

Table A5: Trial 5 observed results using dial gauges

Axis	z (mm)	0	150	300	450	150	300	450	150	300	450	600
	x (mm)	0	350	350	350	700	700	700	1050	1050	1050	1400
Sand load (kg)	UDL (N/mm)	Cumulative deflection (mm)										
		Points										
		edge	1	2	3	4	5	6	7	8	9	edge
0	0	0	0	0	0	0	0	0	0	0	0	0
5	0.08175	0	5.59	6.02	6.964	8.35	9.431	10.263	5.05	6.79	6.36	0
10	0.1635	0	11.08	12.8	11.681	17.38	17.274	16.241	11.28	11.9	10.524	0
15	0.24525	0	19.78	21.32	18.702	27.53	27.626	25.692	17.618	19.3	16.474	0
20	0.327	0	25.16	27.72	24.619	36.8	37.085	35.056	24.068	25.52	21.674	0

Table A6: Trial 6 observed results using dial gauges

Axis	z (mm)	0	150	300	450	150	300	450	150	300	450	600
	x (mm)	0	350	350	350	700	700	700	1050	1050	1050	1400
Sand load (kg)	UDL (N/mm)	Cumulative deflection (mm)										
		Points										
		edge	1	2	3	4	5	6	7	8	9	edge
0	0	0	0	0	0	0	0	0	0	0	0	0
5	0.08175	0	5.85	5.99	6.068	8.87	9.799	11.131	6.18	6.89	6.706	0
10	0.1635	0	11.64	13.86	14.058	19.31	19.695	21.393	13.64	14.33	12.662	0
15	0.24525	0	17.66	20.62	20.624	29.26	28.815	30.641	20.09	20.71	18.084	0
20	0.327	0	23.7	27.22	27.247	38.29	38.156	40.347	26.21	27.03	23.583	0

131

Table A7: Trial 7 observed results using dial gauges

Axis	z (mm)	0	150	300	450	150	300	450	150	300	450	600
	x (mm)	0	350	350	350	700	700	700	1050	1050	1050	1400
Sand load (kg)	UDL (N/mm)	Cumulative deflection (mm)										
		Points										
		edge	1	2	3	4	5	6	7	8	9	edge
0	0	0	0	0	0	0	0	0	0	0	0	0
5	0.08175	0	5.87	6.64	7.304	9.16	9.889	10.542	6.02	7.04	6.136	0
10	0.1635	0	12.85	14.05	13.356	19.04	20.681	22.136	12.24	13.76	12.97	0
15	0.24525	0	15.52	18.07	18.375	22.67	25.875	28.875	14.64	17.42	17.053	0
20	0.327	0	16.51	20.45	21.723	24.74	28.586	33.653	16.74	19.24	19.833	0

Table A8: Trial 8 observed results using dial gauges

Axis	z (mm)	0	150	300	450	150	300	450	150	300	450	600
	x (mm)	0	350	350	350	700	700	700	1050	1050	1050	1400
Sand load (kg)	UDL (N/mm)	Cumulative deflection (mm)										
		Points										
		edge	1	2	3	4	5	6	7	8	9	edge
0	0	0	0	0	0	0	0	0	0	0	0	0
5	0.08175	0	5.24	5.91	7.785	8.33	9.842	10.473	6.17	6.18	6.297	0
10	0.1635	0	10.71	14.52	14.34	18.46	19.288	20.127	17.39	12.71	12.108	0
15	0.24525	0	12.91	16.98	17.936	19.8	22.806	25.341	19.13	16.37	15.183	0
20	0.327	0	14.59	20.69	21.536	21.2	25.93	30.807	27.27	19.12	18.15	0

132

Table A9: Trial 9 observed results using dial gauges

Axis	z (mm)	0	150	300	450	150	300	450	150	300	450	600
	x (mm)	0	350	350	350	700	700	700	1050	1050	1050	1400
Sand load (kg)	UDL (N/mm)	Cumulative deflection (mm)										
		Points										
		edge	1	2	3	4	5	6	7	8	9	edge
0	0	0	0	0	0	0	0	0	0	0	0	0
5	0.08175	0	5.82	7.86	6.566	8.95	11.445	10.508	6.72	7.63	6.819	0
10	0.1635	0	12.15	14	12.985	17.87	19.724	20.367	18.05	13.65	12.767	0
15	0.24525	0	17.85	20.3	19.991	24.75	28.763	30.484	23.55	19.85	18.887	0
20	0.327	0	19.55	22.87	22.829	26.5	32.538	35.267	27.28	23.35	21.948	0

Table A10: Trial 10 observed results using dial gauges

Axis	z (mm)	0	150	300	450	150	300	450	150	300	450	600
	x (mm)	0	350	350	350	700	700	700	1050	1050	1050	1400
Sand load (kg)	UDL (N/mm)	Cumulative deflection (mm)										
		Points										
		edge	1	2	3	4	5	6	7	8	9	edge
0	0	0	0	0	0	0	0	0	0	0	0	0
5	0.08175	0	5.87	5.64	6.518	9.12	9.236	9.528	6.98	5.8	5.767	0
10	0.1635	0	11.2	13.05	13.043	18.92	18.981	19.89	13	12.15	11.172	0
15	0.24525	0	15.45	18.17	18.904	27.57	27.015	28.406	17.56	18.1	16.432	0
20	0.327	0	17.72	21.97	22.937	30.12	30.862	34.328	18.12	21.24	19.988	0

133

APPENDIX B: Tables for Observed Deflection Results Measured with Ruler

Table B1: Trial 1 observed results using dial gauges

Axis	z (mm)	0	150	300	450	150	300	450	150	300	450	600
	x (mm)	0	350	350	350	700	700	700	1050	1050	1050	1400
Sand load (kg)	UDL (N/mm)	Cumulative deflection (mm)										
		Points										
		edge	1	2	3	4	5	6	7	8	9	edge
0	0	0	0	0	0	0	0	0	0	0	0	0
5	0.08175	0	1	1	6	10	1	8	2	2	7	0
10	0.1635	0	12	11	12	17	18	15	9	3	13	0
15	0.24525	0	15	14	14	20	20	18	11	13	14	0
20	0.327	0	16	16	14	21	23	19	16	14	14	0

Table B2: Trial 2 observed results using dial gauges

Axis	z (mm)	0	150	300	450	150	300	450	150	300	450	600
	x (mm)	0	350	350	350	700	700	700	1050	1050	1050	1400
Sand load (kg)	UDL (N/mm)	Cumulative deflection (mm)										
		Points										
		edge	1	2	3	4	5	6	7	8	9	edge
0	0	0	0	0	0	0	0	0	0	0	0	0
5	0.08175	0	7	7	8	11	10	11	7	5	7	0
10	0.1635	0	14	15	14	19	19	20	11	10	13	0
15	0.24525	0	17	18	18	24	25	28	13	15	16	0
20	0.327	0	19	20	23	25	27	35	21	20	21	0

135

Table B3: Trial 3 observed results using dial gauges

Axis	z (mm)	0	150	300	450	150	300	450	150	300	450	600
	x (mm)	0	350	350	350	700	700	700	1050	1050	1050	1400
Sand load (kg)	UDL (N/mm)	Cumulative deflection (mm)										
		Points										
		edge	1	2	3	4	5	6	7	8	9	edge
0	0	0	0	0	0	0	0	0	0	0	0	0
5	0.08175	0	6	6	6	8	9	11	5	7	9	0
10	0.1635	0	13	12	12	20	20	20	11	13	17	0
15	0.24525	0	18	17	17	28	28	28	16	18	22	0
20	0.327	0	25	27	26	40	42	40	23	26	31	0

Table B4: Trial 4 observed results using dial gauges

Axis	z (mm)	0	150	300	450	150	300	450	150	300	450	600
	x (mm)	0	350	350	350	700	700	700	1050	1050	1050	1400
Sand load (kg)	UDL (N/mm)	Cumulative deflection (mm)										
		Points										
		edge	1	2	3	4	5	6	7	8	9	edge
0	0	0	0	0	0	0	0	0	0	0	0	0
5	0.08175	0	6	6	8	9	10	11	5	6	6	0
10	0.1635	0	12	13	14	18	19	21	11	13	14	0
15	0.24525	0	16	16	21	24	29	30	17	18	22	0
20	0.327	0	19	18	25	26	34	37	22	23	27	0

136

Table B5: Trial 5 observed results using dial gauges

Axis	z (mm)	0	150	300	450	150	300	450	150	300	450	600
	x (mm)	0	350	350	350	700	700	700	1050	1050	1050	1400
Sand load (kg)	UDL (N/mm)	Cumulative deflection (mm)										
		Points										
		edge	1	2	3	4	5	6	7	8	9	edge
0	0	0	0	0	0	0	0	0	0	0	0	0
5	0.08175	0	7	7	7	9	9	9	6	6	6	0
10	0.1635	0	13	14	11	17	16	17	12	11	10	0
15	0.24525	0	21	21	20	35	32	31	20	18	22	0
20	0.327	0	26	26	25	45	41	39	26	25	27	0

Table B6: Trial 6 observed results using dial gauges

Axis	z (mm)	0	150	300	450	150	300	450	150	300	450	600
	x (mm)	0	350	350	350	700	700	700	1050	1050	1050	1400
Sand load (kg)	UDL (N/mm)	Cumulative deflection (mm)										
		Points										
		edge	1	2	3	4	5	6	7	8	9	edge
0	0	0	0	0	0	0	0	0	0	0	0	0
5	0.08175	0	5	5	7	8	10	10	5	5	7	0
10	0.1635	0	12	12	10	18	20	20	11	12	16	0
15	0.24525	0	19	21	17	29	30	31	18	19	24	0
20	0.327	0	25	26	22	38	40	41	23	25	32	0

137

Table B7: Trial 7 observed results using dial gauges

Axis	z (mm)	0	150	300	450	150	300	450	150	300	450	600
	x (mm)	0	350	350	350	700	700	700	1050	1050	1050	1400
Sand load (kg)	UDL (N/mm)	Cumulative deflection (mm)										
		Points										
		edge	1	2	3	4	5	6	7	8	9	edge
0	0	0	0	0	0	0	0	0	0	0	0	0
5	0.08175	0	6	7	7	10	9	9	6	6	7	0
10	0.1635	0	12	13	12	20	21	22	13	14	14	0
15	0.24525	0	16	19	18	22	31	28	15	20	21	0
20	0.327	0	18	22	21	25	34	34	17	23	25	0

Table B8: Trial 8 observed results using dial gauges

Axis	z (mm)	0	150	300	450	150	300	450	150	300	450	600
	x (mm)	0	350	350	350	700	700	700	1050	1050	1050	1400
Sand load (kg)	UDL (N/mm)	Cumulative deflection (mm)										
		Points										
		edge	1	2	3	4	5	6	7	8	9	edge
0	0	0	0	0	0	0	0	0	0	0	0	0
5	0.08175	0	6	6	7	9	10	10	6	7	7	0
10	0.1635	0	13	11	12	18	20	19	12	13	13	0
15	0.24525	0	15	14	17	19	26	25	15	17	18	0
20	0.327	0	17	18	22	21	31	31	21	20	23	0

138

Table B9: Trial 9 observed results using dial gauges

Axis	z (mm)	0	150	300	450	150	300	450	150	300	450	600
	x (mm)	0	350	350	350	700	700	700	1050	1050	1050	1400
Sand load (kg)	UDL (N/mm)	Cumulative deflection (mm)										
		Points										
		edge	1	2	3	4	5	6	7	8	9	edge
0	0	0	0	0	0	0	0	0	0	0	0	0
5	0.08175	0	7	7	7	10	10	10	6	8	6	0
10	0.1635	0	14	14	14	19	23	19	11	14	12	0
15	0.24525	0	20	20	22	26	32	30	16	20	18	0
20	0.327	0	22	23	25	28	36	34	27	24	21	0

Table B10: Trial 10 observed results using dial gauges

Axis	z (mm)	0	150	300	450	150	300	450	150	300	450	600
	x (mm)	0	350	350	350	700	700	700	1050	1050	1050	1400
Sand load (kg)	UDL (N/mm)	Cumulative deflection (mm)										
		Points										
		edge	1	2	3	4	5	6	7	8	9	edge
0	0	0	0	0	0	0	0	0	0	0	0	0
5	0.08175	0	6	6	7	9	10	7	6	6	6	0
10	0.1635	0	11	13	14	19	20	17	12	13	12	0
15	0.24525	0	16	18	20	28	28	26	17	19	17	0
20	0.327	0	19	22	24	31	31	32	19	22	21	0

139

APPENDIX C: Pictures of Deflection of BGC from 0 kg to 40 kg

Figure C1: Deflection when sand load = 0 kg

Figure C2: Deflection when sand load = 5 kg

Figure C3: Deflection when sand load = 10 kg

Figure C4: Deflection when sand load = 15 kg

Figure C5: Deflection when sand load = 20 kg

Figure C6: Deflection when sand load = 25 kg

Figure C7: Deflection when sand load = 30 kg

Figure C8: Deflection when sand load = 35 kg

Figure C9: Deflection when sand load = 40 kg

APPENDIX D: Sample Excel Sheets for Hetenyi's Solutions

Hetenyi's solution for simply-supported finite beam on subgrade

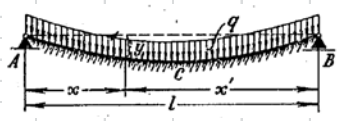

Deflection at any point:

$$y = \frac{q}{k}\left(1 - \frac{Cosh\lambda x \cos\lambda x' + Cosh\lambda x' \cos\lambda x}{Cosh\lambda l + \cos\lambda l}\right)$$

First step: Input required parameters

Beam length, l	1400	mm
Beam width, B	600	mm
Loading, q	0.08175	N/mm
Coefficient of subgrade reaction, k	0.1	N/mm^2
Young's modulus of beam, E	23035.8	N/mm^2
Moment of inertia of beam, I	17111.31	mm^4
Flexural rigidity of beam, EI	3.94E+08	N.mm^2
Characteristic parameter of beam, λ	0.002822	

$$\lambda = \sqrt[4]{\frac{k}{4EI}}$$

Second step: Produce table for deflection

x (mm)	0	100	200	300	400	500	600	700	800	900	1000	1100	1200	1300	1400
x' (mm)	1400	1300	1200	1100	1000	900	800	700	600	500	400	300	200	100	0
y (mm)	0	0.238115	0.450136	0.623049	0.753327	0.842556	0.894124	0.910942	0.894124	0.842556	0.753327	0.623049	0.450136	0.238115	0

Third step: Produce graph for deflection

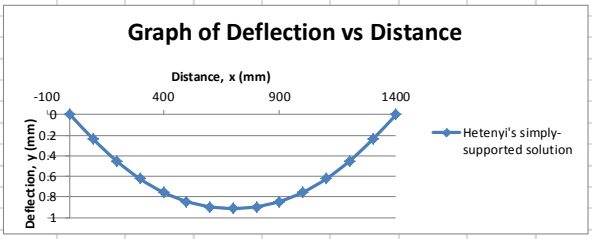

Hetenyi's solution for beam of finite length rested on subgrade

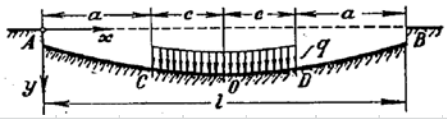

Deflection at end points

$$y_A = y_B = \frac{q}{k}\frac{1}{\sinh\lambda l + \sin\lambda l}[\cosh\lambda a \sin\lambda(l-a) - \sinh\lambda a\cos\lambda(l-a) + \cos\lambda a\sinh\lambda(l-a) - \sin\lambda a\cosh\lambda(l-a)]$$

Deflection for portion C-D

$$y_{C-D} = [y_{A-C}]_{x>a} + \frac{q}{k}[1-\cosh\lambda(x-a)\cos\lambda(x-a)]$$

Deflection at the middle

$$y_o = \frac{q}{k}[1 - \frac{2\left(\sinh\lambda a\cos\lambda c\cosh\frac{\lambda l}{2} + \sin\lambda a\cosh\lambda c\cos\frac{\lambda l}{2}\right)}{\sinh\lambda l + \sin\lambda l}]$$

Deflection line for portion A-C (x<a)

$$y_{A-C} = \frac{q}{k}\frac{1}{\sinh\lambda l + \sin\lambda l}\{\cosh\lambda x\cos\lambda x[\cosh\lambda a\sin\lambda(l-a) - \sinh\lambda a\cos\lambda(l-a) + \cos\lambda a\sinh\lambda(l-a) - \sin\lambda a\cosh\lambda(l-a)] + (\cosh\lambda x\sin\lambda x + \sinh\lambda x\cos\lambda x)[\sin\lambda a\sinh\lambda(l-a) - \sinh\lambda a\sin\lambda(l-a)]\}$$

First step: Input required parameters

Loading, q	0.08175	N/mm
Beam length, l	1400	mm
Beam width, B	600	mm
Coefficient of subgrade reaction, k	7.2	N/mm2
Young's modulus of beam, E	23035.8	N/mm^2
Moment of inertia of beam, I	17111.31	mm^4
Flexural rigidity of beam, EI	394172777	N.mm2
Characteristic parameter of beam, λ	0.0082205	
Distance a	0	mm
Distance c	700	mm

λa	0
λc	5.754327
λl/2	5.754327
λl	11.50865
λ(l-a)	11.50865

Second step: Produce table for deflection (for a = 0 only. If a>0, table needs to be modified)

x (mm)	0	100	200	300	400	500	600	700	800	900	1000	1100	1200	1300	1400
[y(A-C)] for x>a (mm)	-	0.010491	-0.002232	-0.05255	-0.15069	-0.19608	0.171756	-	0.171756	-0.19608	-0.15069	-0.05255	-0.00223	0.010491	-
y (mm)	0.011354	0.011354	0.0113542	0.011354	0.011354	0.011354	0.011354	0.011354	0.011354	0.011354	0.011354	0.011354	0.011354	0.011354	0.011354

Third step: Produce graph for deflection

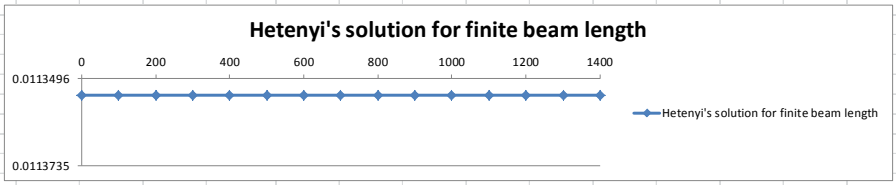

Hetenyi's solution for beam of infinite length rested on subgrade

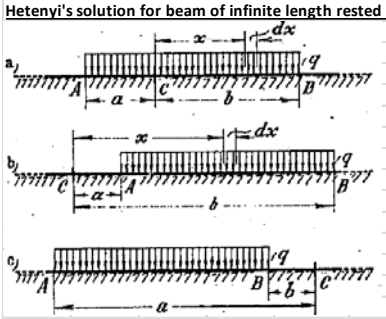

a) Deflection when point C is under the loading:

$$y_c = \frac{q}{2k}[(1 - e^{-\lambda a}\cos\lambda a) + (1 - e^{-\lambda b}\cos\lambda b)]$$

b) Deflection when point C is to the left of the loading:

$$y_c = \frac{q}{2k}[(e^{-\lambda a}\cos\lambda a) - (e^{-\lambda b}\cos\lambda b)]$$

c) Deflection when point C is to the right of the loading:

$$y_c = -\frac{q}{2k}[(e^{-\lambda a}\cos\lambda a) - (e^{-\lambda b}\cos\lambda b)]$$

d) Deflection at point A and B

$$y_{A/B} = \frac{q}{2k}(1 - e^{-\lambda l}\cos\lambda l)$$

First step: Input required parameters

Loading, q	0.08175	N/mm
Beam length, l	1400	mm
Beam width, B	600	mm
Coefficient of subgrade reaction, k	7.2	N/mm2
Young's modulus of beam, E	23035.8	N/mm^2
Moment of inertia of beam, I	17111.31	mm^4
Flexural rigidity of beam, EI	394172715	N.mm2
Characteristic parameter of beam, λ	0.0082205	

Second step: Produce table for deflection

a (mm)	1400	1300	1200	1100	1000	900	800	700	600	500	400	300	200	100	
b (mm)	2800	2700	2600	2500	2400	2300	2200	2100	2000	1900	1800	1700	1600	1500	
x (mm)	-1400	-1300	-1200	-1100	-1000	-900	-800	-700	-600	-500	-400	-300	-200	-100	
y (mm)	2.8E-08	-3.9E-08	-2.7E-07	-6.23E-07	-5.5E-07	1.53E-06	7.57E-06	1.55E-05	8.93E-06	-5.3E-05	-0.00021	-0.00038	-8E-05	0.001699	

a (mm)	0	100	200	300	400	500	600	700	800	900	1000	1100	1200	1300	1400
b (mm)	1400	1300	1200	1100	1000	900	800	700	600	500	400	300	200	100	0
x (mm)	0	100	200	300	400	500	600	700	800	900	1000	1100	1200	1300	1400
y (mm)	0.005677	0.009656	0.011435	0.011731	0.011564	0.011405	0.011338	0.011323	0.011338	0.011405	0.011564	0.011731	0.011435	0.009656	0.005677

a (mm)	1500	1600	1700	1800	1900	2000	2100	2200	2300	2400	2500	2600	2700	2800	
b (mm)	100	200	300	400	500	600	700	800	900	1000	1100	1200	1300	1400	
x (mm)	1500	1600	1700	1800	1900	2000	2100	2200	2300	2400	2500	2600	2700	2800	
y (mm)	0.001699	-8E-05	-0.00038	-0.00021	-5.3E-05	8.93E-06	1.55E-05	7.57E-06	1.53E-06	-5.5E-07	-6.2E-07	-2.7E-07	-3.9E-08	2.8E-08	

Third step: Produce graph for deflection